INFORMATION TO USERS

This manuscript has been reproduced from the microfilm master. UMI films the text directly from the original or copy submitted. Thus, some thesis and dissertation copies are in typewriter face, while others may be from any type of computer printer.

The quality of this reproduction is dependent upon the quality of the copy submitted. Broken or indistinct print, colored or poor quality illustrations and photographs, print bleedthrough, substandard margins, and improper alignment can adversely affect reproduction.

In the unlikely event that the author did not send UMI a complete manuscript and there are missing pages, these will be noted. Also, if unauthorized copyright material had to be removed, a note will indicate the deletion.

Oversize materials (e.g., maps, drawings, charts) are reproduced by sectioning the original, beginning at the upper left-hand corner and continuing from left to right in equal sections with small overlaps. Each original is also photographed in one exposure and is included in reduced form at the back of the book.

Photographs included in the original manuscript have been reproduced xerographically in this copy. Higher quality 6" x 9" black and white photographic prints are available for any photographs or illustrations appearing in this copy for an additional charge. Contact UMI directly to order.

UMI

THE USE OF LAGRANGE MULTIPLIERS FOR ELASTIC STRUCTURE
WITH ARBITRARY BOUNDARY CONDITIONS
SUBJECTED TO THERMAL LOADING

BY

UN-CHIN CHAI

A DISSERTATION PRESENTED TO THE GRADUATE SCHOOL
OF THE UNIVERSITY OF FLORIDA IN PARTIAL FULFILLMENT
OF THE REQUIREMENTS FOR THE DEGREE OF
DOCTOR OF PHILOSOPHY

UNIVERSITY OF FLORIDA

1996

UMI Number: 9709215

.

UMI
300 North Zeeb Road
Ann Arbor, MI 48103

ACKNOWLEDGMENTS

The author sincerely thanks the chairman of his supervisory committee, Dr. Ali A. Seireg, for his guidance and advice throughout the research.

The author wishes to express his appreciation to the other members of his supervisory committee, Dr. Carl, III Crane, Dr. John K. Schueller, Dr. Gloria J. Wiens and Dr. Chen-Chi Hsu, for their valuable comments and suggestions.

The author would like to express his appreciation to his father for his financial support, encouragement and enduring patience throughout this study.

Finally, the author would like to express his deepest appreciation to his wife for her encouragement and support.

ii

TABLE OF CONTENTS

iv

Abstract of Dissertation Presented to the Graduate School
of the University of Florida in Partial Fulfillment of the
Requirements for the Degree of Doctor of Philosopy

THE USE OF LAGRANGE MULTIPLIERS FOR ELASTIC STRUCTURE
WITH ARBITRARY BOUNDARY CONDITIONS
SUBJECTED TO THERMAL LOADING

By

Un-Chin Chai

August, 1996

Chairman: Dr. Ali A. Seireg
Major Department: Mechanical Engineering

The objective of this study is to develop a procedure
for generating "closed-form" finite series solutions for
thermal deformation and stress resulting from any heat input
or temperature distribution throughout the thickness of
multilayered structures of arbitrary shapes and boundary
conditions.

The Rayleigh-Ritz method is used in this study to
evaluate the deflection in structures with boundary
conditions which can be readily satisfied by a preselected
deflection function. For structures with complex boundary
conditions and shapes including holes with arbitrary
geometry, the analysis is accomplished by incorporating the
Lagrange Multipliers approach in the Rayleigh-Ritz method in

v

order to satisfy the constraints at the boundaries in a discrete manner.

A simplified finite difference method is also utilized for rapid evaluation of the transient temperature distribution in homogeneous and composite structures due to arbitrary heat flux conditions.

In all the cases considered for illustration, the CPU time required to reach a converging solution is found to be orders of magnitude smaller than that required to solve this class of problems by finite element analysis. An important advantage of the proposed approach is that the solution is a continuous finite series rather than discrete numerical data at the nodes or elements of the selected mesh.

CHAPTER 1
INTRODUCTION

The Thermal Loading

Thermal stress analysis of structures has been studied by investigators for years. The thermal stress evaluation in composite laminates is also extensively discussed in the literature. Examples include simply supported sandwich panels[1], laminated shells[2,3,4,5] and fiber-reinforced composites[6]. Other examples include the structural elements in nuclear power plants[7] where the thermal-structural behavior and performance is of critical importance. There are many techniques which evaluate the thermal stress in various structures such as the case of beams during hot dip galvanizing[8], plates with different material properties[2,3,9,10,12] and three-dimensional solid structures[3,11]. Most of the previous techniques are based on discrete numerical methods such as finite element method(F.E.M.) or finite difference method for calculating the temperature and stress distribution. Since the highest thermal stress and deformation in structures often do not take place at steady state condition, the transient temperature distribution[12,13,14,15] at which the maximum conditions occur plays an important role in thermal stress analysis.

1

In this study, the transient thermal analysis is performed by a simplified finite difference method[16]. This technique combines the principle of conservation of energy and the theory of heat penetration distance to calculate the temperature field at any instant of time. The finite difference equations of incremental control volumes are generated by using the principle of conservation of energy. These control volumes can be determined by utilizing the heat penetration distance. Therefore, two-dimensional and three-dimensional transient thermal analyses can always be possible to reduced to one-dimensional problems.

Finite Element Analysis

Recent developments in modern digital computers have resulted in extensive activity in the field of structural design and thermal analysis. Of particular importance is the use of the finite element method in this class of problems. It is a very flexible and general method which can be applied to most of the elastic-plastic and thermal-elastic problems, even in the nonlinear domain[17,18]. It also can handle complex shapes, loading and material properties[19].

Modified Rayleigh-Ritz Method by Utilizing Lagrange Multiplier

There are numerous classical methods which have been developed on the basis of the minimum energy principle. Most of these methods are based on the "principle of minimum potential energy" such as the Rayleigh-Ritz method. The application of the Rayleigh-Ritz method in simple structural analysis can be found in many references[20,21,22]. These applications are generally limited to simple problems, such as a simply-supported beam, or simply-supported plate. Since the Rayleigh-Ritz method requires that the assumed deflection function has to satisfy the boundary conditions, it may not be always possible to find a solution which meets all the boundary condition requirements and minimizes the assumed function at the same time.

In order to solve problems with complex shapes and arbitrary boundary conditions, the Rayleigh-Ritz method is modified to incorporate the Lagrangian approach for dealing with equality constraints [23,24,25,26]. In this approach, the boundary conditions are forced to be satisfied with the use of a Lagrangian function which includes the necessary equality constraints with undetermined multipliers. By applying this method, a finite series solution can be obtained for many difficult elasticity problems with arbitrary shapes and boundary conditions.

The main objective of this study is to developed a closed-form solution for thermo-elastic problems with arbitrary shapes and boundary conditions. The proposed method is divided into two parts: the first part generates the solution for the transient temperature distribution and transforms it to an equivalent mechanical loading, the other part evaluates the deformation and thermal stress for the structure subjected the equivalent mechanical loading. By combining the two techniques, the thermo-elastic problems can be solved in a very small fraction of the CPU time required when using the F.E.A. Furthermore, the solution is obtained in the form of a finite series which is applicable to the entire geometry without the need for preprocessing, postprocessing or making decisions on the structure of the mesh for each problem.

Several numerical examples will be considered to evaluate the merits of the proposed approach. A detailed illustration of the proposed process with the calculated numerical data will be given in the Appendix. It can be used as a demonstration of the different steps involved in the analysis and the numerical results from each step.

All the considered examples were also analyzed by using the finite elements method for comparison. The finite element models are created and analyzed by commercial F.E.M. software (COSMOS/M version 1.71). Both the F.E.M. and the proposed approach are implemented on a 486-DX2 personal computer.

CHAPTER 2
THE TEMPERATURE DISTRIBUTION

The General Formulation of the Finite Difference Algorithm

Before solving for the deformation of the structure under thermal loading, it is necessary to perform the thermal analysis by which the temperature field in this structure is achieved. There are many methods that have been developed to resolve the heat transfer problems. In this dissertation, the transient heat transfer problems are solved by using the finite difference method[16]. The general concepts of finite difference are based on the principle of conservation of energy(the first law of thermodynamics) and the theory of heat penetration distance.

From the principle of conservation of energy, the temperature at each control volume is determined by sets of difference equations. In this approach, the control volumes have to be defined beforehand. The theory of control volume is discussed in later sections of this chapter for different types of shapes.

After formulating the difference equations for the temperatures of the control volumes, the heat penetration distance at that instant of time has to be monitored. If the control volume is beyond the heat penetration distance,

5

there is no heat transfer on the boundary of the control volume. Therefore, by using the temperature difference equations and the theory of heat penetrate distance, the temperature of each control volume can be evaluated. The temperature field of the structure can be numerically determined at any instant by the calculated temperatures of control volumes.

In later sections, the finite difference results will be compared with the results of finite element analysis (F.E.A.) models. Since the finite difference method is a simplified one-dimensional heat transfer for all kinds of geometrical shapes, it is expected that the finite difference method would be much faster than F.E.A.

One-Dimensional Problems

For one-dimensional single-material problems, The heat flows only in one direction. For problems of beams with surface heat input, this direction is the direction of the thickness of the beam. In figure 2.1, the thickness of the beam is divided into a number of layers whose thickness is the thickness of the control volume. The volume and surface area of heat transfer of each control volume are defined in equations (2.1) and (2.2).

The surface area of each control volume is

$$A = A_1 = A_2 = A_3 = ... = A_n = A_{n+1} = bL \qquad (2.1)$$

The volume of each control volume

$$V_1 = V_{n+1} = \frac{bL\Delta h}{2}$$

(2.2a)

$$V_2 = V_3 = \ldots = V_{n-1} = bL\Delta h$$

(2.2b)

where b : width of beam
      L : length of beam
      h : thickness of beam
     Δh : thickness of layers except first and last
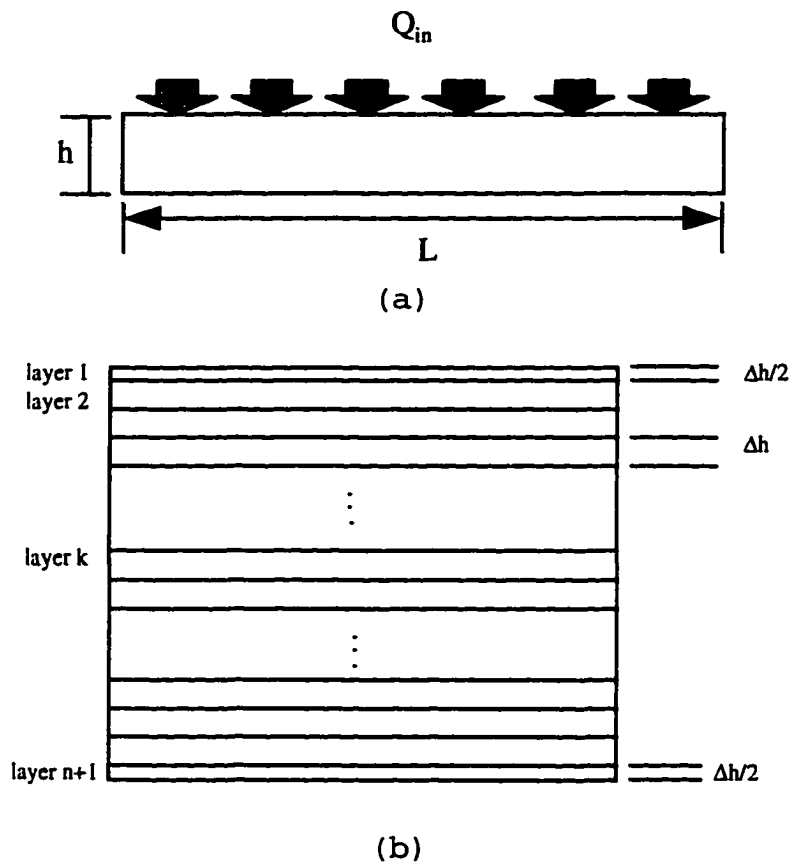   layers

(a)

(b)

Figure 2.1 (a) The beam configuration with heat source Q_{in}
           (b) The control volume of the beam

The assumptions for this case are as given below:

1. The temperature is assumed uniform within any layer.

2. This analysis considers the transient temperature variations along the depth of the beam and neglects the less significant variations along the length.

3. The beam is subjected to a uniform heat rate Qin at its external upper surface.

4. There is no heat loss from the boundary of the beam to the surrounding.

The conservation of energy principal shown in equation (2.3) is essentially an energy balance. The stored energy in the material is what makes the temperature of the material rise.

$$Q_{in} - Q_{out} = Q_{stored} \qquad (2.3)$$

The finite difference scheme is a simplified one dimensional finite difference analysis. The beam shown in figure 2.1 is divided into n+1 layers. The temperatures at every surface(upper or lower) are the main parameters in this case. Their evaluation is based on the conservation of energy principal for a control volume(the shade area in figure 2.2).
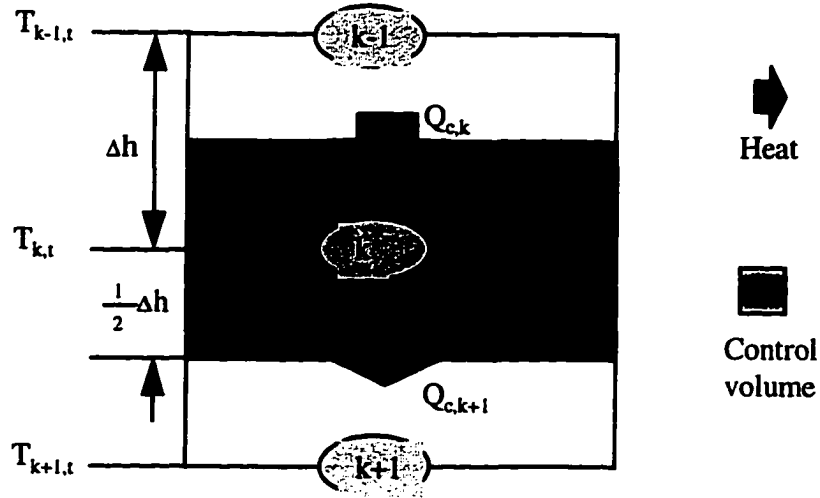
Figure 2.2   The heat transfer for the control volume

$$Q_{c, k} = \frac{KA(T_{k - 1, t} - T_{k, t})}{\Delta h} \Delta t = \frac{K\Delta t}{\Delta h} A(T_{k - 1, t} - T_{k, t}) \qquad (2.4)$$

$$Q_{c, k + 1} = KA\Delta t \frac{T_{k, t} - T_{k + 1, t}}{\Delta h} = \frac{KA\Delta t}{\Delta h} (T_{k, t} - T_{k + 1, t})) \qquad (2.5)$$

$$Q_{stored} = \rho c V_k (T_{k, t + 1} - T_{k, t}) \qquad (2.6)$$

where K : thermal conductivity

Applying equation (2.3), the temperature $T_{k, t+1}$ after a time step Δt can be presented in equation (2.7).

$$\rho c V_k (T_{k, t + 1} - T_{k, t}) = \frac{KA\Delta t}{\Delta h} (T_{k - 1, t} - T_{k, t}) - \frac{KA\Delta t}{\Delta h} (T_{k, t} - T_{k + 1, t})$$

$$T_{k, t + 1} = \frac{K\Delta t A}{\rho c V_k \Delta h} (T_{k - 1, t} + T_{k + 1, t}) + (1 - \frac{2K\Delta t A}{\rho c V_k \Delta h}) T_{k, t} \qquad (2.7)$$

Similar expressions can be obtained for the temperature at the bottom and top surfaces.   The difference equation (2.8) can be written as:
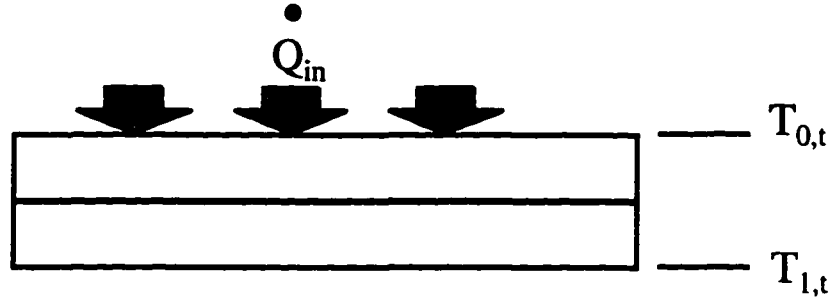
For the top surface:

Figure 2.3 Heat transfer for the first layer

$$\rho c V_1 (T_{0,\ t+1} - T_{0,\ t}) = A\dot{Q}_{in}\Delta t - \frac{KA\Delta t}{\Delta h}(T_{0,\ t} - T_{1,\ t})$$

$$T_{0,\ t+1} = \frac{2\Delta tA}{\rho c V_1}\dot{Q}_{in} + (1 - \frac{2K\Delta tA}{\rho c V_1 \Delta h})T_{0,\ t} + \frac{2K\Delta tA}{\rho c V_1 \Delta h}T_{1,\ t} \quad (2.8)$$

At the bottom layer of the beam shown in figure 2.4, it is assumed that the heat does not transfer to the surrounding, and the only inputs are from the upper layer. The difference equation can be written as:
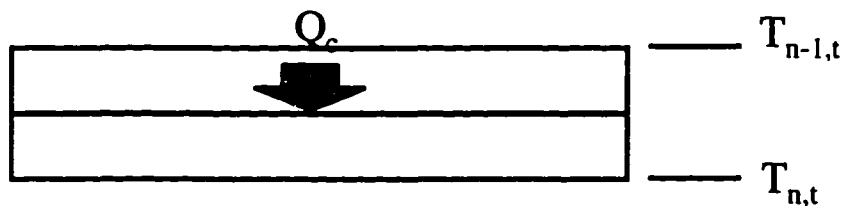

Figure 2.4 Heat transfer for the last layer

$$\rho c V_n(T_{n,\ t\ +\ 1} - T_{n,\ t}) = \frac{KA_\Delta t}{\Delta h}(T_{n\ -\ 1,\ t} - T_{n,\ t})$$

$$T_{n,\ t\ +\ 1} = \frac{2KA_\Delta t}{\rho c V_n \Delta h} T_{n\ -\ 1,\ t} + (1 - \frac{2KA_\Delta t}{\rho c V_n \Delta h})T_{n,\ t} \qquad (2.9)$$

The current time is automatically updated in the program and it can determine the distance that the heat penetrates into the beam. This penetration distance shown in equation (2.10) is modified in the temperature difference equations based on the particular instant of time according to the following relationship:

$$t_p = 0.0891\frac{D_p^2}{\beta} \quad \text{or}$$

$$D_p = \sqrt{\frac{t_p * \beta}{0.0891}} \qquad (2.10)$$

where t_p : penetration time (sec)
D_p : penetration distance
β : thermal diffusivity($K/\rho c$)

When the distance between the heat source and heat exchange surface of the control volume is more than the penetration distance, no heat exchange occurs. The general procedure is therefore as described below:

1. Input the dimensions of the beam:
   beam thickness(h)
   beam width(b)
   beam length(L)

2. Input the material constants
   Density of the material(ρ)
   Thermal conductivity(k)
   Specific heat(c)

3. Input heat source (Qin) and total heating time, t

4. Set up time step(Δt)

5. Calculate the volume and surface area of the control volume

6. Record the current time = time+ Δt

7. Compute how many layers have heat exchange.

8. Solve the temperature difference equation

9. Repeat steps 6 to 8 until the current time is equal to the total heating time.

The flow chart for the program is shown in figure 2.5.

For the case of a composite beam shown in figure 2.6, the surface area of the control volume for each material and the volume of control volume for the material 1 are the same as in the single material case. Due to the theory of heat penetration distance, the volume of control volume for the rest of the materials can be determined in equation (2.12).

For the layers of the first material:

$$V_{1,1} = V_{n1+1,1} = \frac{bL_\Delta h_1}{2}$$

(2.11a)

$$V_{k,1} = bL_\Delta h_1, \quad k=2 \text{ to } n1$$

(2.11b)

For the rest:

$$\Delta h_i = \sqrt{\frac{\beta_i}{\beta_1}} \Delta h_1$$

$$V_{1,i} = V_{n2+1,i} = \frac{bL_\Delta h_i}{2}$$

(2.12a)

$$V_{k,i} = bL_\Delta h_i, \quad k=2 \text{ to } n2$$
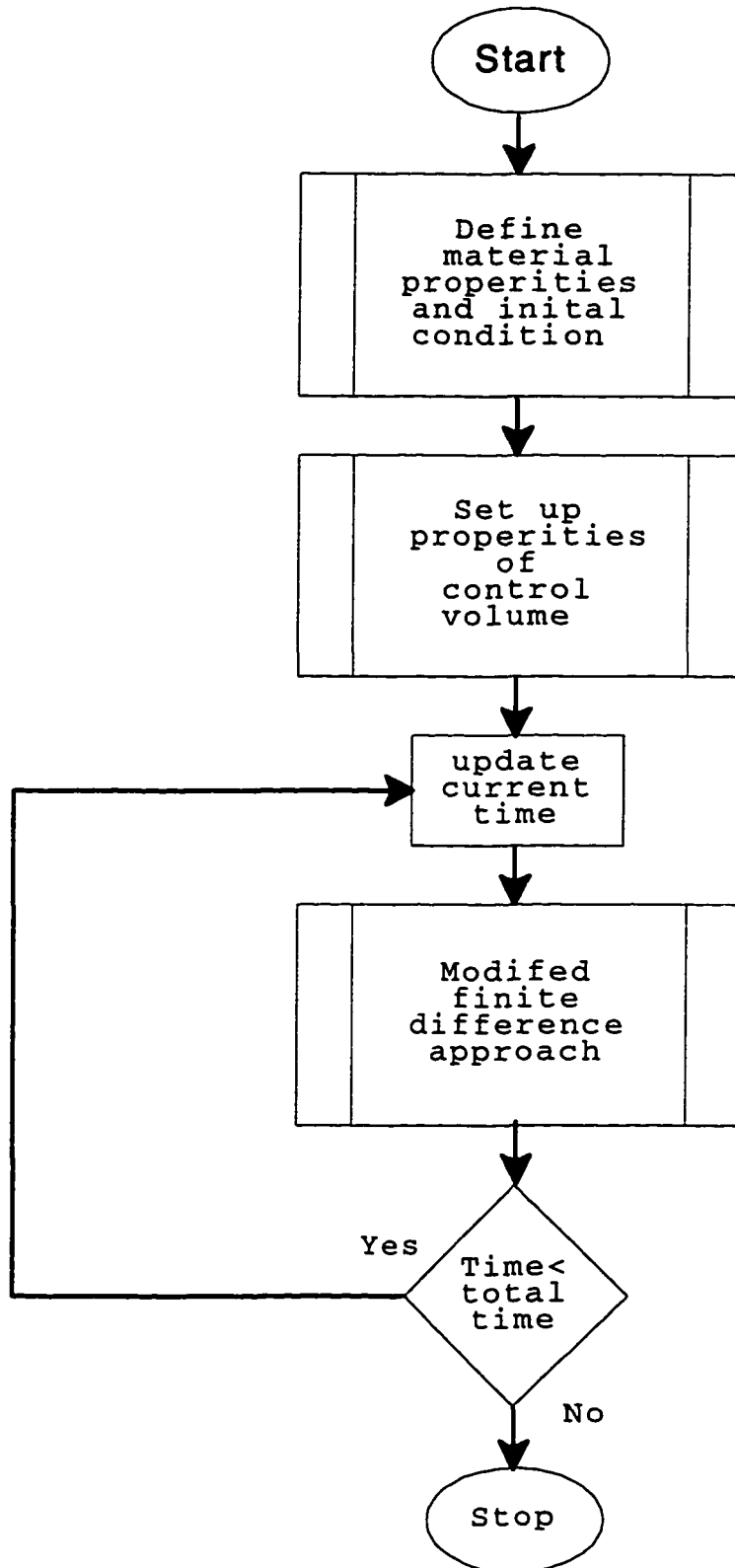
(2.12b)

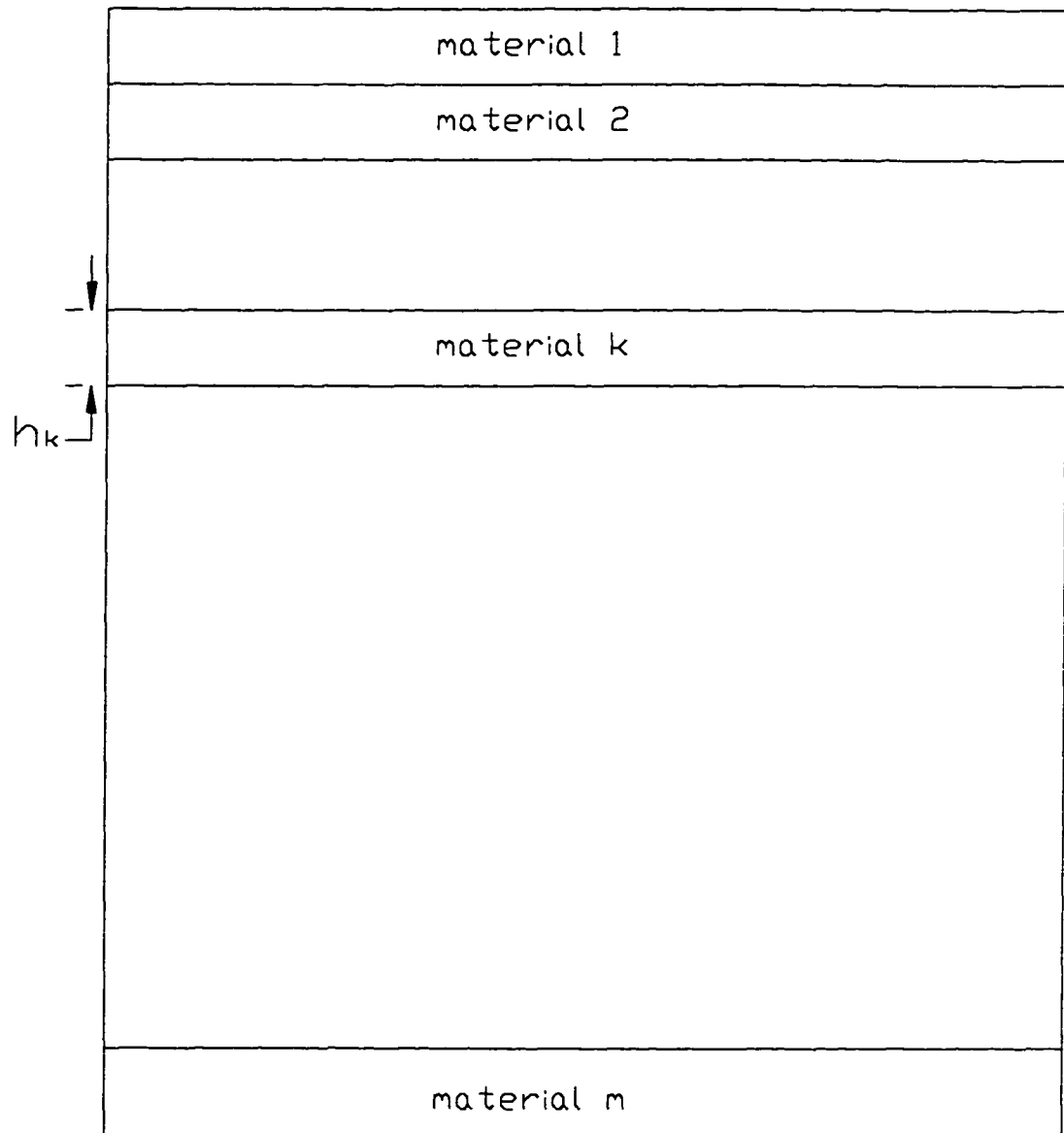Figure 2.5 The flow chart of one dimensional heat transfer

Figure 2.6 The configuration of composite beam

It is more convenient to define the heat density, HD, for each layer in the different material.

For a layer of material i,

$$HD_k = \rho_{ici}V_{j,i}\Delta h_i \tag{2.13}$$

Where $k = \sum_{i} n_i + j$ is the global count of the layer number

The temperature difference equations, as modified by replacing the ρcV part into the HD, are given in equations (2.14), (2.15) and (2.16).

For the first layer:

$$T_{0,t+1} = \frac{2\Delta t A \Delta h_1}{HD_1} \dot{Q}_{in} + (1 - \frac{2K_1\Delta tA}{HD_1})T_{0,t} + \frac{2K_1\Delta tA}{HD_1} T_{1,t}$$

$$\tag{2.14}$$

For the last layer:

$$T_{n,t+1} = \frac{2K_m\Delta tA}{HD_n} T_{n-1,t} + (1 - \frac{2K_m\Delta tA}{HD_n})T_{n,t} \tag{2.15}$$
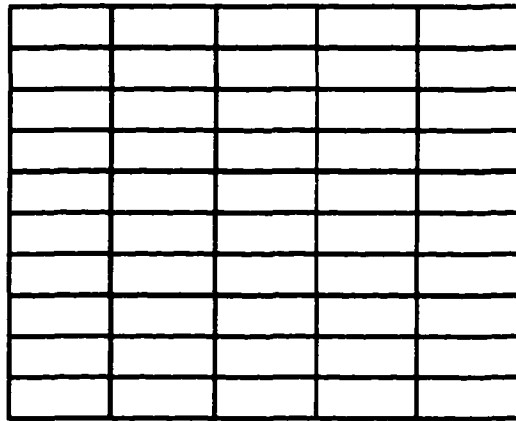
where Δh_1: the layer thickness of the last material

For the remaining layers in material j:

$$T_{k,t+1} = \frac{K_k\Delta tA}{HD_k} (T_{k-1,t} + T_{k+1,t}) + (1 - \frac{2K_k\Delta tA}{HD_k})T_{k,t} \tag{2.16}$$

As can be seen, the general procedure is the same as in the single material case. The only difference between the two cases is the algorithm used to generate the finite difference equations.
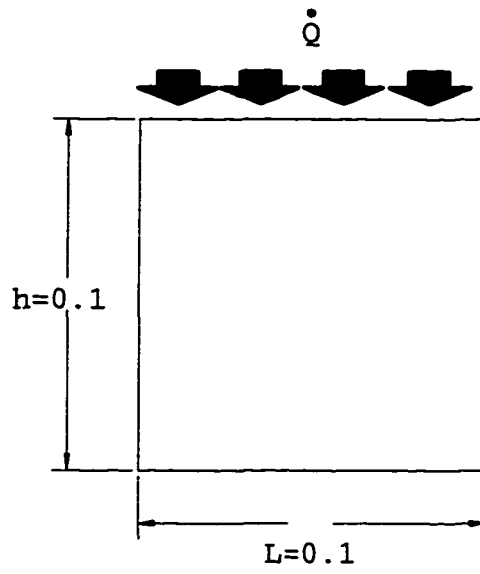
Figure 2.7
(a) The configuration of the beam with thermal loading
(b) The F.E.A. model of Example 2.1(66 nodes, 50 elements and 100 time steps)

Illustrative example

Example 2.1

In this case, a homogeneous beam is subjected to a heat flux at its upper surface. The configuration of the beam is shown in figure 2.7a. The finite element model is shown in figure 2.7b.

The material properties, initial heat input conditions and the dimension of the beam are given below:

```
For Steel:
Density of  material(steel),ρ=7900  (Kg/m³)
Thermal conductivity(steel),  k = 45  (W/m-°C)
Specific heat(steel),  c=460  (J/kg-°C)

heat input,  Q̇=10 Watt
Heat time,  t=60  (sec)

the dimension of the beam:
beam thickness, h=0.1  (m)
beam width, b=0.01  (m)
beam length, L=0.1  (m)
```

The performance of the finite difference(F.D.) method is compared with the finite element analysis(F.E.A.) with regard to temperature distribution as shown in table 2.1 and figure 2.8, as well as the CPU running time as shown in table 2.2. It can be seen that very close results are obtained by the F.D. method and the F.E.A. The F.D. method, however, is much faster than the F.E.A.

Table 2.1 The comparison of temperature distribution between F.E.A. and F.D.

thickness	F.D.	F.E.A.
0	216.4819	203
0.01	90.1579	90.3
0.02	50.6328	51.9
0.03	29.7326	31.1
0.04	17.3734	18.6
0.05	9.8916	10.9
0.06	5.4076	6.21
0.07	2.7893	3.46
0.08	1.3114	1.91
0.09	0.4953	1.14
0.1	0	0.91
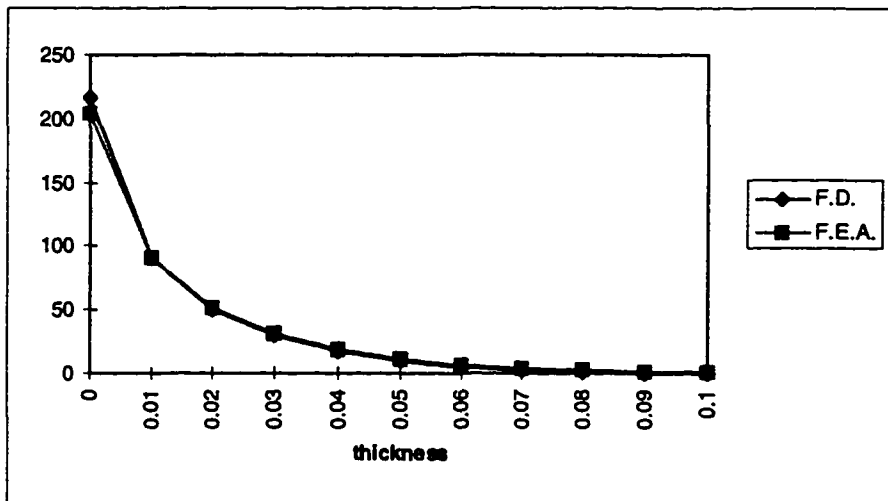
Figure 2.8 The comparison of temperature distribution through the thickness between F.E.A. and F.D.

Table 2.2   the comparison of running time of CPU
between F.E.A. and F.D.

	F.E.A.	F.D.
CPU Time (sec)	56	5

Example 2.2

This example considers a composite structure with two materials, Steel and Aluminum, subject to a heat input at the upper surface. The configuration of the beam with the thermal loading is shown in figure 2.9a. The finite element model is shown in figure 2.9b.

The material properties and initial conditions for this case as follows:

For Steel:
Density of material of Steel ,ρ=7900 (Kg/m^3)
Thermal conductivity of Steel, k = 45 (W/m-°K)
Specific heat of Steel, c=460 (J/kg-°K)

For Aluminum:
Density of material of Aluminum,ρ=2700 (Kg/m^3)
Thermal conductivity of Aluminum, k = 200 (W/m-°K)
Specific heat of Aluminum, c=900 (J/kg-°K)
Heat input time, t=120 (sec), Q_{in}=1. (Watt)
beam width b=0.01 (m)

The performance of the finite difference method is compared with the finite element analysis with regard to the temperature distribution as shown in table 2.3 and figure 2.9, as well as the CPU running time as shown in table 2.4. Again, the results of F.D. and F.E.A are very similar and the F.D. is much faster than the F.E.A.

(a)

| | Steel |
| | Aluminium |
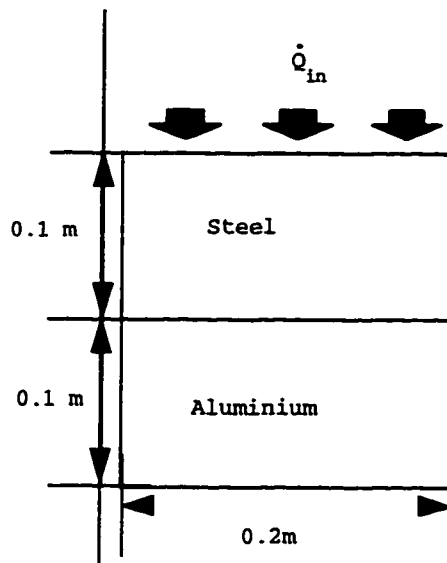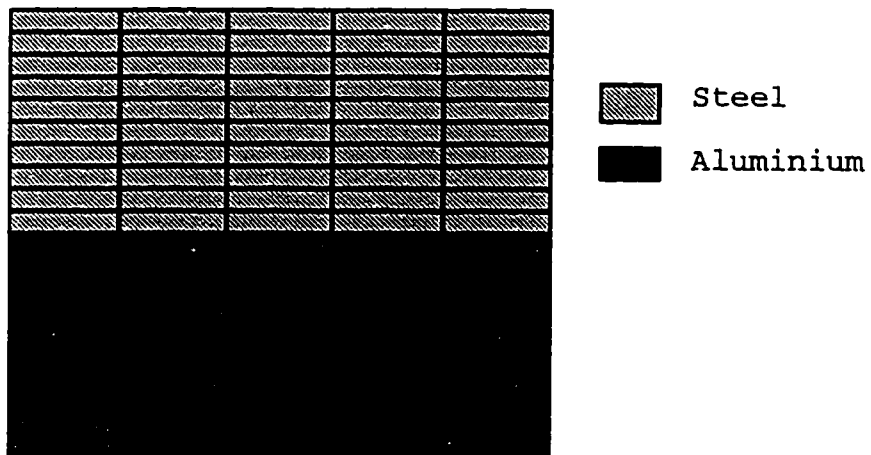
(b)

Figure 2.9
(a) The configuration of the beam with thermal loading
(b) The F.E.A. model for Example 2.2 (126 nodes, 100 elements and 100 time steps)

Table 2.4   the comparison of running time of CPU
between F.E.A. and F.D.
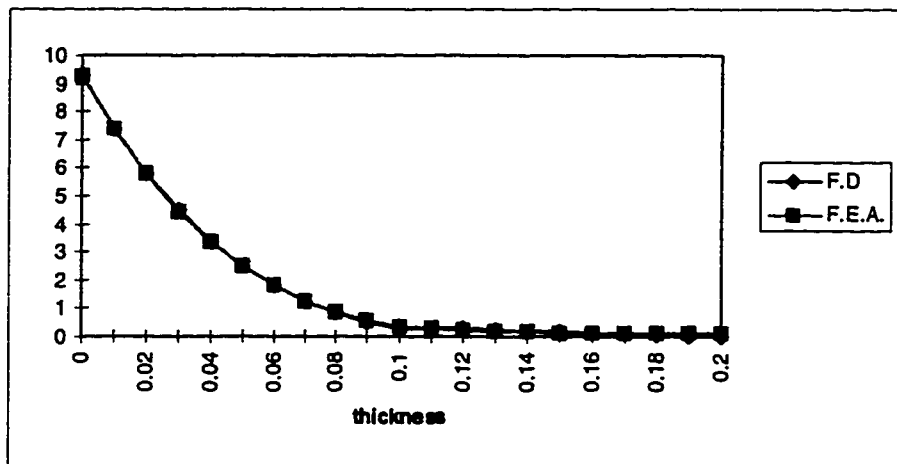
	F.E.A.	F.D.
CPU Time	75	5

Figure 2.10 The comparison of temperature distribution
between F.E.A. and F.D.

Table 2.3 The comparison of temperature distribution between F.E.A. and F.D.

thickness	F.D.	F.E.A.
0	9.2623	9.25
0.01	7.3997	7.39
0.02	5.8079	5.8
0.03	4.4745	4.46
0.04	3.3805	3.37
0.05	2.5011	2.49
0.06	1.8077	1.8
0.07	1.2699	1.27
0.08	0.857	0.86
0.09	0.5397	0.552
0.1	0.2886	0.316
0.11	0.2726	0.267
0.12	0.2566	0.226
0.13	0.2274	0.192
0.14	0.1887	0.163
0.15	0.1521	0.14
0.16	0.1255	0.122
0.17	0.0988	0.108
0.18	0.0634	0.0984
0.19	0.0252	0.0928
0.2	0	0.0909

The two-Dimensional Problem

For the case where the heat input is applied only at a portion of the upper surface of the beam, the surface of control volume is no longer one dimensional (planar). It is

assumed that all the points at the surface of the same control volume have the same heat penetration time. Since the heat flows radically from the position of heat input, the shape of control volume for the single material beam, shown in figure 2.11, is therefore cylindrical.

The surface area and volume of control volume have to be consider in two parts: left-hand-side and right-hand-side of heat input due the probability of non-symmetry in the shape with respect to the heat input. At each boundary, there are four different types of control volumes that need different approaches to obtain their surface areas and volumes. The four types of control volumes are shown in figure 2.12.

For type 1(shown in Figure 2.12(a)):

$$arc\_ab = \frac{\pi r}{2} \qquad\qquad (2.17)$$

$$area\_oab = \frac{\pi r^2}{4} \qquad\qquad (2.18)$$

For type 2(shown in figure 2.12(b)):

$$arc\_ab = (\frac{\pi}{2} - \theta_a)r \qquad\qquad (2.19)$$

$$area\_ocab = \frac{\sin(2\theta_a) + \pi - 2\theta_a}{4} r^2 \qquad\qquad (2.20)$$

where θ_a : the angle between line_oc and line_oa

For type 3(shown in figure 2.12(c)):

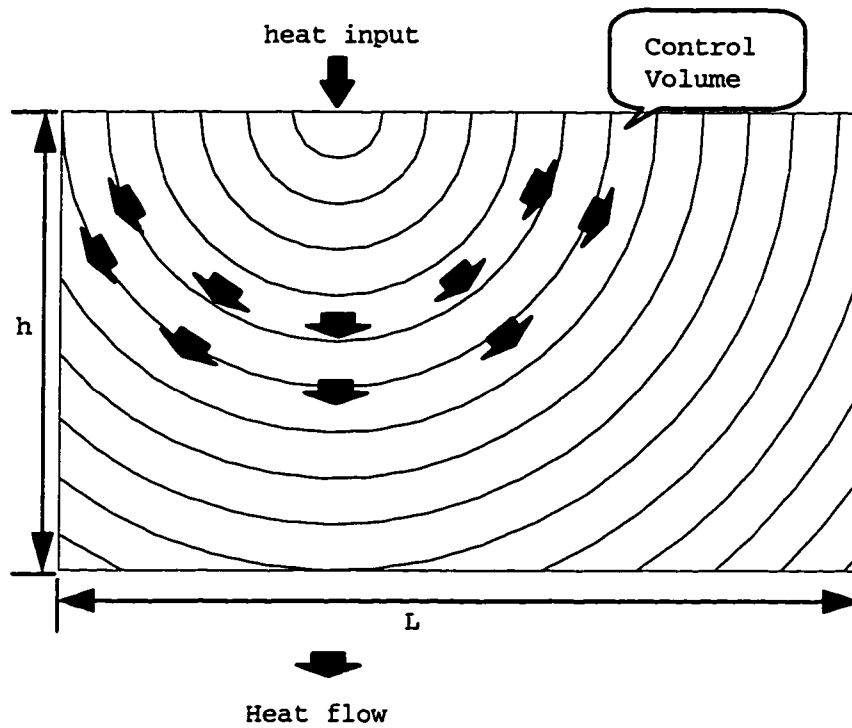$$arc\_ab = \theta_b r \qquad\qquad (2.21)$$

heat input

Control Volume

h

L

Heat flow

Figure 2.11 The control volumes for single material beam

$$area\_\,oabc = \frac{\sin(2\theta_b) + 2\theta_b}{4}\,r^2$$ (2.22)

where θ_b : the angle between line_oa and line_ob

For type 4(shown in figure 2.12(d)):

$$arc\_\,ab = (\theta_b - \theta_a)r$$ (2.23)

where θ_a : the angle between line_oc and line_oa
where θ_b : the angle between line_oc and line_ob

$$area\_\,ocabd = \frac{\sin(2\theta_a) + \sin(2\theta_b) + 2(\theta_b - \theta_a)}{4}\,r^2$$ (2.24)
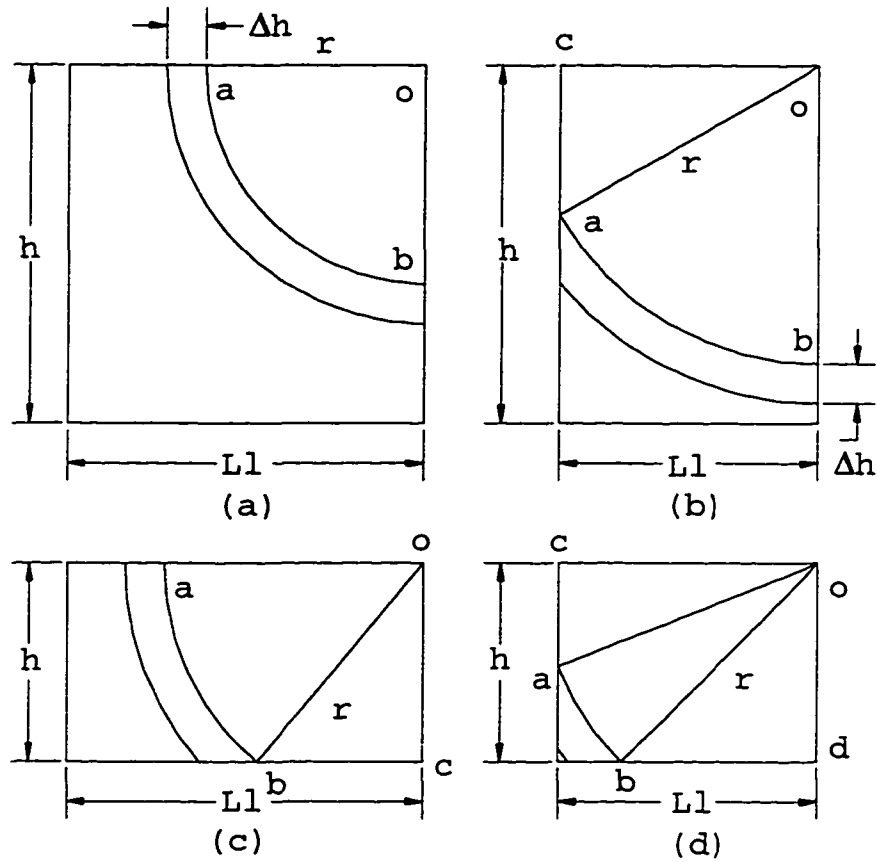
Figure 2.12 Four different types of C.V.
in the single material case

The same procedures is repeated for the other side of the beam. The surface area and volume of each control volume is the superposition of L.H.S. and R.H.S. The heat density (HD) of each layer is also determined in the same way.

$$HD_k = \rho c V_k \Delta h \qquad (2.25)$$

Since the heat penetration time at any point on the surface of each control volume is the same, it is assumed that the heat flow is always perpendicular to the surface of control volume. Therefore this two-dimensional-shape heat transfer problem can be simplified to the one dimensional heat transfer case. The temperatures of the control volumes are obtained by using the same finite difference equations (2.14),(2.15) and (2.16).

For the composite beam, the surface of the control volume still remains cylindrical in the first material part. However, due to the theory of heat penetration distance, the surface of control volume in the rest of materials is no longer cylindrical. An illustration of the profile of the control volume for the two-material composite beam is shown in figure 2.13. The surface of the control volume in the second material can be determined by the heat penetration distance.

Due to the theory of heat penetration distance, the ratio between r_2 and $R-r_1$ is equal to the square root of ratio between thermal diffusivities of material 2 and 1.

$$\frac{R - r_1}{r_2} = \sqrt{\frac{\beta_1}{\beta_2}} \qquad\qquad (2.26)$$

$$\sqrt{\frac{\beta_2}{\beta_1}}R = \sqrt{\frac{\beta_2}{\beta_1}}r_1 + r_2 \qquad\qquad (2.27)$$

Where β_1: thermal diffusivity of material 1
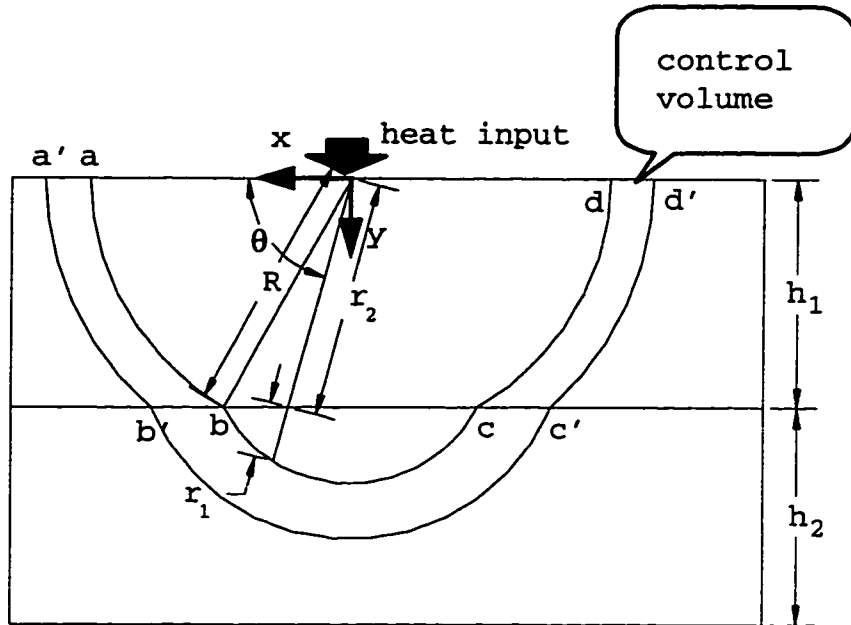Where β_2: thermal diffusivity of material 2

Figure 2.13 The control volume for
two-material composite beam

It is more convenient to represent the profile of the surface in a cylindrical coordinate system. The point on the profile can be noted as (r, θ). By combining equations (2.28) and (2.29), the profile equation is obtained in equation (2.30).

$$r_2 = h_1 \csc{(\theta)})$$

(2.28)

$$r = r_1 + r_2$$

$$r = r_1 + \sqrt{\frac{\beta_2}{\beta_1}}R - r_1\sqrt{\frac{\beta_2}{\beta_1}}$$

(2.29)

$$r = \sqrt{\frac{\beta_2}{\beta_1}}R + (1 - \sqrt{\frac{\beta_2}{\beta_1}})r_1$$

$$r = \sqrt{\frac{\beta_2}{\beta_1}}R - (1 - \sqrt{\frac{\beta_2}{\beta_1}})h_1 \csc{(\theta)}$$

$$r = P - Q\csc{(\theta)}$$

(2.30)

where

$$P = \sqrt{\frac{\beta_2}{\beta_1}} R$$

$$Q = (1 - \sqrt{\frac{\beta_2}{\beta_1}}) h_1$$

Technically, if the end points of the profile are known, then the surface area and volume of control volume are determined by integrating equation (2.30). The area and length integration are shown in equations (2.31) and (2.32). There are still some details that should be discussed. There are four different combinations of end points for the profiles shown in figure 2.14 for the left-hand-side boundary. In each combination, the end points of the profile will define the values of the volume and area of each control volume.

$$area(\alpha, \beta) = \int_{\alpha}^{\beta} (P - Q \csc(\theta))^2 d\theta$$

$$= P^2(\beta - \alpha) - 2PQ[\ln(\left|\frac{\csc(\beta) - \cot(\beta)}{\csc(\alpha) - \cot(\alpha)}\right|)] - Q^2(\cot(\beta) - \cot(\alpha))$$

(2.31)

$$curve(\alpha, \beta) = \int_{\alpha}^{\beta} (P - Q \csc(\theta)) d\theta$$

(2.32)

$$= P(\beta - \alpha) + Q \ln(\left|\csc(\beta) - \cot(\alpha)\right|)$$

For type a, the profile(curve from point a to point b) shown in figure 2.14a is complete. For type b, shown in figure 2.14b, the left end point(point a) of the profile is

on the left boundary of the beam and the lowest point(point

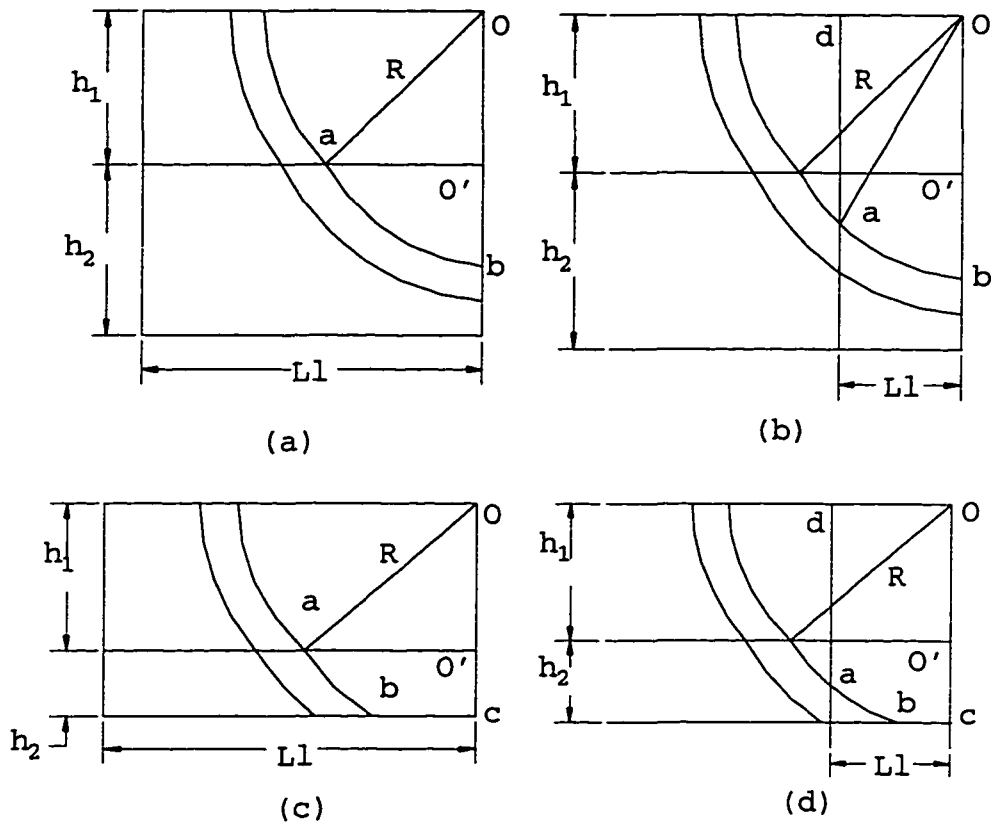b) of the profile is above the bottom surface of the beam.

Figure 2.14 The profiles of the control volumes for
difference boundary effect

For type c, shown in figure 2.14c, the left end

point(point a) of the profile is on the common surface of

the two materials and the lowest point of the profile is

below the bottom surface of the beam. Therefore, the right

end point of the profile(point b) is on the bottom surface

of the beam. For type d, shown in figure 2.14d, the left

end point(point a) of the profile is on the left boundary of the beam. The right end point of the profile(point b) is on the bottom surface of the beam. After calculating the end points for each type, the area and volume for each control volume are determined by utilizing equations (2.31) and (2.32).

After defining the area and volume of each control volume, the heat density(HD) for each control volume is calculated in the same way. By using the same finite difference equations (2.14), (2.15) and (2.16), the temperature field of the beam under thermal loading is computed. The procedure is as given below:

1. Input the position of heat source: The beam is divided into two parts (left-hand-side(LHS) and right-hand-side(RHS)) to calculate the surface area and volume of each control volume.

2. Input the layer(control volume) thickness in the first material

3. Calculate the surface area and volume of each layer of material 1 for the left hand side of the beam.

4. Calculate the surface area and volume of each layer of material 2 for the left hand side of the beam.

5. Repeat (3) and (4) for right hand side of the beam.

6. Superimpose the results from the L.H.S. and R.H.S. of the beam.

7. Update the current time and heat penetration distance.

8. Update and solve the finite difference equations.

9. Repeat (7) to (8) until heating time is over.

For a beam that is composed of more than two materials, the procedure is essentially the same.

Illustrated examples

Example 2.3

In this example, a homogeneous structure is subjected to the heat input at a point on the top surface of the beam. The configuration of the beam and heat input location is shown in figure 2.15a. The finite element model is shown in figure 2.15b. The results are compared with the finite element method in figure 2.16 and table 2.5 to illustrate the accuracy and efficiency of the two methods.

The material of the structure: Steel

The heat input: Qin=10 Watt for 60 sec

The dimension of the structure:

L=0.2 m
L1=0.1 m
h=0.1 m
b=0.01 m

$\dot{Q}in$

L1

h

L
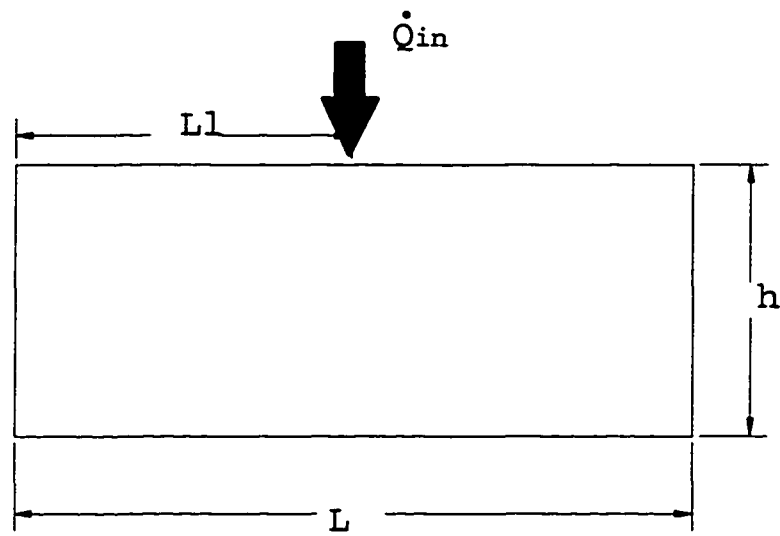
(a)
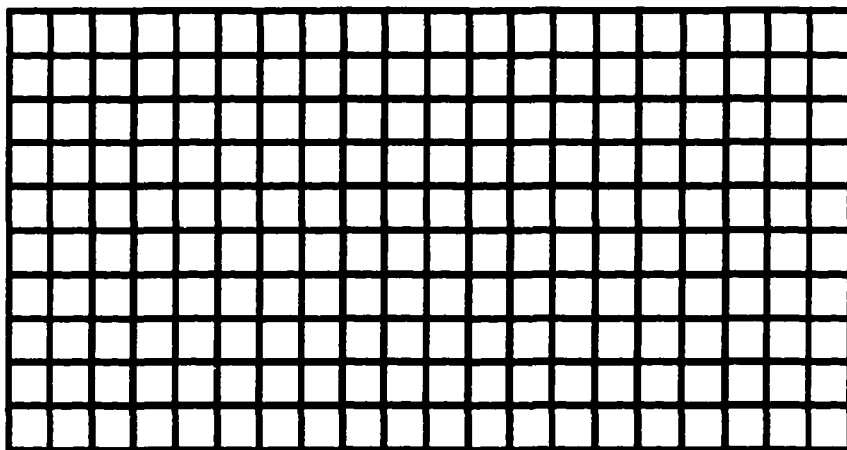
(b)

Figure 2.15 (a) The configuration of the beam and heat input for example 2.3 (b) The F.E.A. model for example 2.3 (231 nodes, 200 elements and 100 time steps)
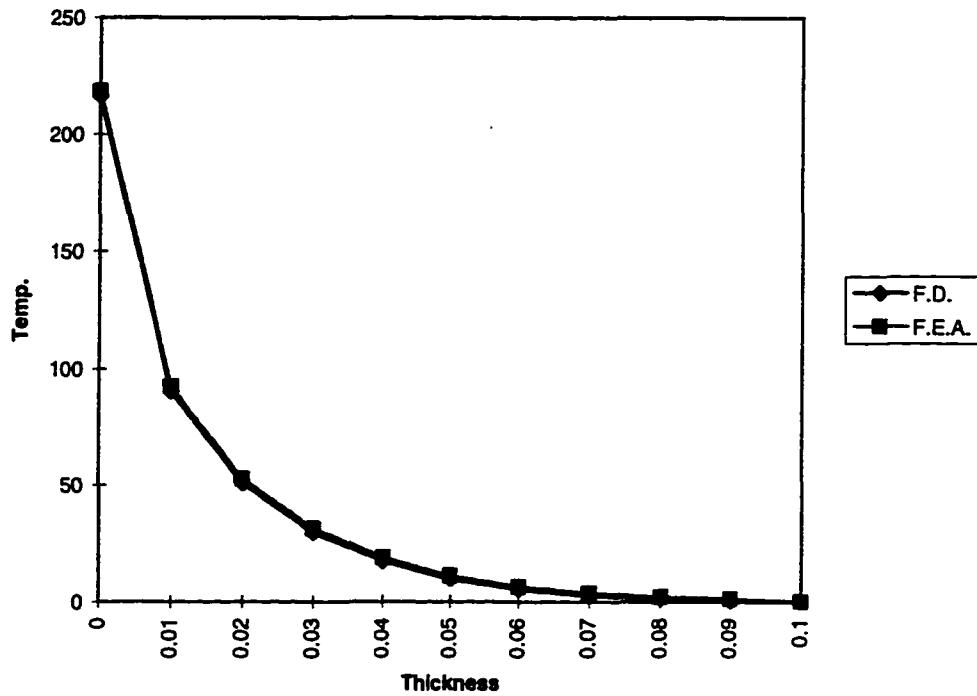
Figure 2.16 The comparison between F.E.A. and F.D. for
the temperature distribution through the thickness
below the location of the heat input

Table 2.5 The comparison between F.E.A. and F.D.
for the CPU running time

	F.E.A.	F.D.
CPU Time	125	6

Example 2.4

In this example, a composite beam is subjected to heat

input at a point on the top surface of the beam. The

configuration of the beam and heat input location is shown in figure 2.17a. The finite element model with initial condition is shown in figure 2.17b. The results are compared with the finite element method to illustrate the accuracy and computational efficiency of the proposed method.

The heat input: Qin=10 Watt for 120 sec

The dimension of the structure:
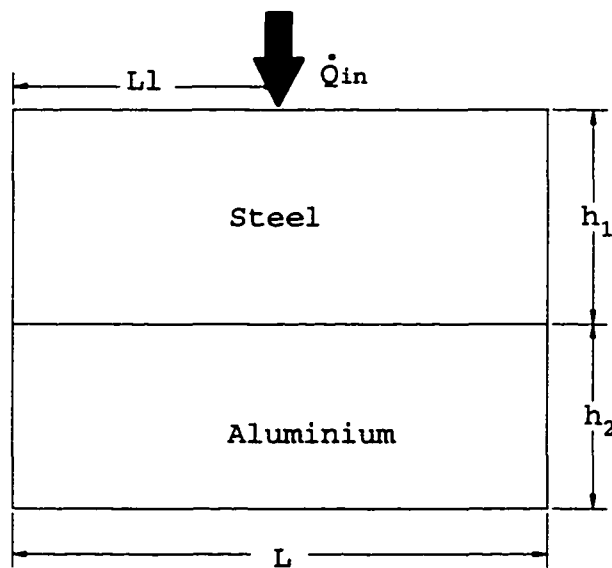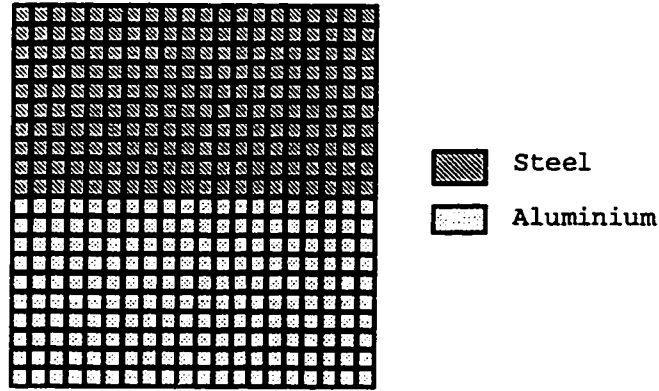L=0.2 m
L1=0.1 m
h_1=0.1 m
h_2=0.1 m
b=0.01

(a)

(b)

Figure 2.17(a) The configuration of the beam and heat input
for Ex. 2.4 (b) The F.E.A. model for example 2.4 (441 nodes,
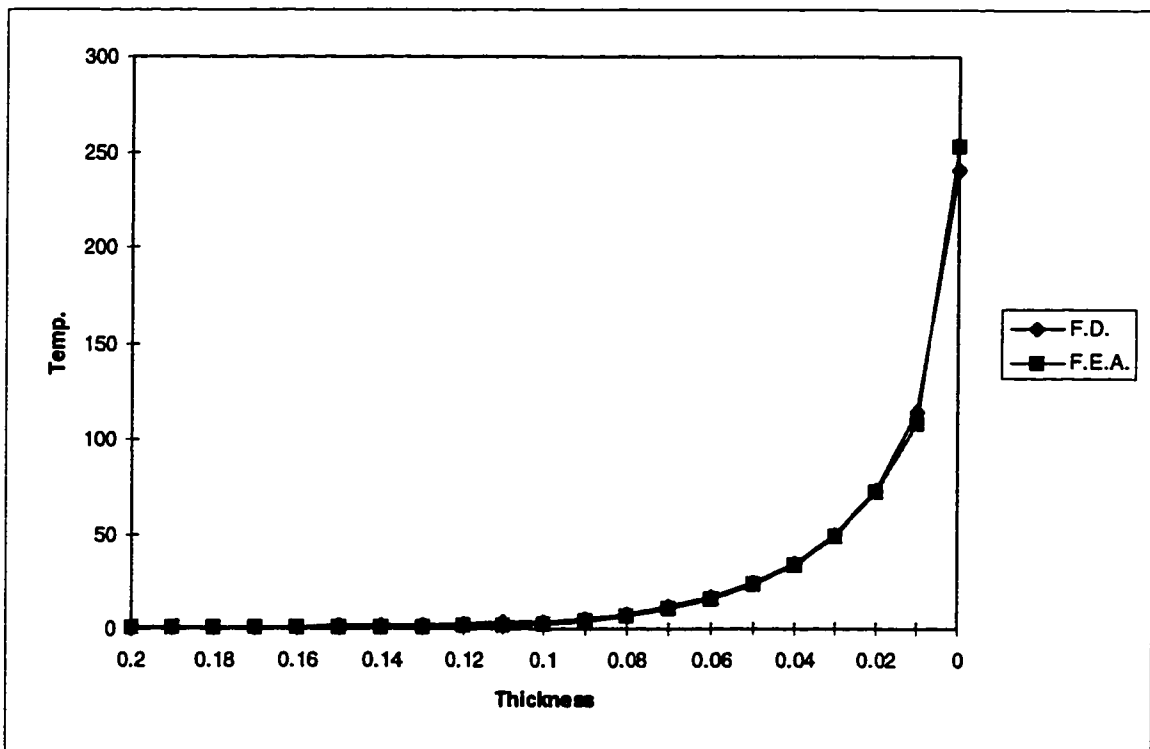400 elements and 100 time steps)

Figure 2.18 The comparison between F.E.A. and F.D.
for the temperature distribution through the thickness the
below location of the heat input

Table 2.6 The comparison between F.E.A. and F.D.
for the CPU running time

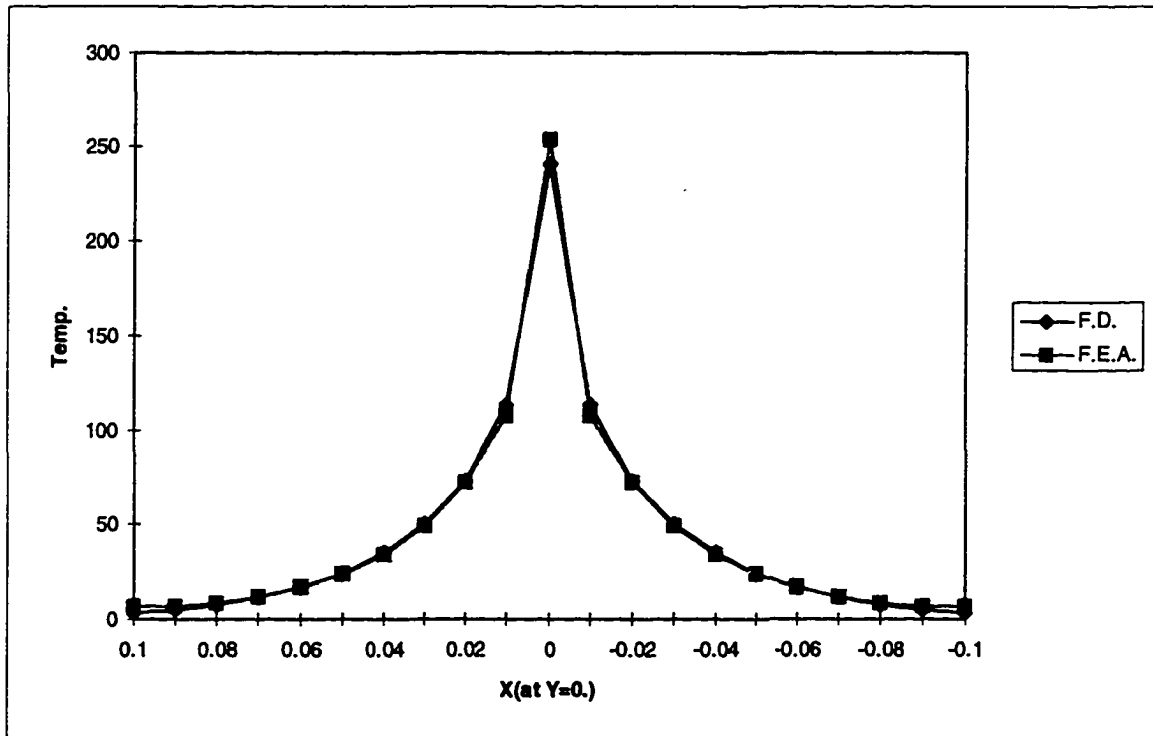|	F.E.A.	F.D.
CPU Time	273	6

Figure 2.19 The comparison between F.E.A. and F.D.
for the temperature on the top surface

Three-Dimensional Problems

If the heat input is on a portion of the top surface of a plate, the shape of control volume is now expanded into three-dimensional space. The surface area and volume of each control volume of the structure are defined by the principle of heat penetration distance as in the case of the one or two dimensional problems. Although the computation becomes more complex in three dimensional problems, the approach is very similar to two dimensional problems.

Two examples are considered for illustration. One is a single-material plate and the other is a composite plate. Both examples are subjected to heat input on the top surfaces of the plate.

Illustrate examples

Example 2.5

In this example, a homogeneous square plate is subjected to heat input at the center of the top surface of the plate. The plate configuration is as shown in figure 2.20a. The finite element model is shown in figure 2.20b. Because of the symmetry of the geometry, loading, and boundary conditions of this problem, only one quarter of the structure is used for the F.E.A. model. Its result is compared with finite the element method in figure 2.21 and

table 2.7 to illustrate the accuracy and computational efficiency of the proposed method.

The dimension of the plate:
$L_1=0.2$ m
$L_2=0.2$ m
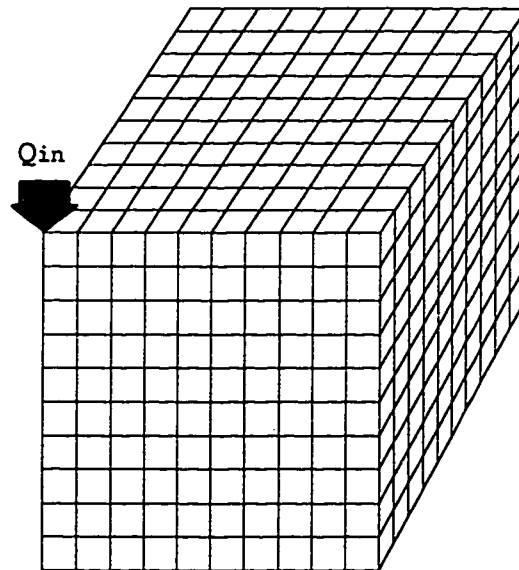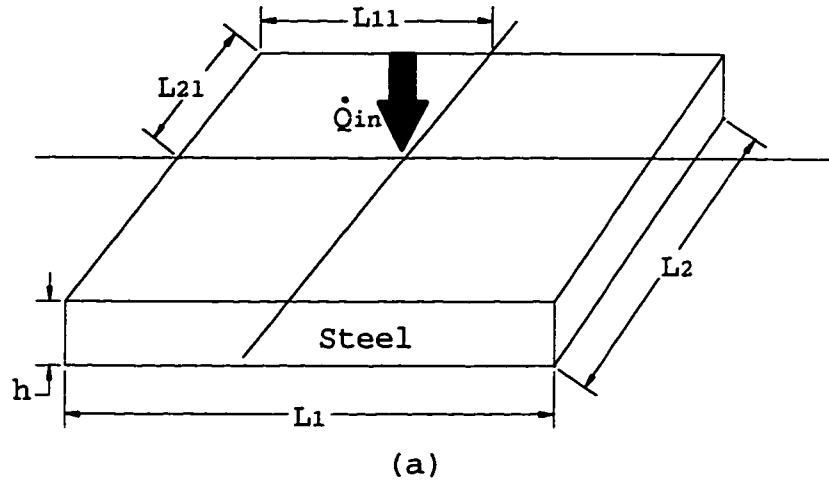$L_{11}=L_{21}=0.1$ m
$h=0.1$ m

(a)

(b)

Figure 2.20 (a) The plate configuration and heat input $Q_{in}=10$ Watt (b) F.E.A. model for example 2.5 (1331 nodes, 1000 elements and 50 time steps)

Table 2.7 The comparison between F.E.A. and F.D.
for the CPU running time

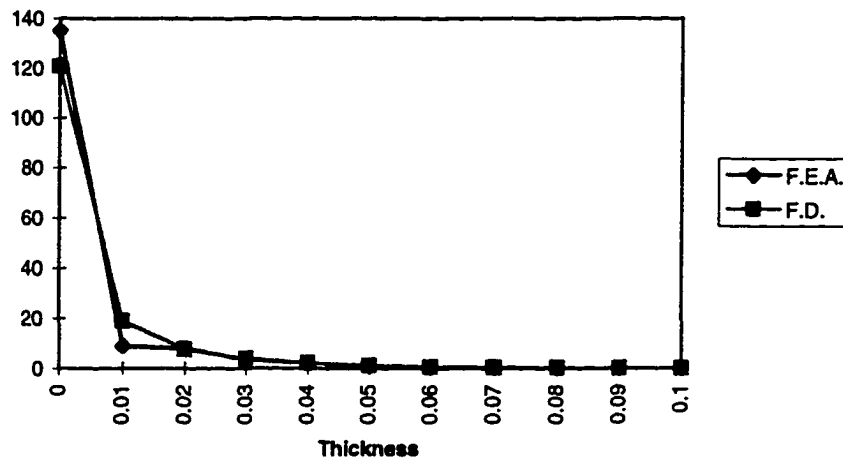|	F.E.A.	F.D.
CPU Time	584	6

Figure 2.21 The comparison between F.E.A. and F.D.
for the temperature distribution through the thickness
below the location of the heat input

Example 2.6

In this case, a composite square plate is subjected to heat input at the center of the top surface of the plate. The plate configuration is shown in figure 2.22a. The finite element model is shown in figure 2.22b. The result is compared with the finite element method to illustrate the accuracy and computational efficiency of the proposed method.
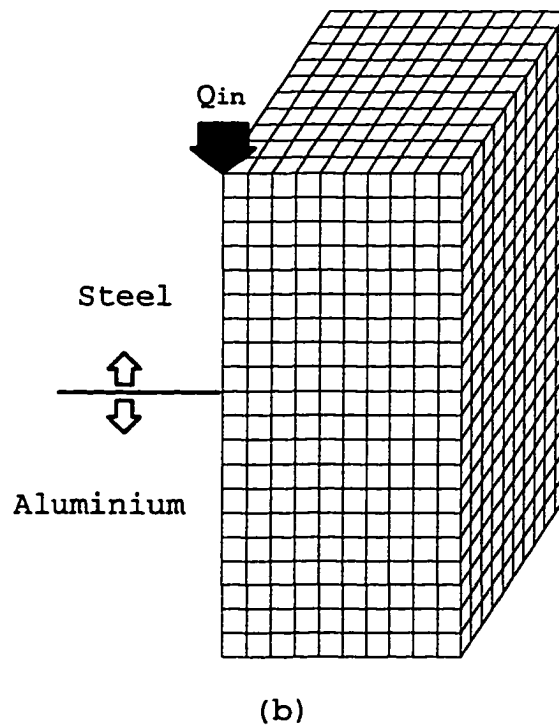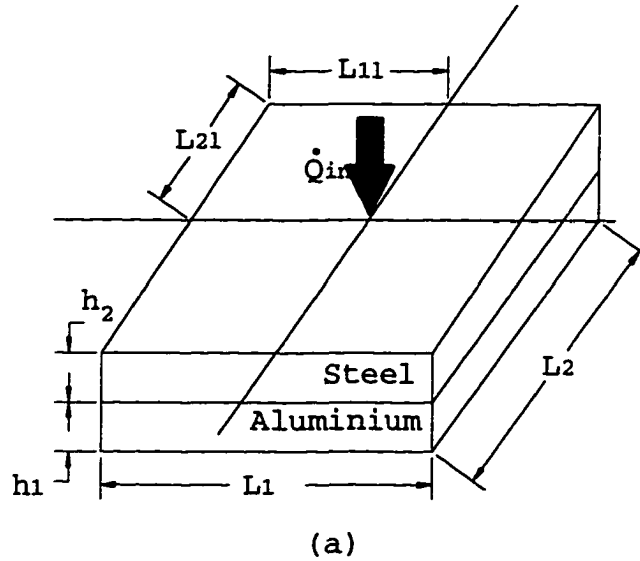
(a)

(b)

Figure 2.22 (a) The plate configuration and heat input of example 2.6 ($L_{11}=L_{21}=0.1$, $L_1=L_2=0.2$, $h_1=h_2=0.1$, $Q_{in}=10$ Watt)(b) F.E.A. model for example 2.6(2531 nodes, 2000 elements and 30 time steps)

Table 2.8 The comparison between F.E.A. and F.D.
for the CPU running time

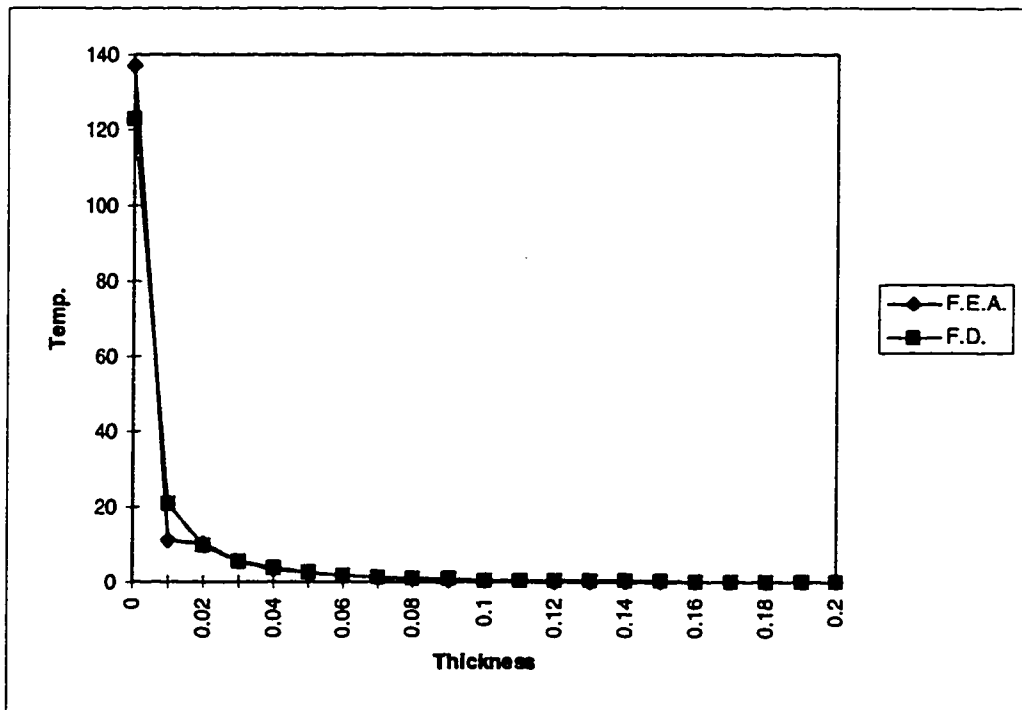|	F.E.A.	F.D.
CPU Time	824	7

Figure 2.23 The comparison between F.E.A. and F.D.
for the temperature distribution through
the thickness at the center of the beam

CHAPTER 3
THERMAL DEFLECTION AND STRESS DISTRIBUTION

The General Concept

When a structure is heated above the ambient temperature, it will expand. Due to the heat input into the structure, the thermal loading(temperature field) will cause deflection as well. The procedure of obtaining the temperature field of the structure is discussed in chapter 2. In this chapter, the main goal is to obtain the thermal deflection and stress by assuming that the temperature field in the structure is known.

The purpose of this study is to develop a new method to obtain the deflection of the structure under thermal loading. In the proposed method, the thermal loading of the structure is transformed to an equivalent mechanical loading that can produce exactly the same deflection as the thermal loading. The details of how to transform the thermal loading(temperature field) to an equivalent mechanical loading will be discussed later in this chapter.

After obtaining the equivalent mechanical loading of the structure, the deflection due to the equivalent mechanical loading is evaluated by utilizing the energy method with Lagrange multipliers. The application of the

42

energy method with Lagrange multipliers in structural analysis is presented in references[23,24,25,26]. The traditional energy method ,such as Rayleigh-Ritz method, is generally limited to the simplest problems where all the boundary conditions can be satisfied by the assumed deflection function. Through the use of Lagrange multipliers, the problems with complex boundary conditions can be solved.

In this method, the potential energy function is obtained by assuming a deflection function composed of a set of coordinate functions Φ_n with unknown coefficients. The Lagrange multipliers are then utilized to insure the satisfaction of any boundary conditions which are not satisfied by the assumed deflection function. The unknown coefficients of the assumed deflection function can be determined by minimizing the Lagrangian function which includes the potential energy and the constraints.

The One-Dimensional(Beam) Problem

A beam is first considered for illustrating the proposed method. For example, a multiple material beam as shown in figure 3.1 is assumed to be subjected to a temperature distribution through the thickness as a result of thermal loading. Assuming that the cross section of the beam remains plane, the neutral axis of the beam can be determined by geometric consideration as follows:
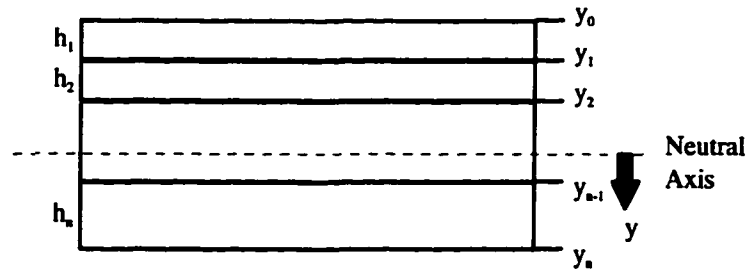
Figure 3.1 The cross section of the composite beam

The i-layer of the beam has a thickness h_i. The y_{i-1} and y_i are the distances from the neutral axis to the top surface and the lower surface of i-layer. The y_i can be expressed as:

$$y_i = y_0 + \sum_{j=1}^{i-1} h_j \qquad \text{for } j=1 \text{ to } n \qquad (3.1)$$

Therefore, for any layer in the beam, the distances of the top and lower surfaces are functions of the distance from the neutral axis to the top surface of the first layer(y_0). Since the first moment calculated about the neutral axis is zero, the y_0 is calculated by using equation (3.2). The position of N.A. can be therefore determined from:

$$\sum_{i=1}^{n} E_i \int_{y_{n-1}}^{y_n} y dA = 0 \qquad (3.2)$$

The total flexural rigidity **D** can be obtained as the sum of the rigidities of the different layers with respect to the neutral axis(N.A.).

$$D = \sum_{k=1}^{n} E_k I_k^*$$ (3.3)

where $I_k^* = \frac{bh_k^3}{12} + bh_k d_k^2$

$$d_k = y_{k-1} - \frac{1}{2} h_k$$

The longitudinal thermal expansion of the beam αT will generally cause uniform expansion as well as bending. Since the beam is free to expand in the x-direction and there is no other mechanical loading other than the thermal loading, the resultant stress is the superposition of the thermal stress (σ_t), uniform stress (σ_{ave}) and bending stress(σ_m). In order to satisfy the equilibrium conditions, the total force due to the stress distribution in x-direction has to be zero and the total moment about the neutral axis should be also zero.

Therefore, for the single material beam with depth h:

$$\sigma_t = -\alpha ET$$

$$\sigma_{ave} = \int_{-h/2}^{h/2} \alpha ET dy$$ (3.4)

$$\sigma_m = \frac{12y}{h^3} \int_{-h/2}^{h/2} \alpha ET y dy$$

where: E : Young's Modulus
α : Thermal expansion coefficient
T : Temperature rise value at any point through the thickness of the beam

Similarly for the composite(n-layers) beam:

For layer i:

$$\sigma_{t(i)} = -\alpha_i E_i T \tag{3.5}$$

$$\sigma_{ave(i)} = \frac{E_i}{\displaystyle\sum_{j=1}^{n} h_j E_j} \sum_{i=1}^{n} \int_{y_{j-1}}^{y_j} \alpha_j E_j T \, dy \tag{3.6}$$

$$\sigma_{m(i)} = \frac{E_i y}{D} \sum_{j=1}^{n} \int_{y_{j-1}}^{y_j} \alpha_j E_j T y \, dy \tag{3.7}$$

The resultant stress for any layer of the beam can be calculated as:

$$\sigma = \sigma_t + \sigma_{ave} + \sigma_m \tag{3.8}$$

The deflection of the beam is the superposition of uniform expansion and pure bending. The uniform expansion is caused by σ_{ave} and pure bending is caused by σ_m. Assuming that the length of the beam is much greater than the beam's total thickness, the effect of the uniform expansion on deflection can be ignored. Therefore the deflection of the beam with thermal loading can be simulated as the deflection of the beam with an equivalent thermal moment M_t through the length of the beam. This equivalent moment, shown in Equation (3.9), is the total moment caused by the bending stress(σ_m) about the neutral axis. The deflection of the beam with $T(x,y)$ can be simulated as loading with an equivalent moment $M_t(x)$ acting on the beam.

$$M_t(x) = \sum_{j=1}^{n} b \int_{y_{j-1}}^{y_j} \alpha_j E_j T(x, y) y \, dy \qquad (3.9)$$

Where b: the width of the beam

If the temperature distribution T is dependent on y only, the M_t is constant along the length of the beam. If the T is a function of x(the length of the beam) and y(the thickness of the beam), the equivalent thermal moment M_t is function of x.

For the beam case, the potential energy is the sum of strain energy and the work done by loading. The strain energy can be expressed as function of deflection(v) as given in equation (3.10). The work done by external force or moment also can be presented as a function of deflection. Therefore, the potential energy is a function of deflection. The deflection of the beam v(x) is assumed to be a linear combination of a set of prescribed coordinate functions $\Phi_n(x)$ as in equation (3.11).

$$U = \int_{0}^{l} \frac{EI}{2} (v'')^2 dx \qquad (3.10)$$

$$v = \sum_{n=1}^{N} A_n \Phi_n(x) \qquad (3.11)$$

where A_n are unknown parameters

From the previous discussion, the thermal loading T(x,y) can be transformed to an equivalent moment $M_t(x)$.

The work done by the thermal loading can be expressed as follows:

$$w = \int_0^l M_t(v'')dx \qquad (3.12)$$

If the beam is subject to the constraints:

$$G_j(A_1, A_2, \cdots, A_N) = 0 \qquad j=1,2,\ldots,I_c \qquad (3.13)$$

By using the constraints with Lagrange Multipliers, the Lagrangian function(L) can be written as follows:

$$L = U - w + \sum_{i=1}^{I_c} \lambda_i G_i \qquad (3.14)$$

By minimizing the Lagrangian function as shown in equations (3.15) and (3.16), the unknown parameters(A_n, n=1...N) can be readily evaluated. The deflection of the beam is therefore determined by substituting these parameters in equation (3.11).

$$\frac{\partial L}{\partial A_n} = 0 \qquad \text{for } n=1,2,\ldots,N \qquad (3.15)$$

$$\frac{\partial L}{\partial \lambda_j} = 0 \qquad \text{for } j=1,2,\ldots,\ I_c \qquad (3.16)$$

The procedure of the proposed method is summarized as below:

1. Input material properties and solve for the position of N.A. and the flexural rigidity **D**

2. Input the thermal loading(temperature field)

3. Transfer the thermal loading to the equivalent mechanical loading

4. Assume the series of deflection function

5. Calculate the potential energy

6. Add any unsatisfied boundary conditions with Lagrange multipliers to the equation of potential energy to form the Lagrangian function

7. Develop and solve the set of linear equations obtained by partial derivatives of the Lagrangian function with respect to the unknown coefficients and the Lagrange Multipliers.

8. Substitute back the unknown coefficients and the deflection is determined

Illustrated examples

In order to illustrate the accuracy and the computational efficiency of the proposed method, the results from the proposed method are compared with the results from the finite element method for all the considered examples.

Examples 3-1 to 3-3 are for single material beams subjected to three different sets of boundary conditions. Examples 3-4 to 3-6 are two-material composite beams subjected to the same sets of boundary conditions as examples 3-1 to 3-3. Examples 3-7 to 3-9 are two-material composite beams symmetrically structured and also subjected to the same sets of boundary conditions as examples 3-1 to 3-3.

The temperature loading for these nine cases are assumed to be the same. The temperature difference between top and bottom surfaces is 120° and the temperature distribution through the thickness of the beam is assumed to be linear. In all examples, the length and deflection units are in meters and the temperature units are in °C.
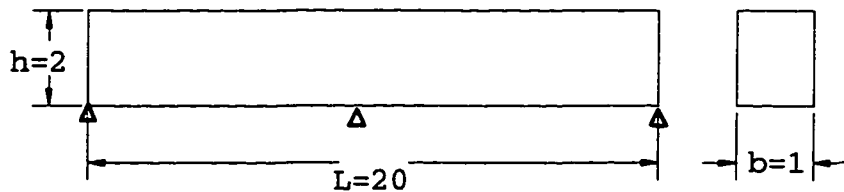
Example 3.1

Figure 3.2 The configuration of the beam subjected to thermal loading in example 3.1

For the homogeneous beam shown in figure 3.2, the boundary conditions are zero deflection at both ends and at the middle of the beam. Since sine functions already satisfy these boundary conditions at both ends, only one constraint for the middle point is necessary for this case. The assumed deflection function(sine series) is given in equation (3.17). The potential energy of the beam can be expressed by equation (3.18) as derived from the assumed deflection function. The boundary conditions of the beam can be considered as constraints at discrete locations as shown in equation (3.19). The equilibrium of the beam is satisfied

when the beam has minimum potential energy. By using the method of Lagrange multipliers, the Lagrangian function is represented as equation (3.20). The partial derivatives with respect to A_i and λ_j equal zero become a set of linear equations((3.21) and (3.22)). The unknown coefficients(A_i) of the finite series are obtained by solving these equations. The process can be repeated with expansion of the series until the solution converges with satisfactory accuracy.

$$v = \sum_{n=1}^{n} A_n \sin\left(\frac{n\pi x}{L}\right))$$ (3.17)

Since $\int_0^L \sin\left(\frac{n\pi x}{L}\right)\sin\left(\frac{m\pi x}{L}\right) = 0$ for $m \neq n$

Therefore

$$\int_0^L (v'')^2 dx = \int_0^L (\sum_{n=1}^{n} (n\pi)^2 A_n \sin\left(\frac{n\pi x}{L}\right))(\sum_{n=1}^{n} (n\pi)^2 A_n \sin\left(\frac{n\pi x}{L}\right))$$

$$\int_0^L (v'')^2 dx = \sum_{n=1}^{n} \int_0^L n^4 \pi^4 A_n^2 \sin^2\left(\frac{n\pi x}{L}\right))$$

$$\int_0^L (v'')^2 dx = \sum_{n=1}^{n} \frac{n^4 \pi^4}{4L^3} A_n^2$$

The potential energy Π in this beam:

$$U_e - W = \frac{D}{2} \int_0^L (v'')^2 dx - \int M_c(v'') dx$$

$$= \sum_{n=1,2,3...}^{N} (\frac{D}{4} n^4 \pi^4 A_n^2) - 2 \sum_{n=1,3,5...}^{N} M_c n\pi A_n$$ (3.18)

The constraint:

$$G = \sum_{n=1}^{N} A_n \sin\left(\frac{n\pi x}{L}\right) = 0$$ (3.19)

The Lagrangian function is :

$$L = U - w + \lambda G \qquad (3.20)$$

$$\frac{\partial L}{\partial A_i} = 0 \qquad \text{for } i=1 \text{ to } n \qquad (3.21)$$

$$\frac{\partial L}{\partial \lambda} = 0 \qquad (3.22)$$

The temperature distribution T(y) is as follow:

$$T(y) = 120(1 - \frac{(y + 1)}{2})) \qquad (3.23)$$

The model for the finite element analysis used for comparison is shown in figure 3.3. Since the boundary conditions and the thermal loading are symmetrical about the center location, this model only contains half of the beam with 55 nodes and 40 elements.
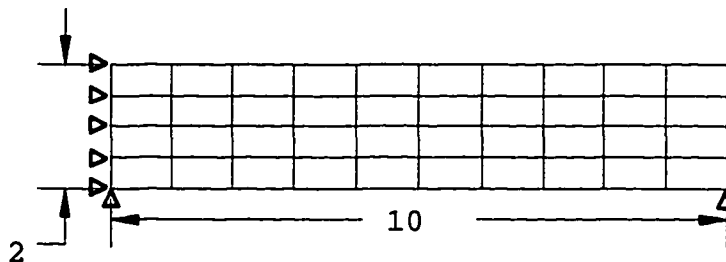
Figure 3.3 The F.E.A. model for example 3.1

The results of the proposal method for different number of terms N are shown in figure 3.4. The assumed deflection function converge at N=7. The comparison between the proposed method and the F.E.A. is shown in figure 3.5. The difference in the maximum deflection(x=16.) is about 9%. The CPU time for calculating deflection by the F.E.A. is 9

sec. The proposed method gives the solution in less than 1 sec.

The results illustrate that the proposed method is much faster than the F.E.A. and the two methods give very close deflection values.
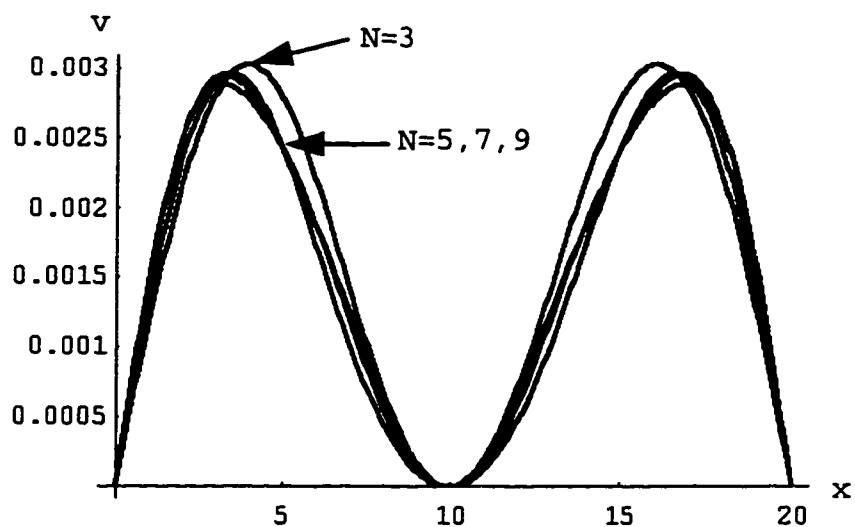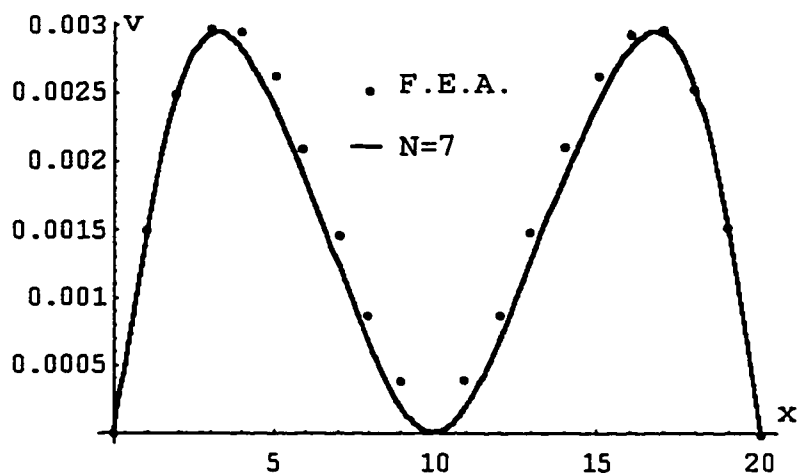

Figure 3.4 the computed deflections for N=3,5,7,9

Figure 3.5 Deflections by the proposed method(N=7) and the F.E.A.

Example 3.2

Consider a clamped-supported homogeneous beam as shown in figure 3.6 subjected to the same temperature distribution $T(x,y)$ given in equation (3.23).
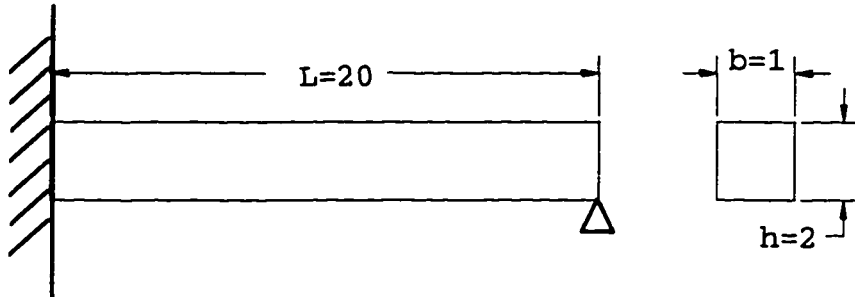

Figure 3.6 The configuration of the beam in example 3.2

By choosing the same deflection function, the formulation of the total potential energy is the same as that in example 3-1. The boundary conditions, however, are not all satisfied by this function. The unsatisfied boundary condition is $v'=0$ at $x=0$, which can be written as:

$$G = \sum_{n=1}^{N} A_n n = 0 \qquad (3.24)$$

The same procedure as in example 3-1 is applied to solve for the A_n and λ. The model of the finite element analysis used for comparison is shown in Figure 3.7. Since the boundary conditions and the thermal loading are not symmetrical in x direction, this model contains the full configuration of the beam with 105 nodes and 80 elements.
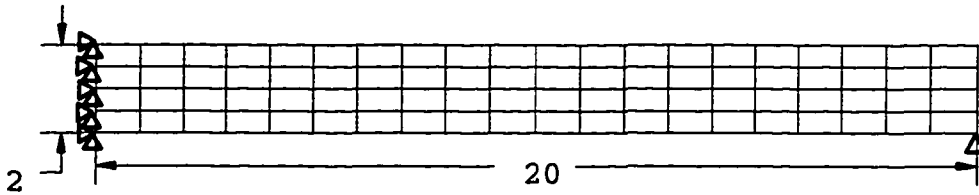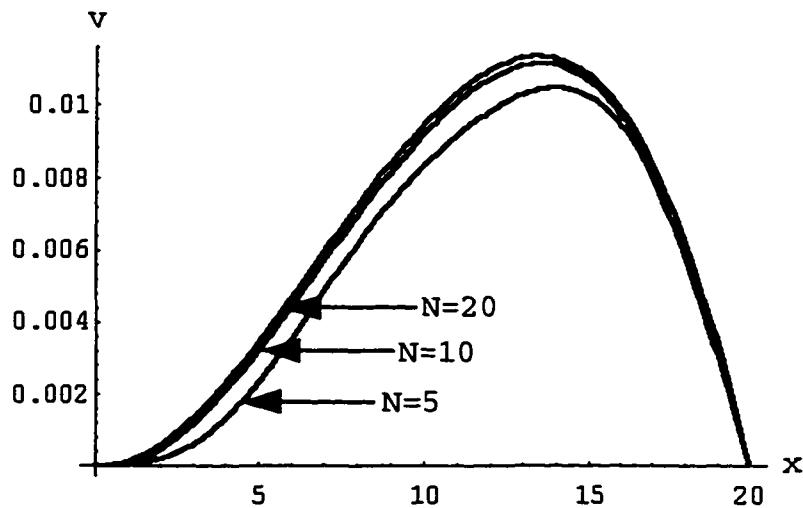
eid

Figure 3.7 The F.E.A. model for example 3.2

Figure 3.8 the computed deflections for N=5,10,20

The results from the proposed method for different terms N are shown in Figure 3.8. The assumed deflection function converges at N=10. The comparison between the proposed method and the F.E.A. is shown in figure 3.9. The difference in the maximum deflection(x=14) is approximately 0.88%. The CPU time for calculating deflection by the F.E.A. is 11 sec. The proposed method requires less than 1 sec.

Again, the results illustrate that the proposed method is much faster than the F.E.A. and that the two methods give almost identical results.
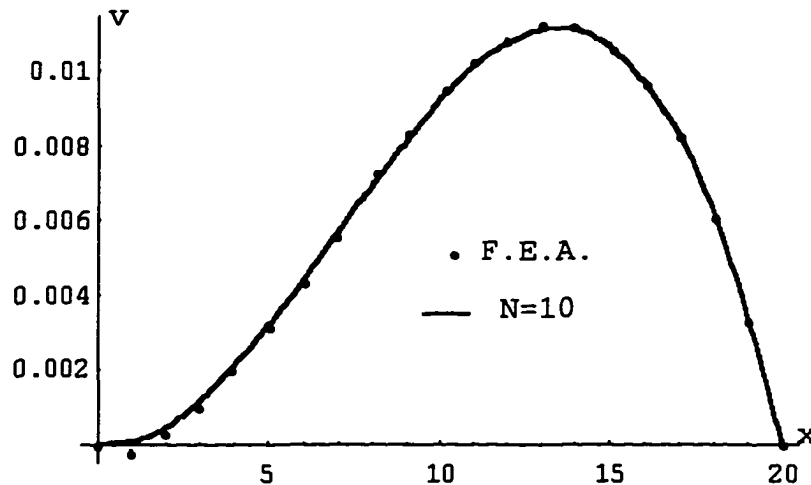

Figure 3.9 Deflections by the proposed method(N=10)
and the F.E.A.

Example 3.3

Under certain conditions, for example a homogeneous cantilever beam, it is necessary to use a more complete Fourier series, such as a series including both sine and cosine functions. The nature of the sine functions alone makes it difficult to provide a deflection at the free end.

Assuming that the deflection is a complete Fourier series as follows:

$$v = A_0 + \sum_{n=1}^{N} A_n \cos\left(\frac{n\pi x}{L}\right) + \sum_{n=1}^{N} B_n \sin\left(\frac{n\pi x}{L}\right) \tag{3.25}$$

The strain energy stored in the beam for this assumed deflection is:

$$U = \frac{EI\pi^4}{4L^3} \left\{ \sum_{n=1}^{N} (A_n{}^2 + B_n{}^2) + \right.$$

$$\left. \sum_{n=1}^{N} \sum_{\substack{m=1 \\ m \neq n}}^{N} \left\{ A_n B_n \frac{4n^2 m^3}{(n^2 - m^2)\pi} \left(\cos(n\pi) \cos(m\pi) - 1 \right) \right\} \right\} \tag{3.26}$$

The work done by the equivalent moment $M_t(x)$ is still the same as equation (3.12). The boundary conditions are $y=0$ and $y'=0$ at $x=0$, and $y''=0$ and $y'''=0$ at $x=L$, none of which are satisfied by equation (3.25). The constraints are thus:

$$G_1 = A_0 + \sum_{n=1}^{N} A_n = 0 \tag{3.27}$$

$$G_2 = \sum_{n=1}^{N} n B_n = 0 \tag{3.28}$$

$$G_3 = \sum_{n=1}^{N} A_n n^2 \cos(n\pi) = 0 \tag{3.29}$$

$$G_4 = \sum_{n=1}^{N} B_n n^3 \cos(n\pi) = 0 \tag{3.30}$$

The Lagrangian function L can be formulated as:

$$L = U - W + \sum_{i=1}^{4} \lambda_i G_i \qquad (3.31)$$

Equating the partial derivatives of the Lagrangian function with respect to parameters λ_i (i=1,2,3,4) A_0, A_n and B_n (n=1,2,...N) to zero, a set of (2N+5) linear equations with (2N+5) unknowns is obtained. Therefore all the unknown coefficients can be solved and the deflection function of the beam is determined.

The F.E.A. model used for comparison is the same as in example 3-1-2 except for the boundary conditions. The results from the proposed method for different number of coefficients N are shown in figure 3.10. The assumed deflection function converges at N=8. The comparison between the proposed method and the F.E.A. is shown in Figure 3.11. The difference in the maximum deflection(x=20) is approximately 1.48%. The CPU time for calculating deflection by the F.E.A. is 12 sec. The proposed method only requires less than 2 sec.

Again, the results illustrate that the proposed method is much faster than the F.E.A. and that the two methods give almost identical deflections values.
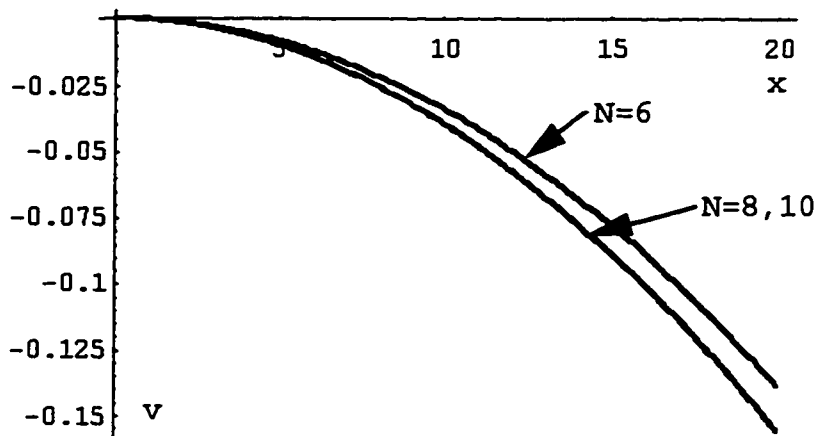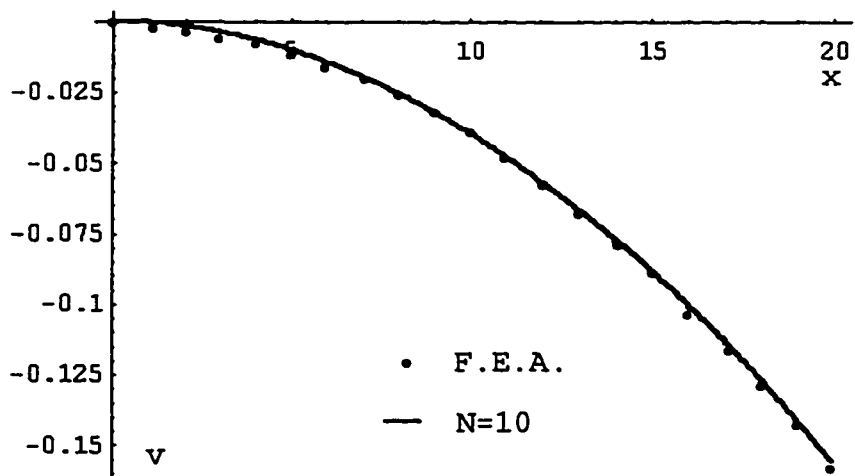
Figure 3.10 the computed deflections for N=6,8,10

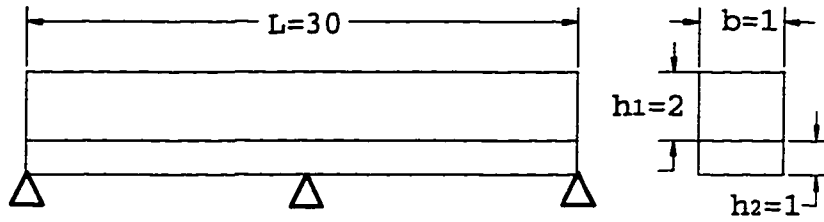Figure 3.11 Deflections by the proposed method(N=8)
and the F.E.A.

Example 3.4

Figure 3.12 The configuration and boundary conditions of the beam in example 3-4
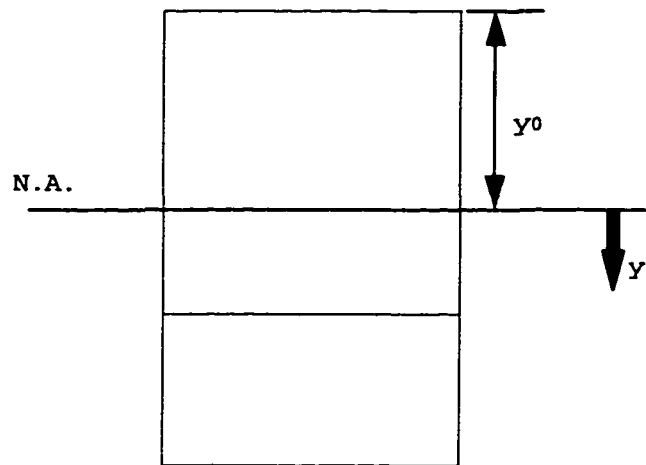

Figure 3.13 The cross section of the beam in example 3-4

For a composite beam shown in figure 3.12, the temperature distribution of the beam is assumed to be

$$T(y) = 120(1 - \frac{(y + Y_0)}{3}))$$

(3.32)

$$\sum_{i=1}^{n} E_i \int_{y_{n-1}}^{y_n} ydA = 0$$

$$\int_{y_0}^{y_0+h_1} E_1 ydA + \int_{y_0+h_1}^{y_0+h_1+h_2} E_2 ydA = 0$$

(3.33)

where h_1 : the thickness of material 1(Steel)

h_2 : the thickness of material 2 (Aluminum)
E_1 : the Modulus of material 1
E_2 : the Modulus of material 2

The position of the N.A. (Y_0) shown in figure 3.13 is calculated by using equation (3.33). The flexural rigidity D is calculated as follows:

$$D = b[E_1(\frac{h_1^3}{12} + h_1(\frac{h_1}{2} + y_0)^2] + b[E_2(\frac{h_2^3}{12} + h_2(h_1 + \frac{h_2}{2} + y_0)^2]]$$

where b: width of the beam   (3.34)

The equivalent moment $M_t(x)$ is obtained as follow:

$$M_t(x) = \int_{y_0}^{y_0+h_1} E_1\alpha_1 T(x, y)y\,dy + \int_{y_0+h_1}^{y_0+h_1+h_2} E_2\alpha_2 T(x, y)y\,dy \qquad (3.35)$$

The work done the equivalent moment $M_t(x)$ is:

$$w = \int_0^L M_t v'' dx \qquad (3.36)$$

The potential energy Π in this beam and the constraint are the same as equation (3.18) and (3.19). The Lagrangian function L is also the same as equation (3.20). By the same procedure as equation (3.21) and (3.22), the deflection function of the beam is determined.

The F.E.A. model used for comparison is shown in figure 3.14. Because of the symmetrical geometry and boundary conditions, this model only considers half of the beam that contains 77 nodes and 60 elements. The results from the proposed method for different number of terms N are shown in Figure 3.15. The assumed deflection function converges at

N=7. The comparison between the results from the proposed method and the F.E.A. is shown in Figure 3.16. The difference in the maximum deflection(x=26) is approximately 3.10%. The stress distributions through the thickness from the F.E.A. and the proposed method are shown in figure 3.17. The shear stress at the interface surface of the two materials as obtained by the proposed method is 37.28 MPa. The CPU time for calculating the deflection by the F.E.A. is 12 sec. The proposed method requires less than 2 sec.

The results illustrate that the proposed method is much faster than the F.E.A. and that the two methods give very close deflection values.
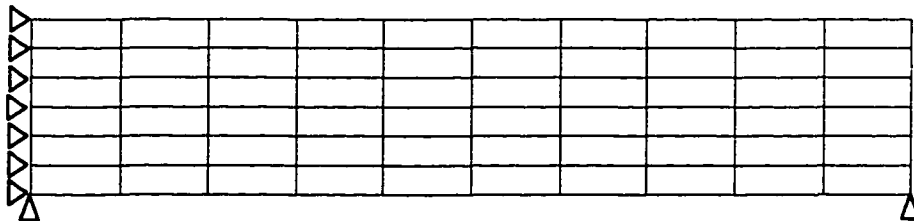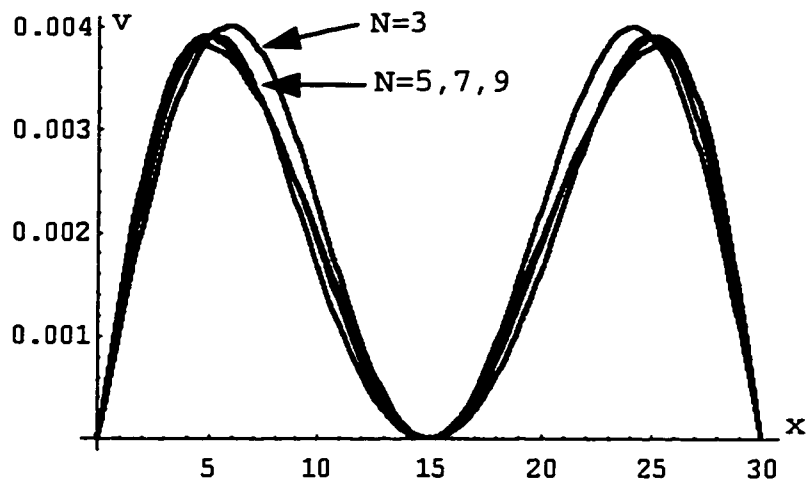

Figure 3.14 The F.E.A. model for example 3.4
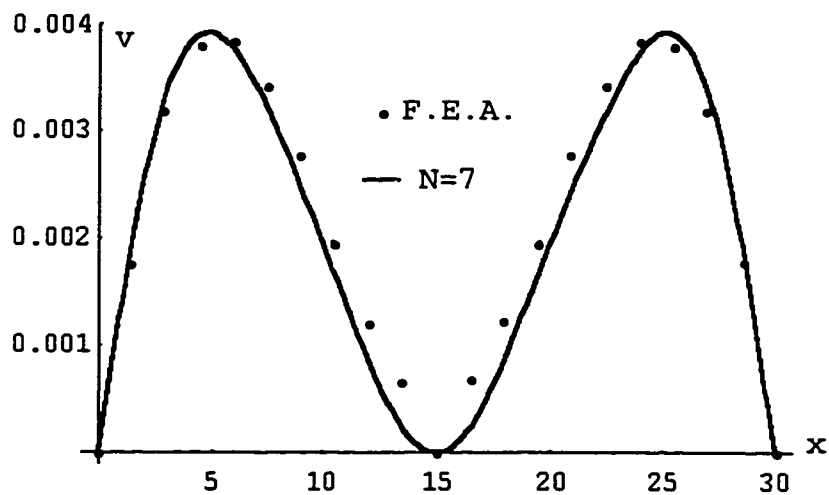
Figure 3.15 the computed deflections for N=3,5,7,9

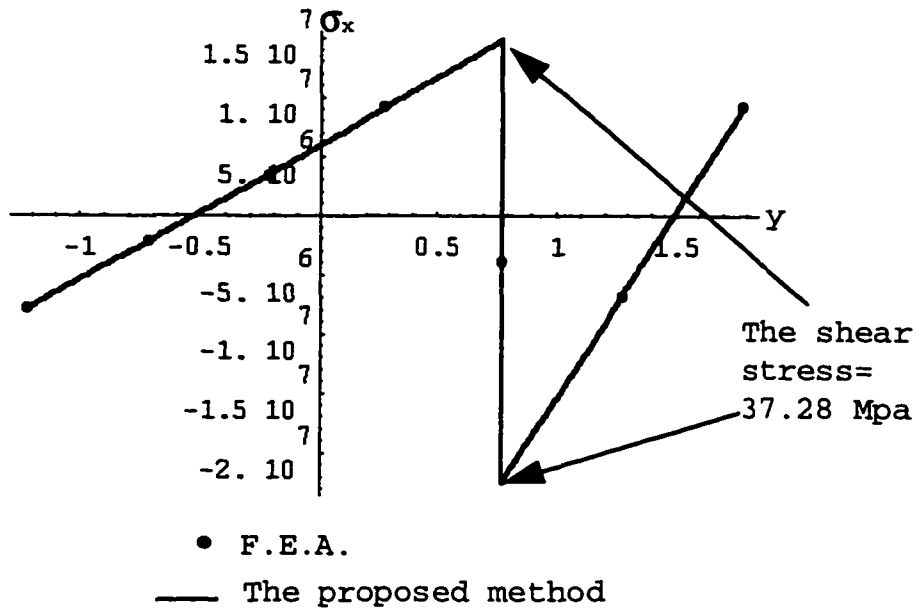Figure 3.16 Deflections by the proposed method(N=7)

and the F.E.A.

Figure 3.17 Stress through the thickness of the beam

Example 3.5

Consider a clamped-supported composite beam as shown in Figure 3.18 subjected to the temperature distribution T(x,y) as shown in equation (3.23). This composite beam is the same as the beam in example 3.4.
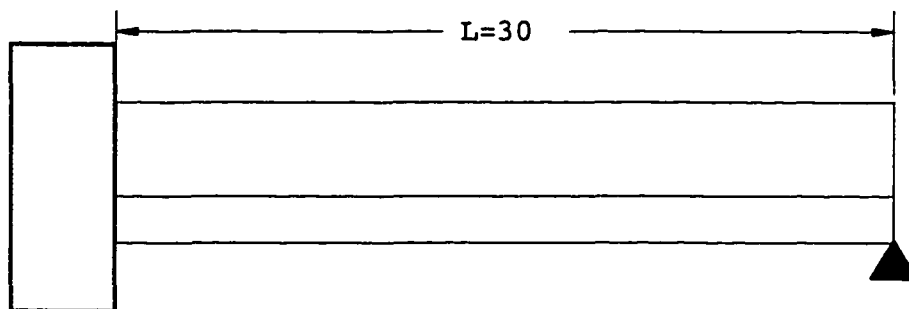

Figure 3.18 The configuration of the beam in example 3.5

Following the same procedure as in example 3.4, the M_t can be obtained. By choosing the same deflection function, the formulation of the total potential energy is the same as that in example 3.2. Since the boundary conditions are not all satisfied, the unsatisfied boundary condition ($v'=0$ at $x=0$) can be written as:

$$G = \sum_{n=1}^{N} A_n n = 0$$

The same procedure as in example 3.2 is applied to solve for the A_n and λ. The F.E.A. model used for comparison is shown in Figure 3.19. Since the boundary conditions and the thermal loading are not symmetrical in the x direction. This model contains the full configuration of the beam with 147 nodes and 120 elements.
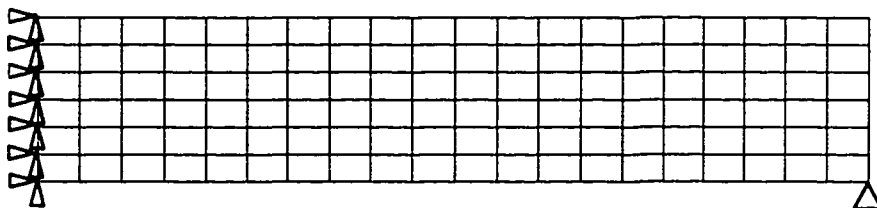

Figure 3.19 The F.E.A. model for example 3.5

The results from the proposed method for different number of term N are shown in figure 3.20. The assumed deflection function converges at N=10. The comparison between the proposed method and the F.E.A. is shown in Figure 3.21. The difference in the maximum deflection(x=20) is approximately 1.69%. Since the temperature loading is the same as in example 3.4, the stress distribution through the thickness of the beam and slip stress is the same as that in example 3-4. The CPU time for calculating deflection by the F.E.A. is 11 sec. The proposal method requires less than 1 sec.
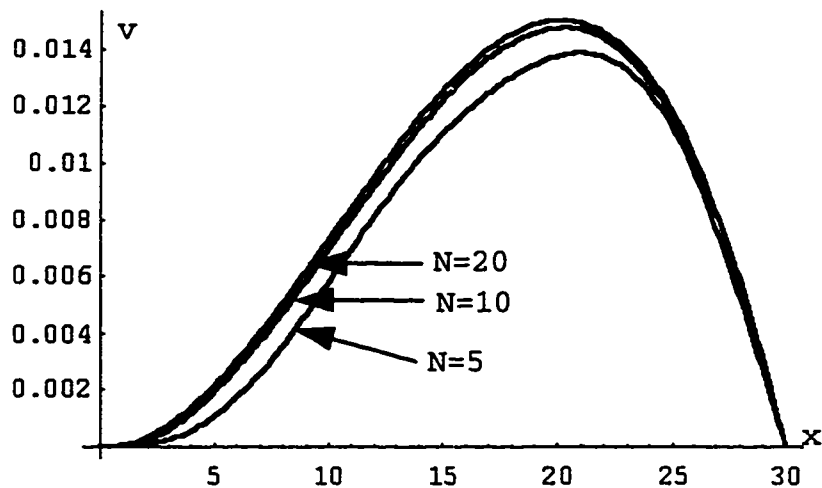

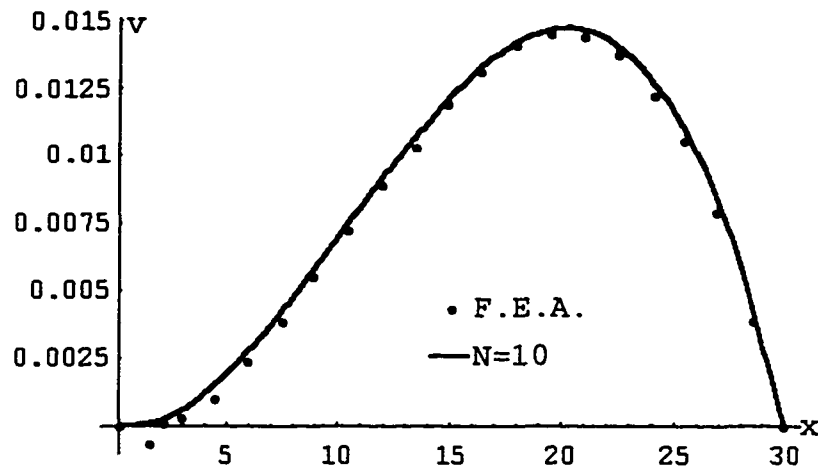Figure 3.20 the computed deflections for N=5,10,20

Figure 3.21 Deflections by the proposed method(N=10)
and the F.E.A.

Again, the results illustrate that the proposed method is much faster than the F.E.A. and that the two methods give almost identical deflection values.

Example 3.6

In this example, we consider a composite beam with the same boundary condition as in example 3.3 and the same configuration of the beam as in example 3.4. The beam in this case is shown in figure 3.22.
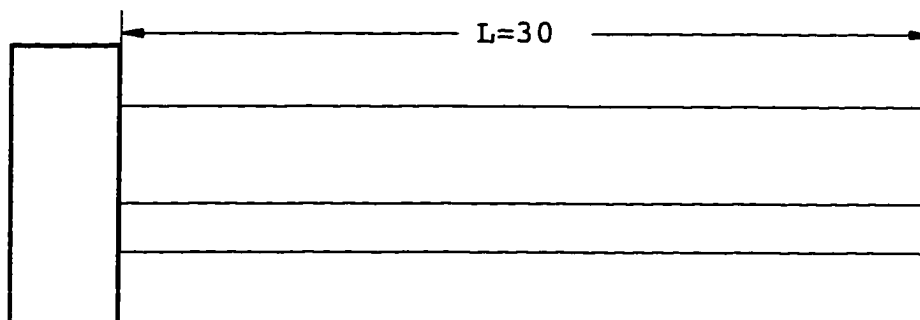
Figure 3.22 The configuration of the beam in example 3-6

Following the same procedure as in examples 3.3 and 3.4, the deflection is obtained. The F.E.A. model used is the same as in example 3.5 with different boundary conditions. The results from the proposal method for different number of terms N are shown in figure 3.23. The assumed deflection function converges at N=8. The comparison between the proposed method and the F.E.A. is shown in Figure 3.24. The difference in the maximum deflection(x=30) is approximately 3.09%. The CPU time for calculating deflection by the F.E.A. is 12 sec. The proposed method requires less than 2 sec.

Again, the results illustrate that the proposed method is much faster than the F.E.A. and those two methods give almost identical deflection values
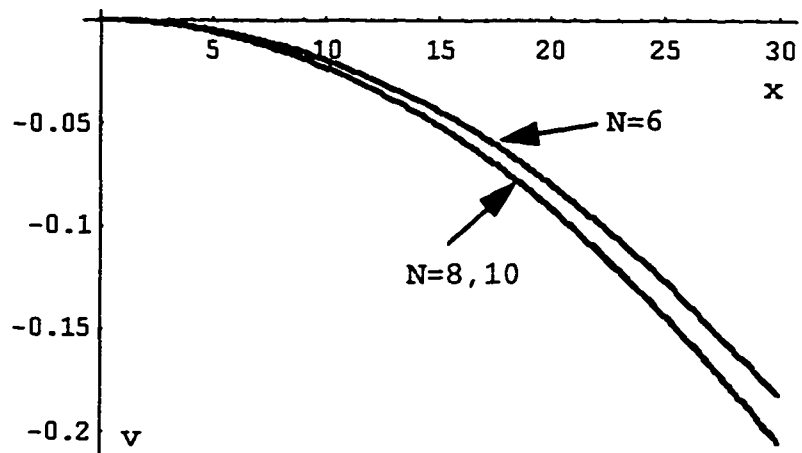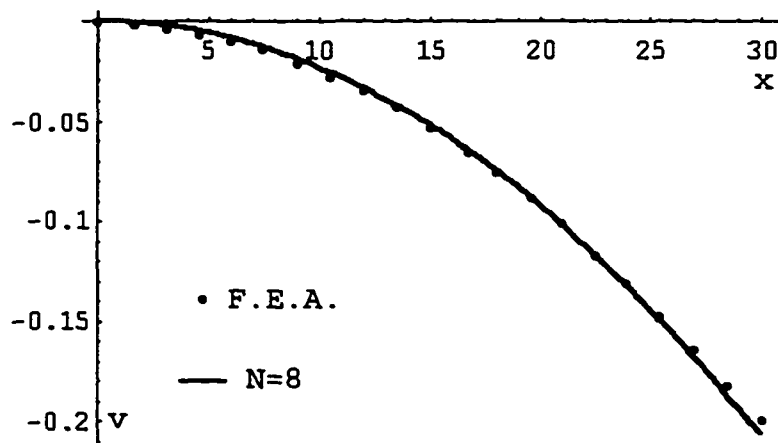
Figure 3.23 the computed deflections for N=4,6,8

Figure 3.24 Deflections by the proposed method(N=8)
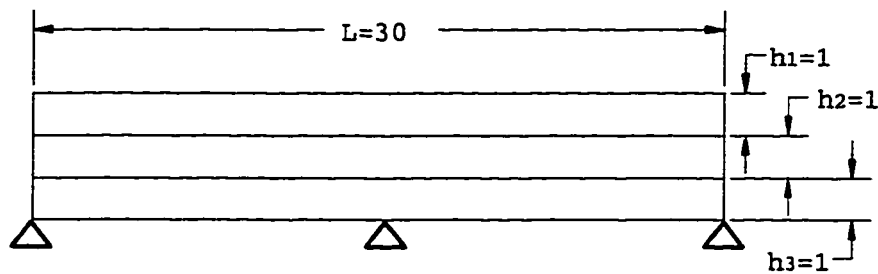and the F.E.A.

Example 3.7

Figure 3.25 the configuration and boundary conditions of the beam in example 3.7

For the composite beam shown in figure 3.25 and a temperature distribution as given by equation (3.37):

$$T(y) = 120(1 - \frac{(y - Y_0)}{3}))$$

(3.37)

$$\sum_{i=1}^{n} E_i \int_{y_{n-1}}^{y_n} y dA = 0$$

(3.38)

$$\int_{y_0}^{y_0+h_1} E_1 y dA + \int_{y_0+h_1}^{y_0+h_1+h_2} E_2 y dA + \int_{y_0+h_1+h_2}^{y_0+h_1+h_2+h_3} E_1 y dA = 0$$

where
h_1 : the thickness of first layer(Steel)
h_2 : the thickness of second layer(Aluminum)
h_3 : the thickness of third layer(Steel)
E_1 : the Modulus of material 1(Steel)
E_2 : the Modulus of material 2(Aluminum)

The position of N.A.(Y_0) can be calculated by using equation (3.38). Since the beam is symmetrically structured, the position of N.A. must be at the center of the thickness($Y_0 = (h_1+h_2+h_3)/2$). The flexural rigidity D is calculated as follow:

$$D = b[E_1(\frac{h_1{}^3}{12} + h_1(\frac{h_1}{2} + y_0)^2]$$

$$+b[E_2(\frac{h_2{}^3}{12} + h_2(h_1 + \frac{h_2}{2} + y_0)^2] \tag{3.39}$$

$$+b[E_1(\frac{h_1{}^3}{12} + h_3(h_1 + h_2 + \frac{h_3}{2} + y_0)^2]$$

where b: width of the beam

The equivalent moment $M_t(x)$ is obtained as follow:

$$M_t = \int_{y_0}^{y_0+h_1} E_1\alpha_1 Ty\,dy + \int_{y_0+h_1}^{y_0+h_1+h_2} E_2\alpha_2 Ty\,dy + \int_{y_0+h_1+h_2}^{y_0+h_1+h_2+h_3} E_1\alpha_1 Ty\,dy \tag{3.40}$$

The work done by the equivalent moment $M_t(x)$ is:

$$w = \int_0^L M_t v''dx$$

The potential energy Π of the beam and the constraints are the same as given by equations (3.18) and (3.19). The Lagrangian function L is also the same as expressed in equation (3.20). Following the same procedure and using equations (3.21) and (3.22), the deflection function of the beam is determined.
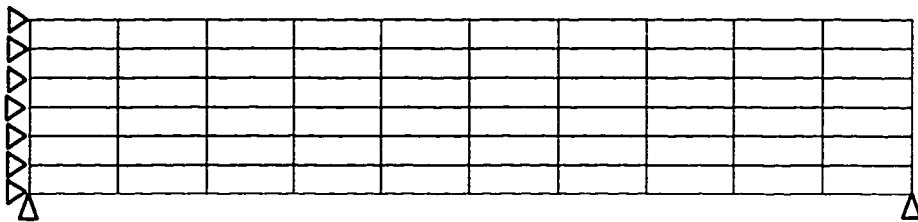

Figure 3.26 The F.E.A. model for example 3.7

The F.E.A. model used for comparison is shown in figure 3.26. This model contains 77 nodes and 60 elements. The results from the proposed method for different number of terms N are shown in Figure 3.27. The assumed deflection function converges at N=7. The comparison between the proposed method and the F.E.A. is shown in Figure 3.28. The difference in the maximum deflection(x=27) is approximately 6.38%. The stress distributions through the thickness obtained by the F.E.A. and proposed method are shown in figure 3.29. The maximum shear stress at the interface surface of the two materials as obtained from the proposed method is 67.2 Mpa. The CPU time for calculating deflection by the F.E.A. is 12 sec. The proposed method requires less than 2 sec.
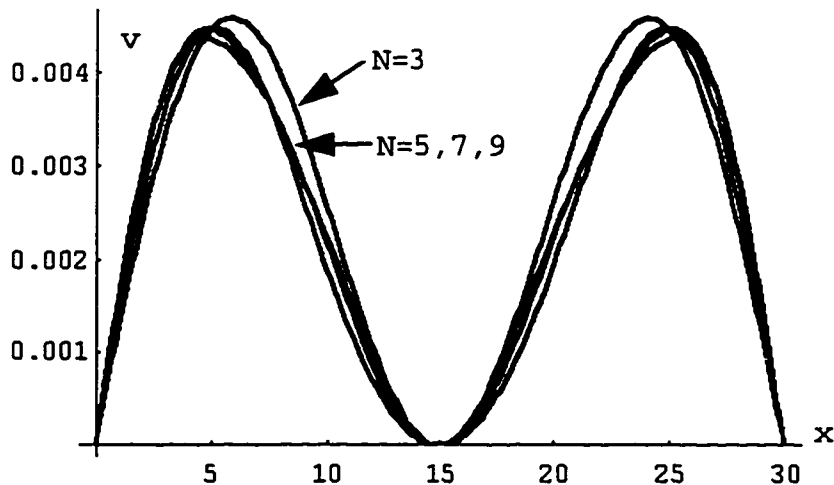

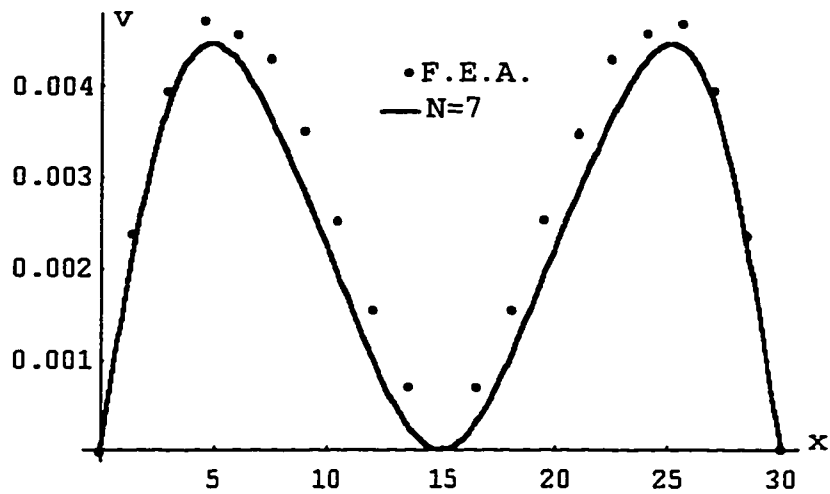Figure 3.27 the computed deflections for N=3,5,7,9

Figure 3.28 Deflections by the proposed method(N=7)
and the F.E.A.

The results illustrate that the proposed method is much
faster than the F.E.A. and that the two methods give very
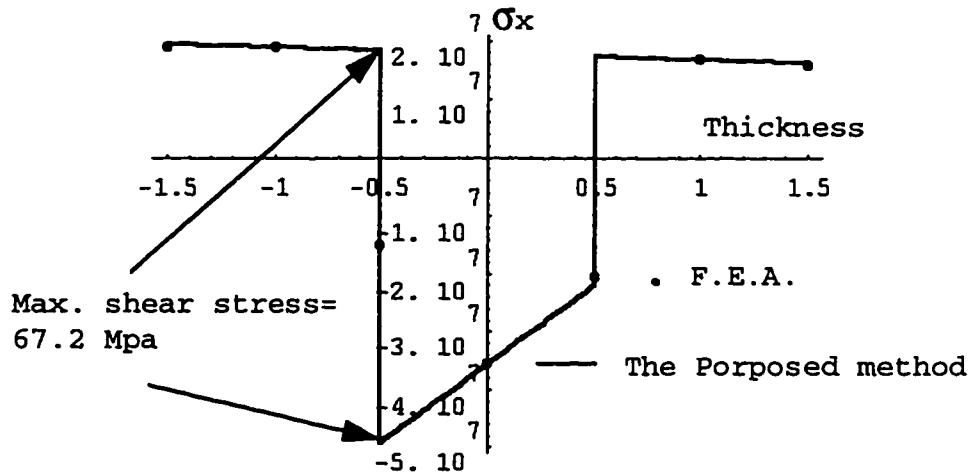close deflection values.

Figure 3.29 Stress through the thickness of the beam

Example 3.8

Consider a clamped-supported composite beam as shown in figure 3.30 subjected to the temperature distribution T(x,y) as shown in equation (3.37). The composite beam in this case is the same as the beam of example 3-7.
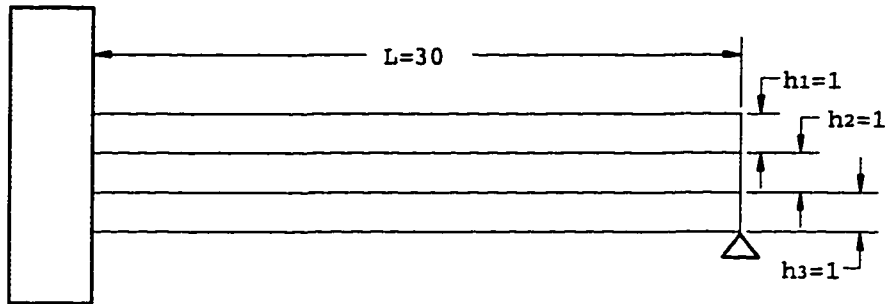
Figure 3.30 The configuration of the beam in example 3.8

The same procedure as in examples 3.7 is followed to obtain M_t. By choosing the same deflection function, the formulation of the total potential energy is the same as that in example 3.2. Since the boundary conditions are not all satisfied, the unsatisfied boundary condition (v'=0 at x=0) can be written as:

$$G = \sum_{n=1}^{N} A_n n = 0$$

The same procedure as in example 3.2 is applied to solve for the A_n and λ. The F.E.A. model used for comparison is shown in Figure 3.31. Since the boundary conditions and the thermal loading are not symmetrical in the x direction,

this model contains the full configuration of the beam with 147 nodes and 120 elements.
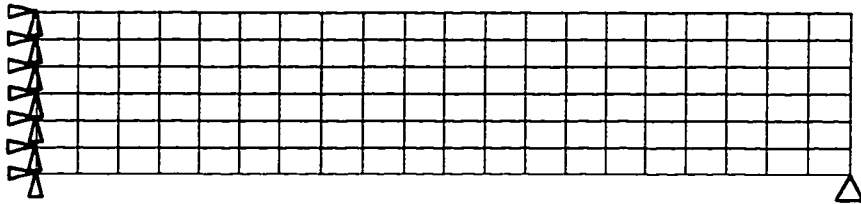
Figure 3.31 The F.E.A. model for example 3.8

The results from the proposed method for different number of terms N are shown in Figure 3.32. The assumed deflection function converges at N=10. The comparison between the proposed method and the F.E.A. is shown in Figure 3.33. The difference in the maximum deflection(x=20) is approximately 1.05%. Since the temperature loading is the same as in example 3-7, the stress distribution through the thickness of the beam and shear stress is the same as that in example 3.7. The CPU time for calculating deflection by the F.E.A. is 11 sec. The proposed method requires less than 1 sec.

Figure 3.32 the computed deflections for N=5,10,20

Again, the results illustrate that the proposed method is much faster than the F.E.A. and that the two methods give almost identical deflection values.

Figure 3.33 Deflections by the proposed method(N=10) and the F.E.A.

Example 3.9

In this example, the composite beam has the same boundary condition as in example 3.6 and the same configuration as in example 3.7. The beam in this case is shown in Figure 3.34.
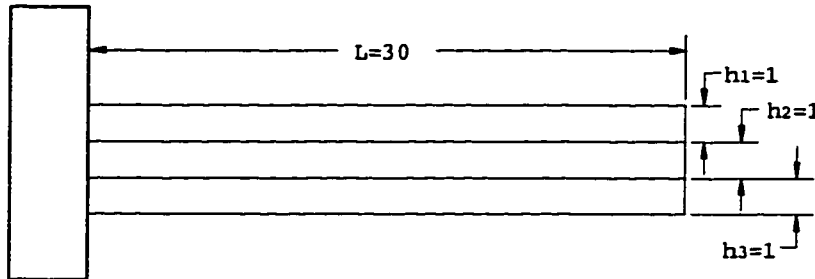
Figure 3.34 The configuration of the beam in example 3-9

Following the same procedure as in examples 3-6 and 3-7, the deflection is obtained. The F.E.A. model used is the same as in example 3.8 with a change in the boundary conditions. The results from the proposed method for different number of terms N are shown in figure 3.35. The assumed deflection function converges at N=8. The comparison between the proposed method and the F.E.A. is shown in Figure 3.36. The difference in the maximum deflection(x=30) is approximately 1.49%. The CPU time for calculating deflection by the F.E.A. is 12 sec. The proposed method requires less than 2 sec.
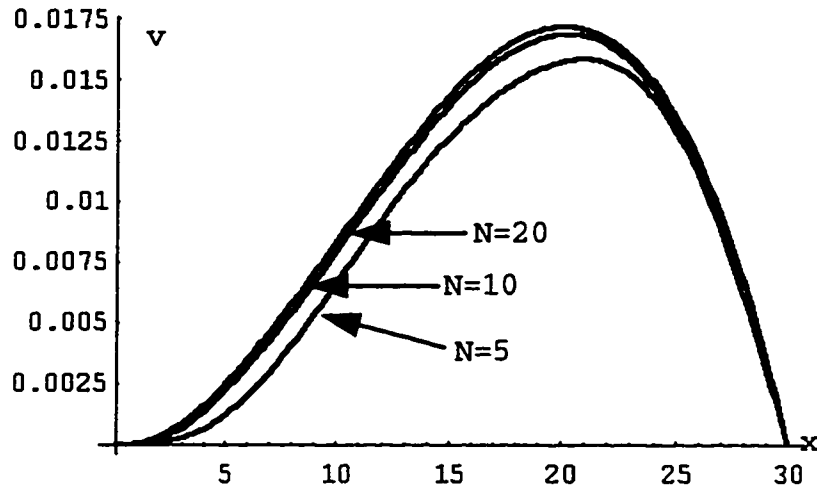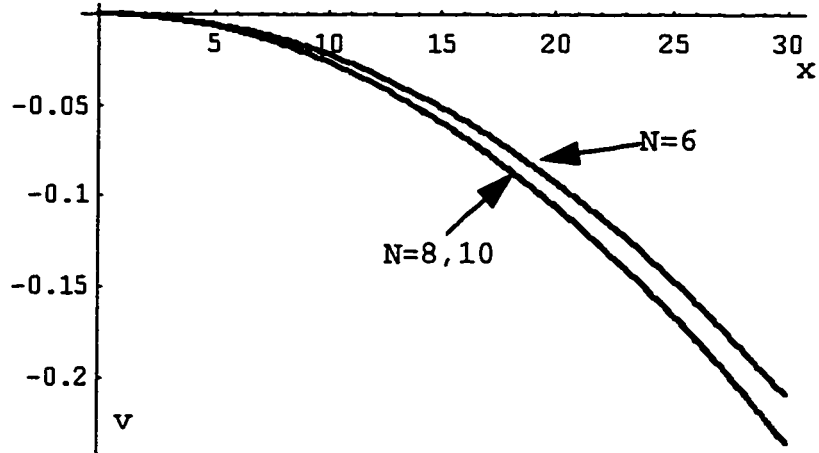
Figure 3.35 the computed deflections for N=4,6,8

Again, the results illustrate that the proposed method is much faster than the F.E.A. and that the two methods give almost identical deflection values
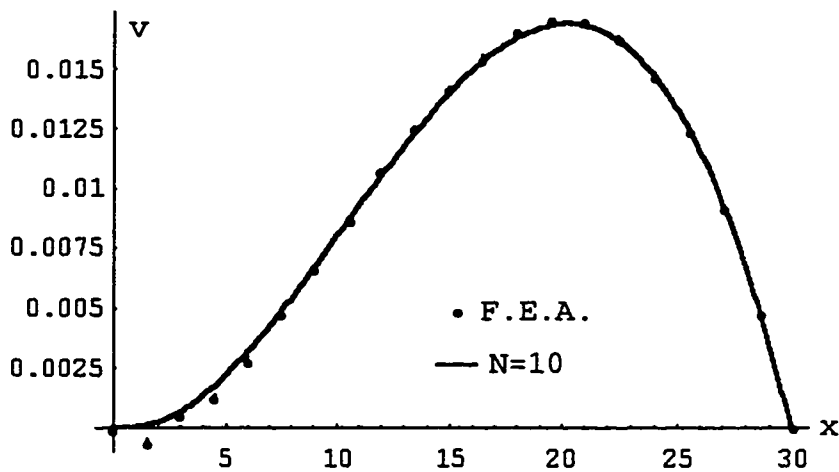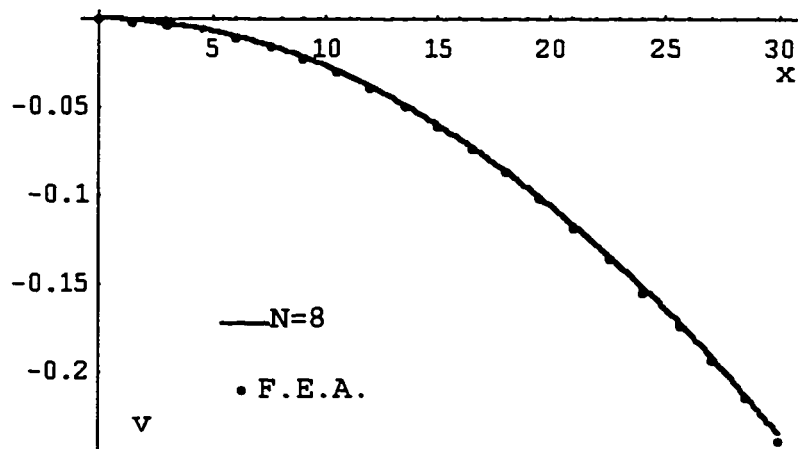
Figure 3.36 Deflections by the proposed method(N=10) and the F.E.A.

The Two-Dimensional (Plate) Problem

In this investigation, a plate is defined as an elastic body bounded by two flat surfaces. The distance between the surfaces is the thickness of the plate. The neutral surface (N.S.) is a plane parallel to the top and bottom surfaces. The position of the N.S. can be obtained in the same fashion as in the beam case. The development of the theory of bending of a thin plate is based on the following assumptions attributed to Kirchhoff[20]:

1. The linear filament of the plate which is initially normal to the N.S. remains straight and normal to N.S. after bending.

2. There is no deformation in the N.S.

3. Normal stress in the direction transverse to the N.S. is small compared to the other normal stresses, and the normal strain in that direction is small enough to be disregarded.

The position of N.S. for a composite plate shown in figure 3.37 is obtained by the same procedure as that used in the beam case. Therefore, the total flexural rigidity D of the composite plate is defined by equation (3.41). The strain energy U for a plate is formulated as equation (3.42).

$$D = \sum_{k=1}^{n} \frac{E_k I_k}{1 - v_k}$$

(3.41)

where $I_k = \frac{h_k^3}{12} + h_k d_k^2$

$d_k = y_{k-1} - \frac{1}{2} h_k$

v : Poisson's ratio

$$U = \frac{D}{2} \int_A \{ (\frac{\partial^2 v}{\partial^2 x} + \frac{\partial^2 v}{\partial^2 y})^2 - 2(1 - v) [\frac{\partial^2 v}{\partial^2 x} \frac{\partial^2 v}{\partial^2 y} - (\frac{\partial^2 v}{\partial x \partial y})^2] \} dA$$

(3.42)

where v : deflection function

A : the surface area of the plate

Due to the effect of Poisson's ratio, the equivalent moment M_t is shown in equation (3.43). The work done by the equivalent moment M_t is given in equation (3.44).
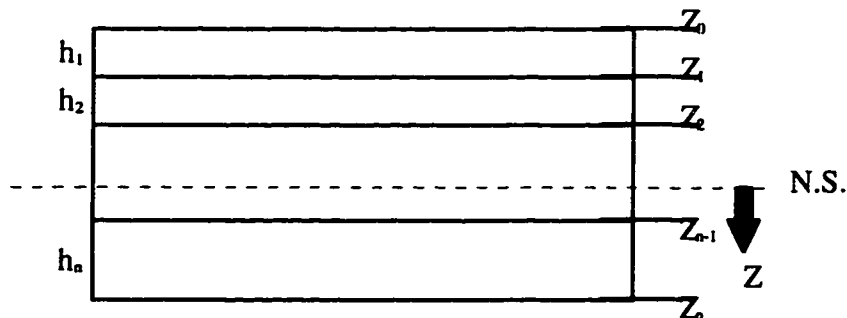
Figure 3.37 The cross section of a composite plate

$$M_t(x, y) = \sum_{i=1}^{n} \int_{z_{i-1}}^{z_i} (1 + v_i) (E_i \alpha_i T(x, y, z) z) dz$$

(3.43)

$$W = \int\limits_{0}^{L_x} \int\limits_{0}^{L_y} M_c(\frac{\partial^2 v}{\partial^2 x} + \frac{\partial^2 v}{\partial^2 y})dxdy \qquad (3.44)$$

The potential energy therefore can be written as follows:

$$\Pi = U - W \qquad (3.45)$$

The boundary conditions at the edges of the plate can be categorized as follows:

1. clamped edge along which v and $\partial v/\partial n$ vanish

2. simply-supported edge along which v and M_n vanish

3. free edge along which M_n and v_n vanish

In the above statements, the derivative with respect to n is the derivative with respect to the normal to the edge, and M_n and v_n denote, respectively, the moment and the shear force in the normal direction to the edges. The procedure of the proposed method is the same as in the beam case.

Illustrative examples

Seven examples are used with different boundary conditions in order to demonstrate the capability of the proposed method. Examples 3.10 to 3.14 are unit homogeneous square plate with dimension $L_x=L_y=1$. In example 3.14, a composite plate is considered in order to demonstrate both the shear stress and deflection. In examples 3.15 and 3.16, the homogeneous plates with holes are considered. In all

examples, the length and deflection units are in meters and the temperature units are in °C.

In order to illustrate the accuracy and the computational efficiency of the proposed method, it is compared with the finite element method for all the considered examples. The thermal loading for these seven cases is assumed to be the same. The temperature difference between top and bottom surfaces is 120° and the temperature distribution through the thickness of the beam is assumed to be linear.
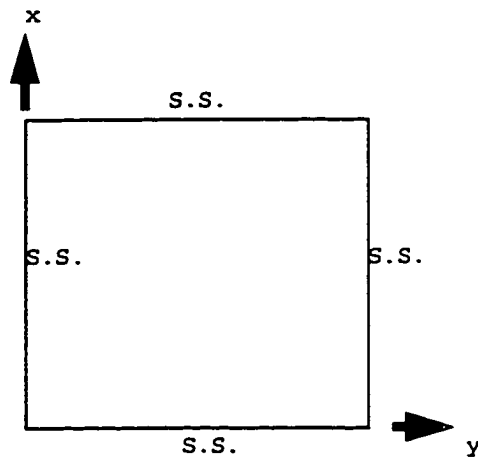
Example 3.10

Figure 3.38 the configuration of the plate with boundary conditions in example 3.10

The problem of a homogeneous plate with all edges simply supported has been cited by many authors (for example Timoshenko[20], Saada[27], and Love[28]) to demonstrate the

usage of Rayleigh-Ritz method in plate problems. Taking a unit square homogeneous plate(thickness h=0.01) as an example, the assumed deflection function(v) is chosen to be a double sine series for both x and y direction.

$$v(x, y) = \sum_{m=1}^{Nm} \sum_{n=1}^{Nn} A_{mn} \sin(m\pi x) \sin(n\pi y)) \qquad (3.46)$$

To simplify the problem, N_m and N_n will be taken the same throughout this study. With the deflection surface approximated by the double sine series shown in equation (3.46), the strain energy U which is obtained by equation (3.42) is expressed as :

$$U = \frac{D\pi^4}{8} \sum_{m=1}^{Nm} \sum_{n=1}^{Nn} A_{mn}^2 (m^2 + n^2)^2 \qquad (3.47)$$

The temperature distribution T(z) is as follow:

$$T(z) = 120(1 - \frac{(z + \frac{1}{2})}{h})) \qquad (3.48)$$

The equivalent moment M_t and The work done by the equivalent moment M_t can be calculated from equations (3.43) and (3.44).

$$M_t(x, y) = \frac{120D\alpha(1 - \upsilon^2)}{h} \qquad (3.49)$$

$$W = \sum_{m=1}^{N} \sum_{n=1}^{N} A_{mn}[M_t \frac{(m^2 + n^2)(1 - \cos(m\pi))(1 - \cos(n\pi))}{mn} \qquad (3.50)$$

Since the second derivative of a sine function vanishes at the edges of the plate, i.e. $\partial^2 v/\partial x^2 = 0$ at x=0 and x=1. and $\partial^2 v/\partial y^2 = 0$ at y=0 and y=1., all boundary conditions are

satisfied by the assumed deflection function and no additional constraint equations are necessary. The Lagrangian function L is equal to the potential energy function in this case.

Using the same approach as in the beam examples, the partial derivatives of L with respect to each A_{mn} are set equal to zero. The unknown A_{mn} coefficients are obtained as:

$$A_{mn} = \frac{480\alpha(1 + \upsilon)\,(1 - \cos(m\pi))\,(1 - \cos n\pi))}{\pi^4 hmn} \qquad (3.51)$$

In view of the above equations, it can be seen that the numerical value of A_{mn} diminishes very quickly as m and n increase.
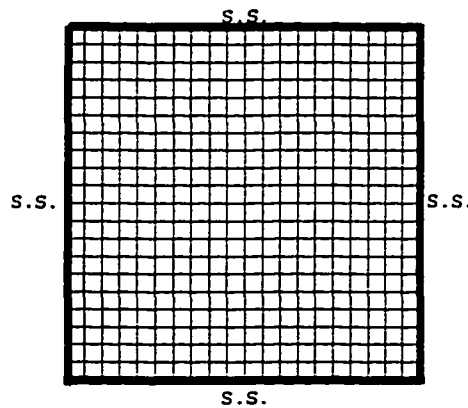
Figure 3.39 The F.E.A. model for example 3.10

The F.E.A. model used for comparison is shown in figure 3.39. This model contains 882 nodes and 400 elements. The

results from the proposed method for different number of terms N are shown in figure 3.40. Figure 3.41 shows the comparison between the F.E.A. model and the proposed method for the deflection curves taken along the section y=0.5. The assumed deflection function converges at N=7. The difference in the maximum deflection (x=0.5) is approximately 0.56%. The deflection of the plate is shown in figure 3.42. The CPU time for calculating deflection by the F.E.A. is 167 sec. The proposed method requires less than 1 sec.
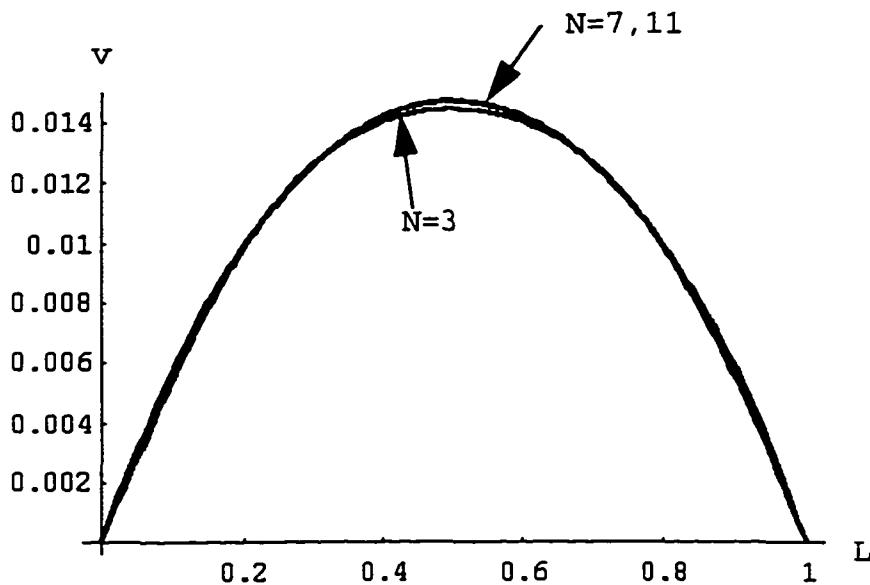
Figure 3.40 the computed deflection function along the section y=0.5
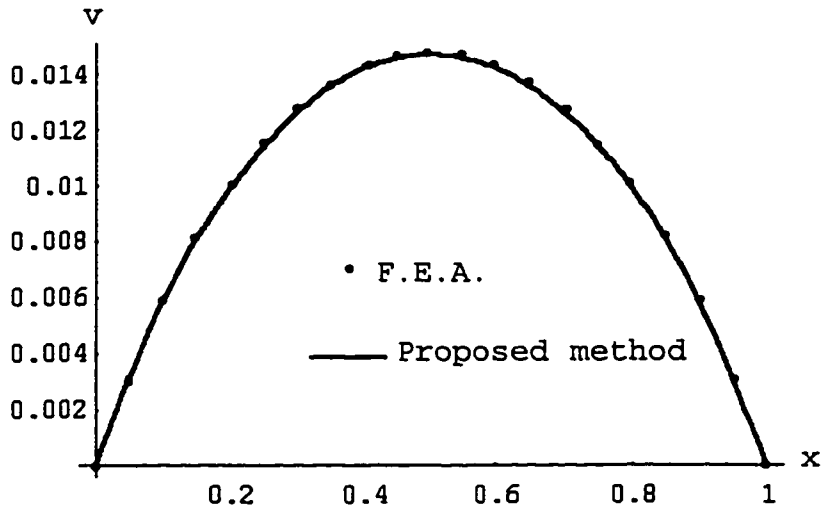
Figure 3.41 the comparison between the F.E.A. model
and the proposed method(N=7) for the deflection curves
along the section y=0.5.

Example 3.11

As illustrated in the previous section, the proposed
method makes it very convenient to convert one plate problem
to another with different boundary conditions. It is also
easy to change the boundary conditions of a plate problem
without any major change in the formulation when using the
proposed method. Consider a unit square homogeneous plate
with three edges simply supported and the fourth edge
clamped as shown in figure 3.43.
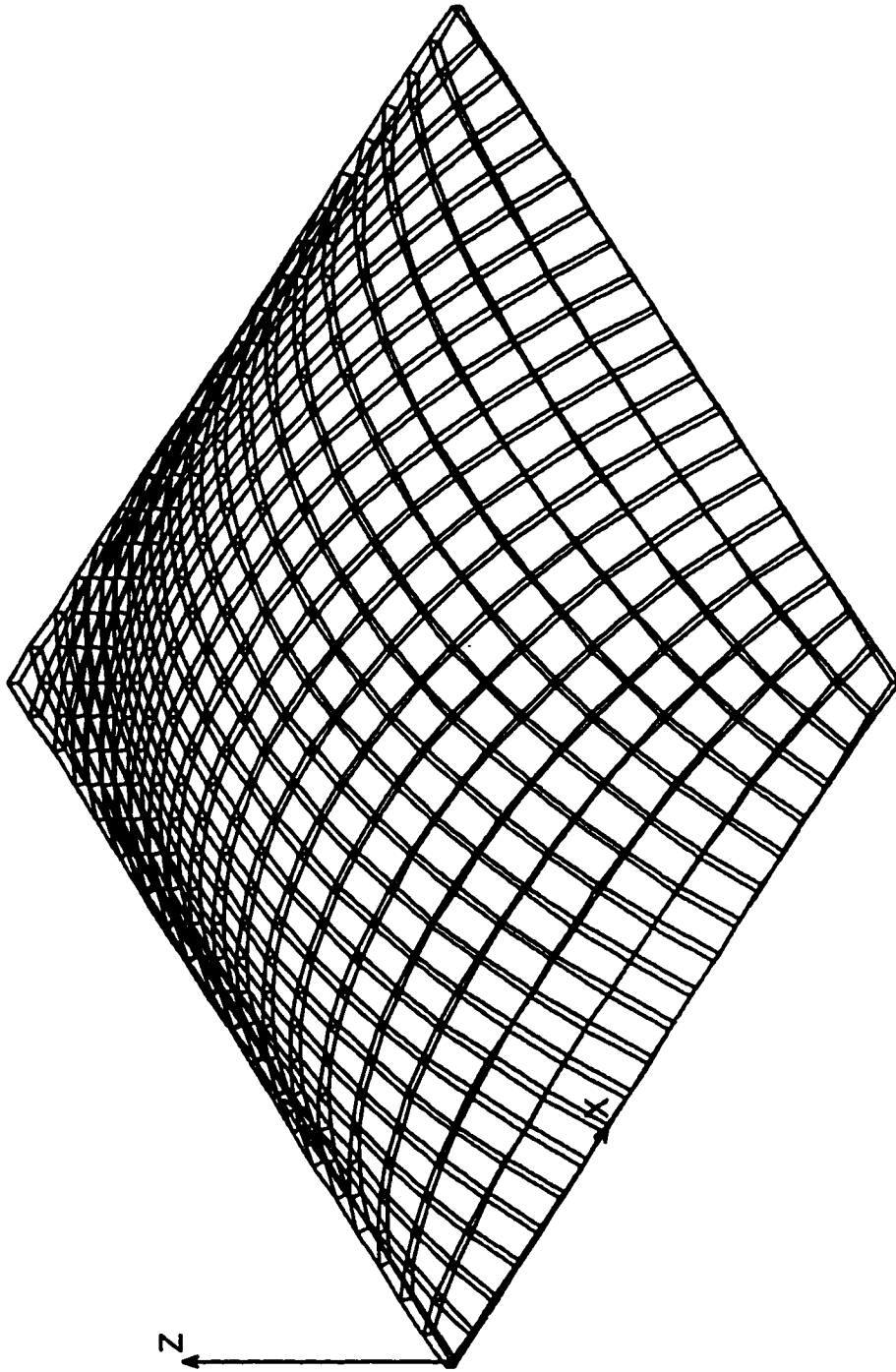
FIGURE 3.42 THE DEFLECTION OF THE PLATE FOR EXAMPLE 3.10

Lin DEF Lc=1
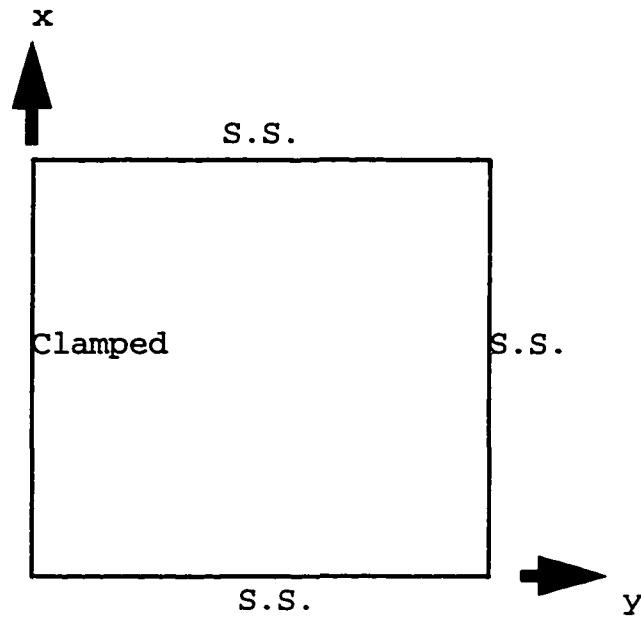
Figure 3.43 the configuration of the plate with boundary
conditions in example 3.11

With the same assumed deflection function as equation
(3.46), the formulations of the strain energy and the work
done by the equivalent moment will be the same as for
example 3.10. Since the boundary conditions are not all
satisfied by the assumed deflection function, the Lagrangian
function L is not only potential energy. The unsatisfied
boundary condition is that the slop at the fixed boundary
must be zero.

$$\frac{\partial v}{\partial x} = 0 \quad \text{for } x=0 \tag{3.52}$$

Since it is extremely difficult to find a continuous
function to force the slop to be zero along the entire edge

x=0, the boundary conditions are only satisfied using Lagrange Multipliers at a finite number of points chosen along the edge x=0. The boundary conditions on the segments between these points are disregarded. In this example, the number of the point is chosen as 9 to provide enough accuracy for the deflection values.

The constraint equations are obtained as follow:

$$G_i(A_{mn}) = \sum_{m=1}^{N} \sum_{n=1}^{N} A_{mn}(m\pi) \sin(n\pi y_i) = 0 \quad i=1 \text{ to } 9 \qquad (3.53)$$

where $y_i = i/10$.

The Lagrangian function L is:

$$L(A_{mn}, \lambda_i) = U - W + \sum_{i=1}^{9} \lambda_i G_i(A_{mn})) \qquad (3.54)$$

Equating the partial derivatives of L with respect to each A_{mn} to zero and combining the result with equation (3.53), there are (N^2+9) linear equations for (N^2+9) unknown coefficients. The deflection function is therefore determined.

The F.E.A. model used for comparison is the same as in example 3.10 with a change in the boundary conditions. The results from the proposed method for different number of terms N are shown in figure 3.44. Figure 3.45 shows the comparison between the F.E.A. model and the proposed method for the deflection curves taken along the section y=0.5. The assumed deflection function converges at N=17. The difference in the maximum deflection (x=0.65) is

approximately 0.90%. The deflection of the entire plate is shown in figure 3.46. The CPU time for calculating deflection by the F.E.A. is 156 sec. The proposed method requires less than 3 sec.

Figure 3.44 the computed deflection function along the section y=0.5

Figure 3.45 the comparison between the F.E.A. model and proposed method(N=17) for the deflection curves along the section y=0.5.

Example 3.12

In this example, the boundary conditions of the unit square homogeneous plate are 2 simply supported edges along x=0 and y=0 and two clamped edges along x=1 and y=1. The formulations of the strain energy U and the work done by the equivalent moment will be the same as in previous example. The constraint equations are obtained as follow:

Lin DEF Lc=1
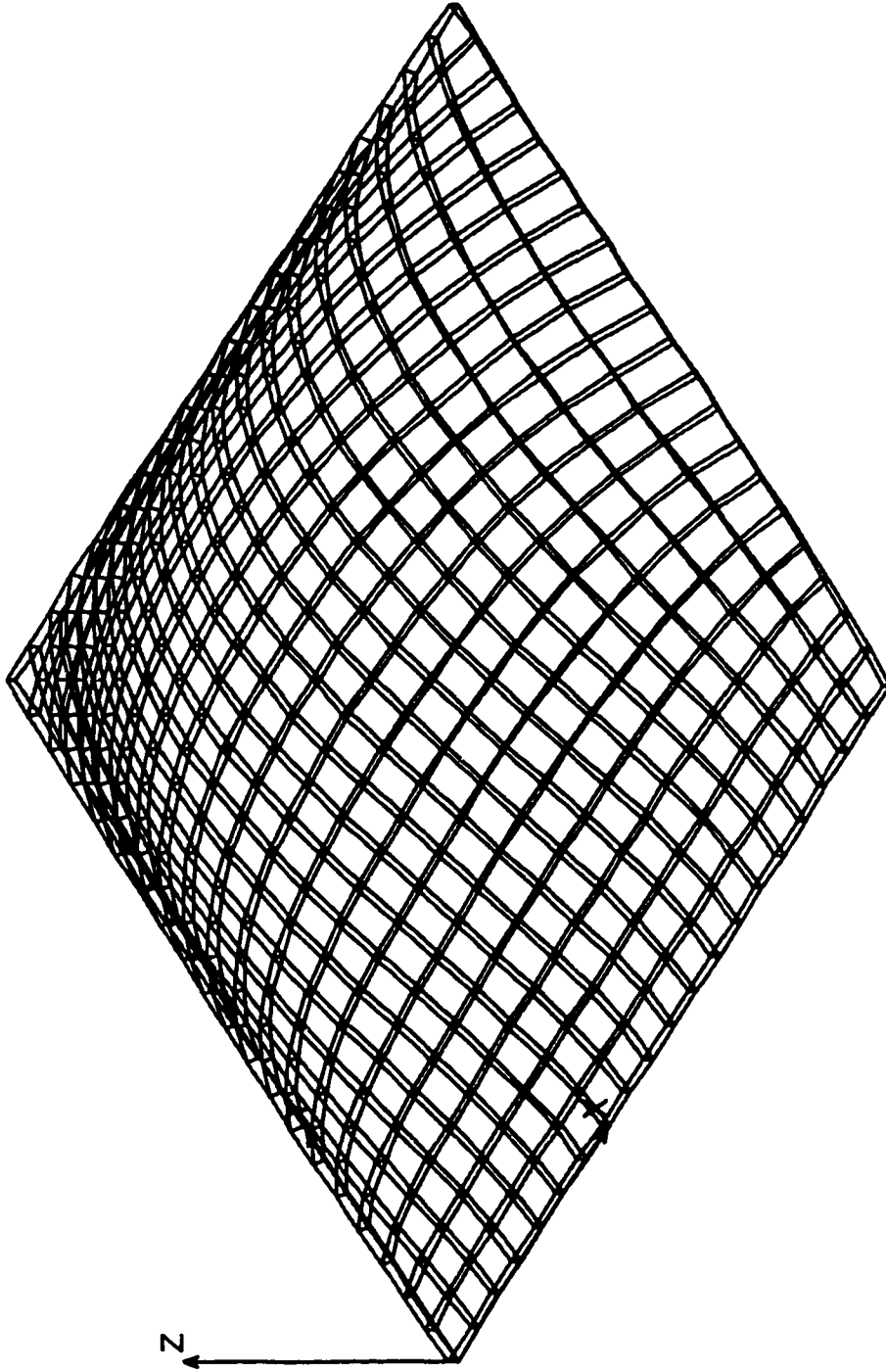
FIGURE 3.46 THE DEFLECTION OF THE PLATE FOR EXAMPLE 3.11

$$G_i(A_{mn}) = \sum_{m=1}^{N} \sum_{m=1}^{N} A_{mn}(m\pi)\sin(n\pi y_i) = 0, \quad I=1 \text{ to } 9 \qquad (3.55a)$$

$$G_j(A_{mn}) = \sum_{m=1}^{N} \sum_{m=1}^{N} A_{mn}(n\pi)\sin(n\pi x_j - 9) = 0, \quad j=10 \text{ to } 18 \quad (3.55b)$$

where $x_i = (i/10)$, $y_i = (i/10)$, $i=1$ to 9

The Lagrangian function L is:

$$L(A_{mn}, \lambda_i) = U - W + \sum_{i=1}^{18} \lambda_i G_i(A_{mn})) \qquad (3.56)$$

Figure 3.47 the configuration of the plate with boundary conditions in example 3-12

Equating the partial derivatives of L with respect to each A_{mn} to zero and combining with equations (3.55a) and (3.55b), there are (N^2+18) linear equations for (N^2+18)

unknown coefficients. The deflection is therefore determined.

The F.E.A. model used for comparison is the same as in example 3.10 with a change in the boundary conditions. The results from the proposed method for different number of terms N are shown in figure 3.48. Figure 3.49 shows the comparison between the F.E.A. model and the proposed method for the deflection curves along the section y=0.5. The assumed deflection function converges at N=17. The difference in the maximum deflection (x=0.7) is approximately 0.9%. The deflection of the entire plate is shown in figure 3.50. The CPU time for calculating deflection by the F.E.A. is 156 sec. The proposed method requires less than 5 sec.
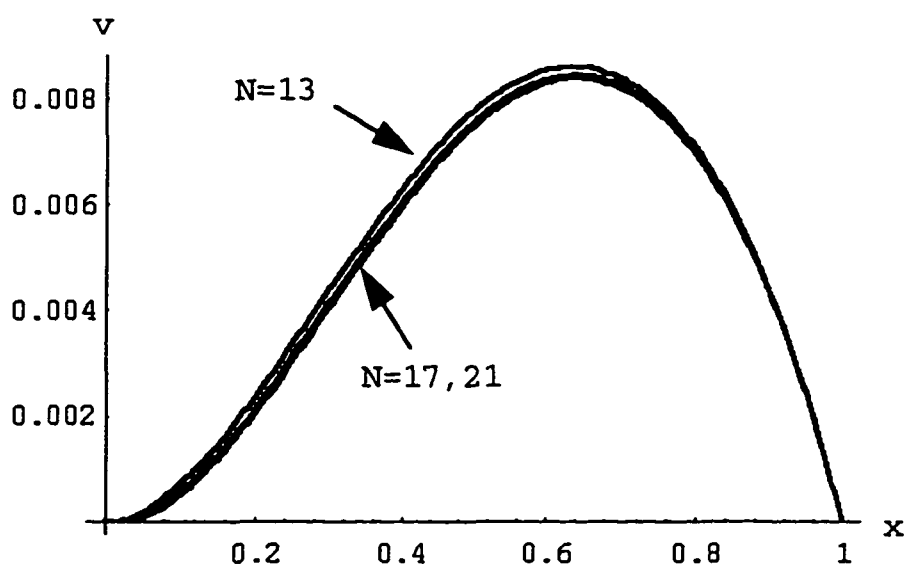

Figure 3.48 the computed deflection function taken along the section y=0.5
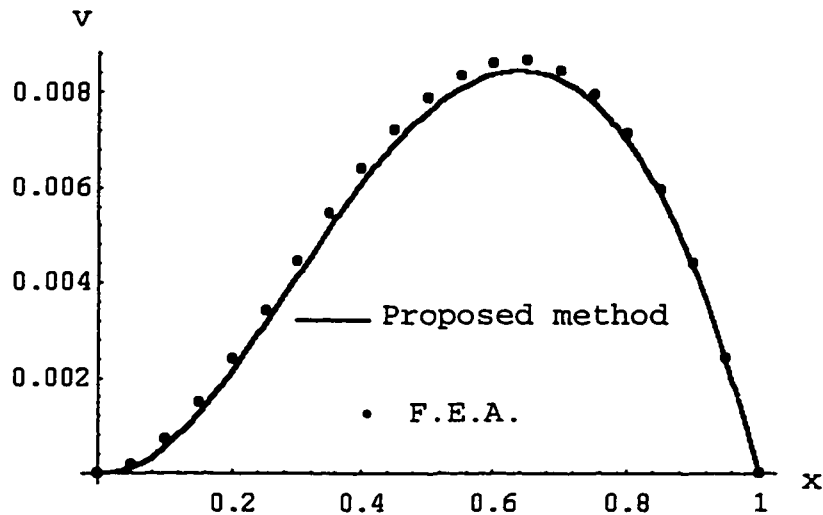
Figure 3.49 the comparison between the F.E.A. model
and the proposed method(N=17) for the deflection curves
along the section y=0.5.

Example 3.13

In this example, the boundary conditions of the unit

square homogeneous plate are 2 simply supported edges along

x=0 and x=1 and two clamped edges along y=0 and y=1. The

formulations of the strain energy U and the work done by the

equivalent moment will be the same as in the previous

example. The constraint equations are obtained as follows:

$$G_i(A_{mn}) = \sum_{m=1}^{N} \sum_{m=1}^{N} A_{mn}(m\pi) \sin(n\pi y_i) = 0, \quad I=1 \text{ to } 9 \qquad (3.55a)$$

FIGURE 3.50 THE DEFLECTION OF THE PLATE FOR EXAMPLE 3.12

Lin DEF Lc=1

97

$$G_j + {}_1(A_{mn}) = \sum_{m=1}^{N} \sum_{n=1}^{N} A_{mn}(m\pi) \sin(m\pi) \sin(n\pi y_j) = 0 \qquad (3.55b)$$
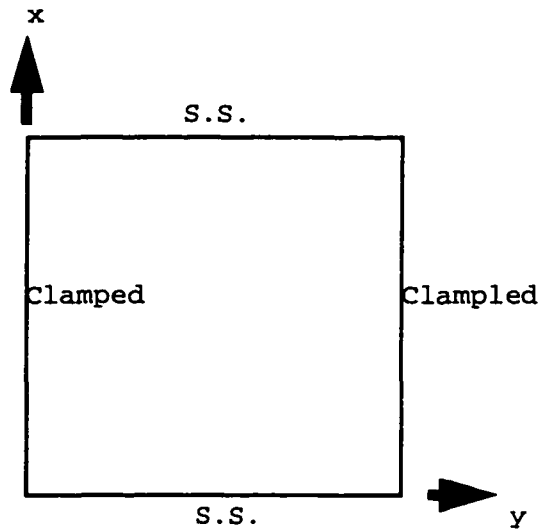
Figure 3.51 the configuration of the plate with the boundary conditions in example 3.13

The Lagrangian function L is:

$$L(A_{mn}, \lambda_i) = U - W + \sum_{i=1}^{18} \lambda_i G_i(A_{mn})) \qquad (3.56)$$

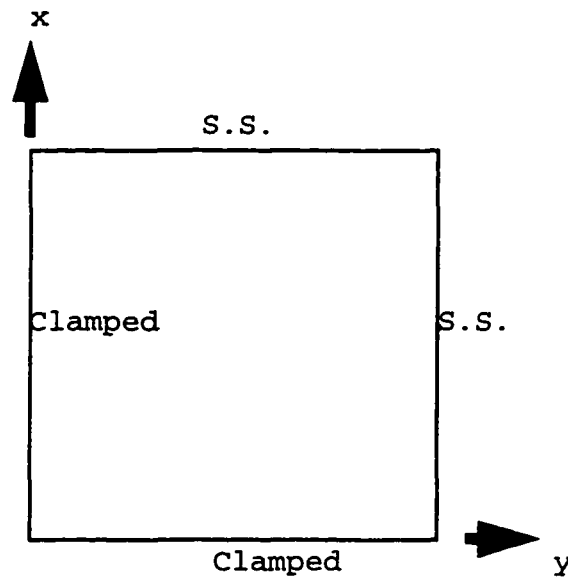Equating the partial derivatives of L with respect to each A_{mn} to zero and combining with equations (3.55a) and (3.55b), there are (N^2+18) linear equations for (N^2+18) unknown coefficients. The deflection function is therefore determined.

The F.E.A. model used for comparison is the same as in example 3.10 with a change in the boundary conditions. The results from the proposed method for different number of terms N are shown in figure 3.52. Figure 3.53 shows the comparison between the F.E.A. model and the proposed method for the deflection curves along the section y=0.5. The assumed deflection function converges at N=17. The difference in the maximum deflection (x=0.5) is approximately 7%. The deflection of the entire plate is shown in figure 3.50. The CPU time for calculating deflection by the F.E.A. is 148 sec. The proposed method requires less than 5 sec.
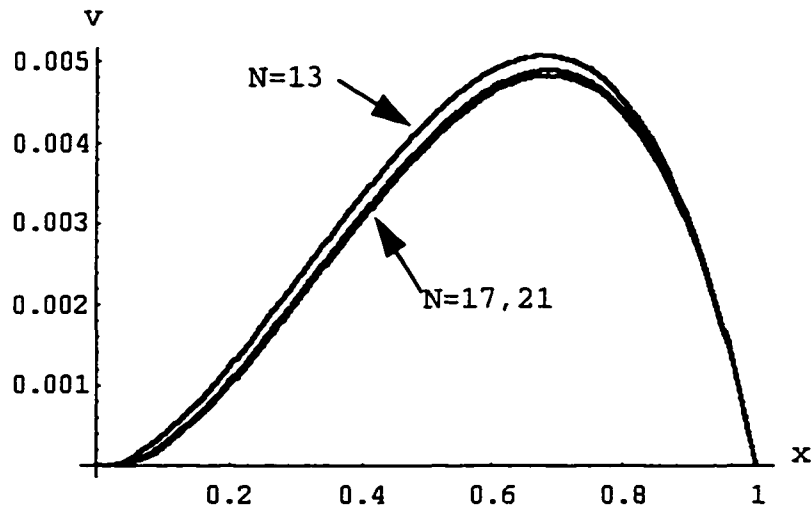

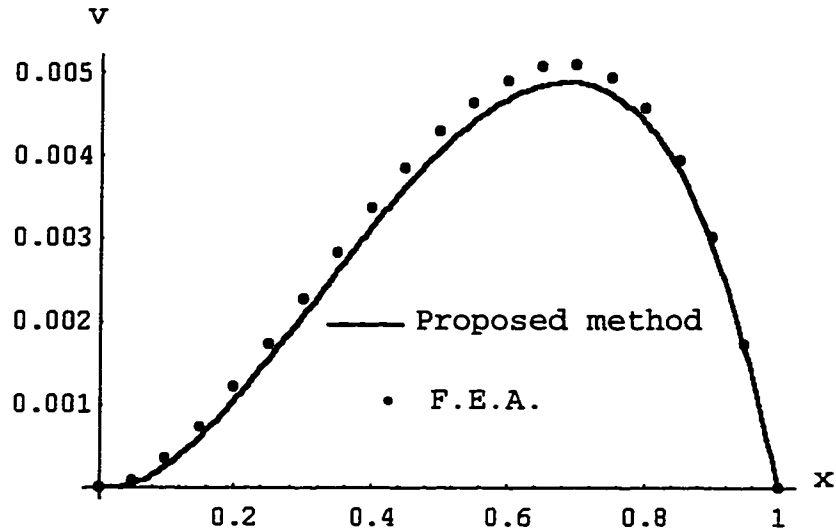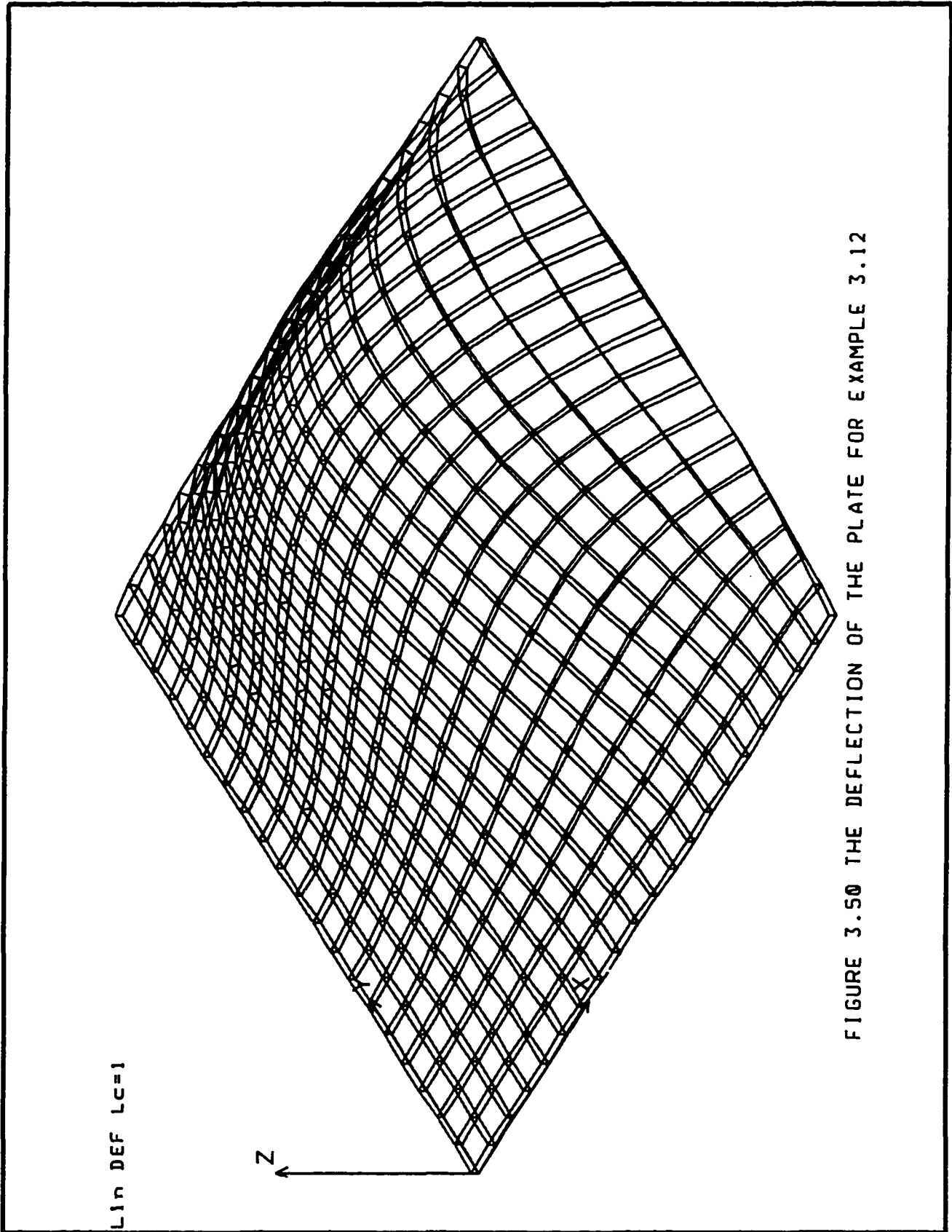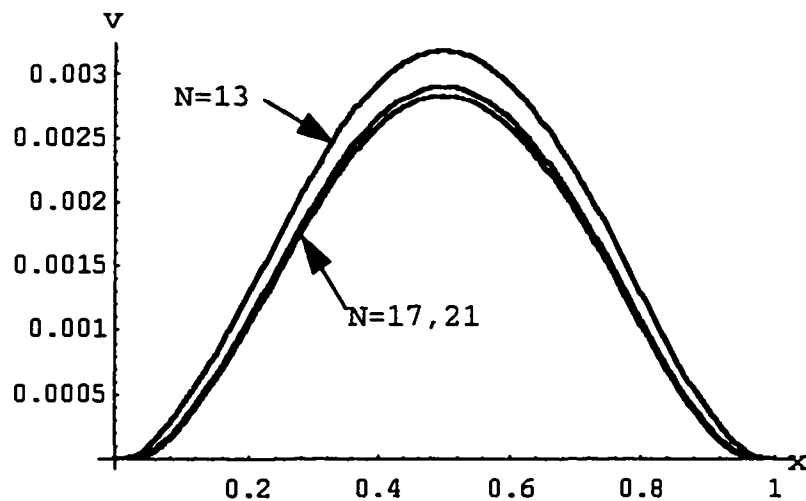Figure 3.52 the computed deflection function taken along the section y=0.5
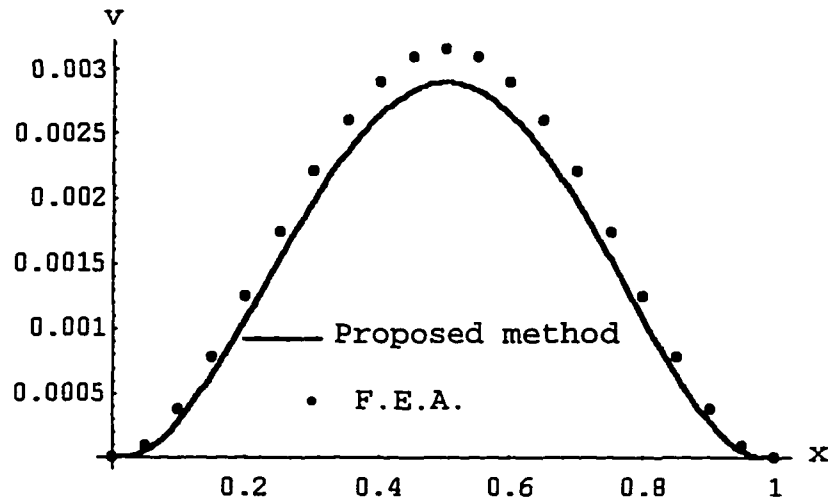
Figure 3.53 the comparison between the F.E.A. model and the proposed method(N=17) for the deflection curves taken along the section y=0.5.

Example 3.14

In this example, a unit square composite plate with all edges simply supported is considered. The temperature of top surface of the plate is 120 degrees. The temperature of the bottom surface of the plate is zero. The temperature distribution through the thickness is assumed linear.

The neutral surface of the plate is obtained by using the same procedure in the beam problems. The total flexural rigidity D of the composite plate is therefore determined by equation (3.41).
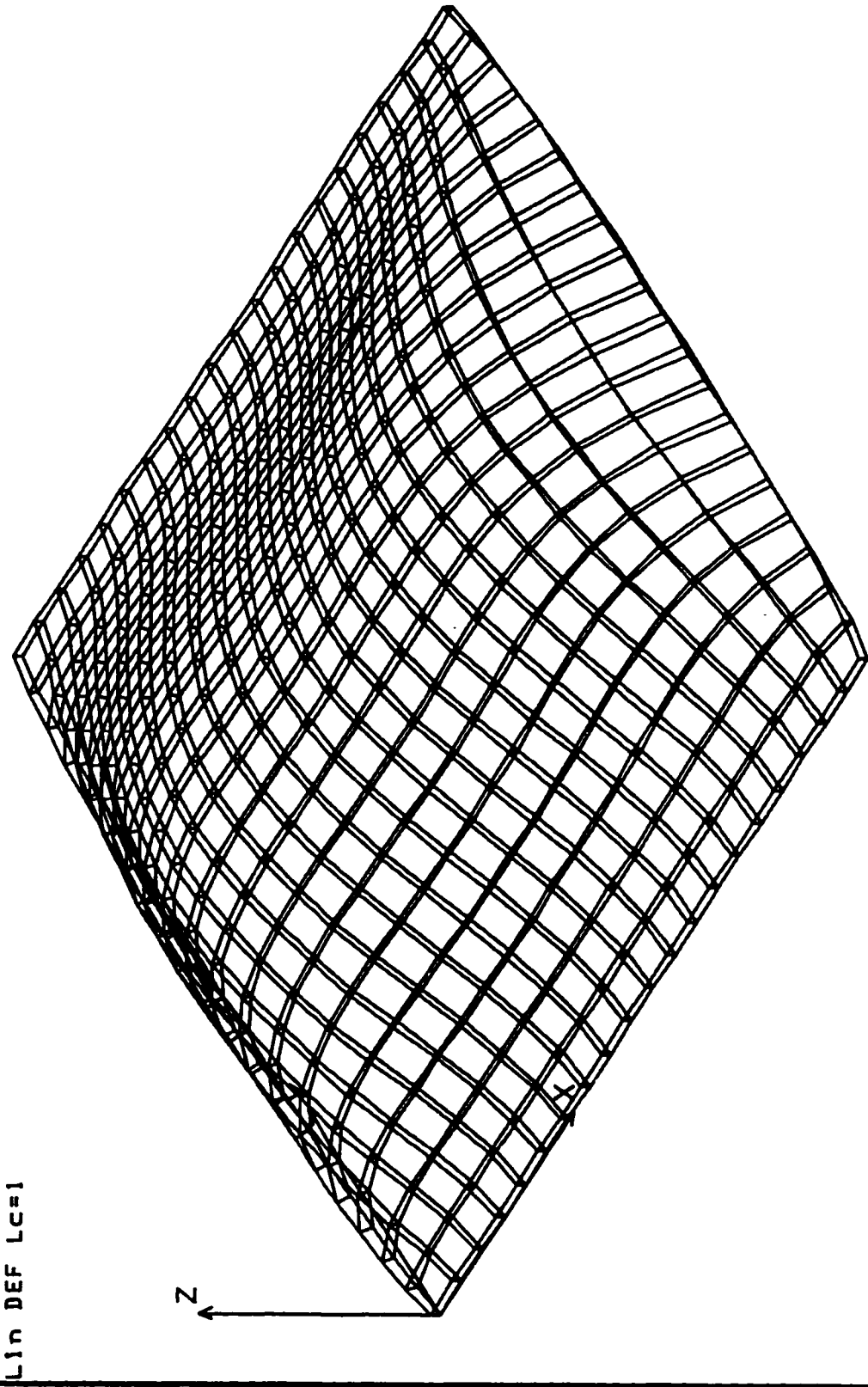
Lin DEF Lc=1

FIGURE 3.54 THE DEFLECTION OF THE PLATE FOR EXAMPLE 3.13

In this example, since the materials are symmetrical about N.S. The N.S. is the central surface throughout the plate.
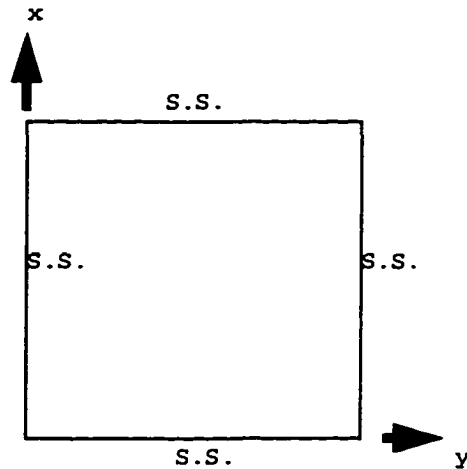
Figure 3.55 The plate for example 3.14
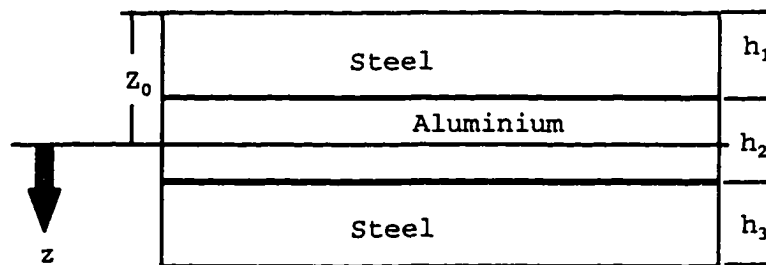
Figure 3.56 The cross section of the plate for example 3.14

The configuration and cross section of the plate are shown in figure 3.56 and the thermal loading for the plate

is as in equation (3.57). The equivalent moment M_t can be determined by substituting in equation (3.43).

$$T(z) = 120(1 - \frac{(z + \frac{h}{2})}{h}))$$

(3.57)

$$M_t(x, y) = \sum_{i=1}^{n} \int_{z_{i-1}}^{z_i} \frac{E_i \alpha_i T(x, y, z)z}{1 - \upsilon_i} dz$$

(3.58)

By assuming the deflection function to be the same as in the previous examples, given in equation (3.46), the strain energy U, the work done by the equivalent moment M_t and potential energy are therefore formulated as:

$$U = \frac{D\pi^4}{8} \sum_{m=1}^{Nm} \sum_{n=1}^{Nn} A_{mn}^2 (m^2 + n^2)^2$$

(3.59)

$$W = \int_0^{L_x} \int_0^{L_y} M_t(\frac{\partial^2 v}{\partial^2 x} + \frac{\partial^2 v}{\partial^2 y}) dxdy$$

(3.60)

$$\Pi = U - W$$

Since the second derivative of a sine function vanishes at the edges of the plate, i.e. $\partial^2 v/\partial x^2 = 0$ at $x=0$ and $x=1$. and $\partial^2 v/\partial y^2 = 0$ at $y=0$ and $y=1$., all boundary conditions are satisfied by the assumed deflection function and no additional constraints are necessary. The Lagrangian function L is equal to the potential energy function.

Using the same approach as in example 3.10, the partial derivatives of L with respect to each A_{mn} set equal to zero. The unknown A_{mn} coefficients are obtained as:

$$A_{mn} = \frac{480\alpha(1 + \upsilon)\,(1 - \cos(m\pi))\,(1 - \cos n\pi)}{\pi^4 hmn} \qquad (3.61)$$

The F.E.A. model used for comparison contains 484 nodes and 300 elements. The results from the proposed method for different number of terms N are shown in figure 3.57. Figure 3.58 shows the comparison between the F.E.A. model and the proposed method for the deflection curves along the section y=0.5. The assumed deflection function converges at N=7. The difference in the maximum deflection (x=0.5) is approximately 8.62%. The shear stress distribution through the thickness of the plate obtained by The F.E.A. and the proposed method are shown in figure 3.58.

Figure 3.57 the assumed deflection function along the section y=0.5
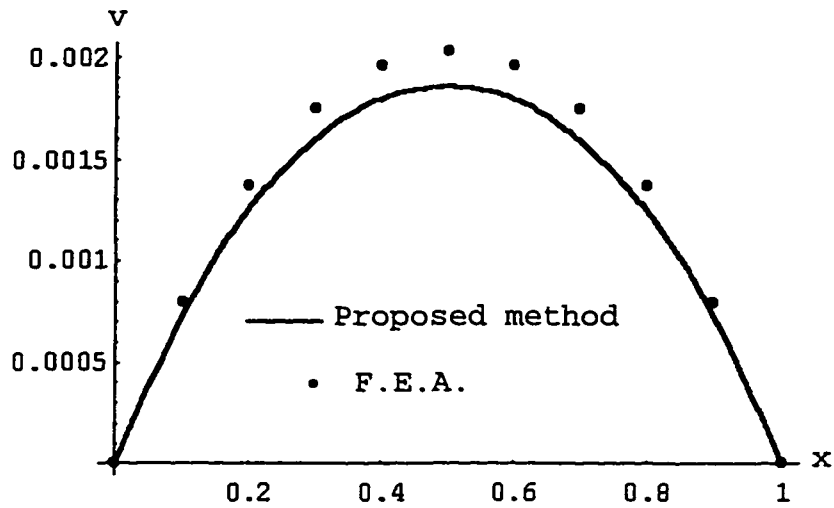
Figure 3.58 the comparison between the F.E.A. model and the proposed method(N=7) for the deflection curves along the section y=0.5.

Figure 3.59 shear stress distributions through the thickness of the plate obtained by The F.E.A. and proposed method

Lin DEF Lc=1
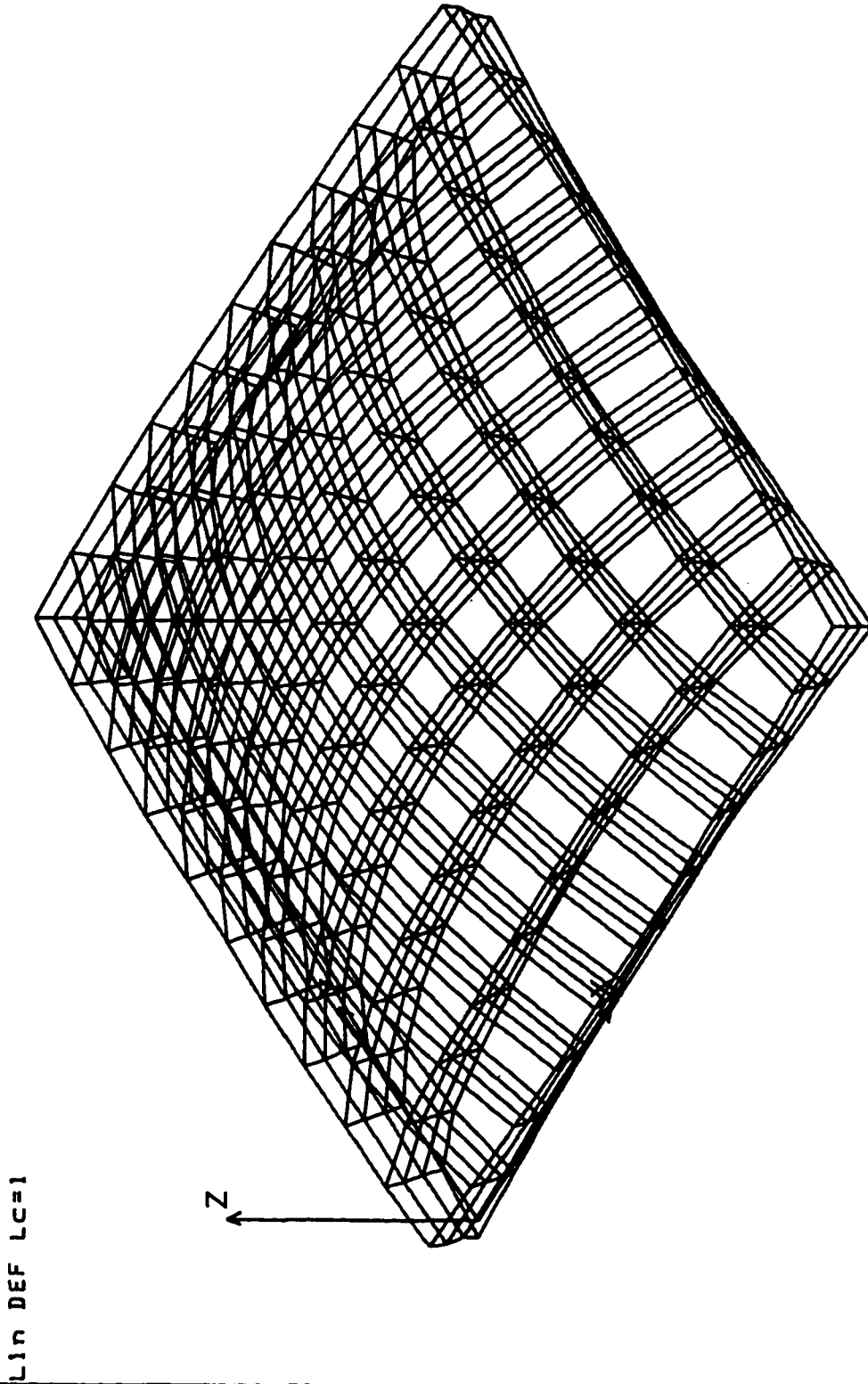
FIGURE 3.60 THE DEFLECTION OF THE PLATE FOR EXAMPLE 3.14

The CPU time for calculating deflection by the F.E.A. is 110 sec. The proposed method requires less than 1 sec. The deflection of the plate is shown in figure 3.60.

Example 3.15

A plate with arbitrarily shaped holes is a common structural element, but is extremely difficult to handle by the classical theory of plates. The finite element method, so far, is the approach that analysts generally use. However, the results from the F.E.A. is not a continuous function. It can only produce the stress and deflection at some discrete points(nodes). In order to obtain the deflection values by F.E.A. which match the same density of the results from the proposed method, F.E.A. would require considerably more CPU time than the proposed method.

In this example, the unit square homogeneous plate with clamped square hole is considered. The edges of the hole are clamped and the boundary of the plate is simply supported.

In the proposed method, a pseudo plate of the same size as the hole can be fitted into the hole, with its boundary clamped. The pseudo plate can then be integrated with the original plate, inside which the hole is located, and analyzed as a whole with the same procedure shown in example 3.10. The pseudo plate inside the hole can be then disregarded.
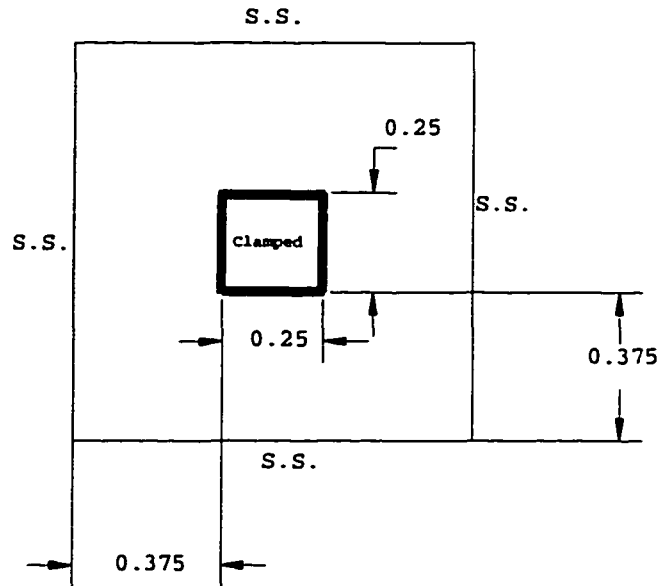
Figure 3.61 The configuration of the plate for example 3.15

By assuming the same deflection function as equation (3.46), the formulation of the Lagrangian function L remains the same. The constraints are zero deflection and zero normal slope along the edges of the hole. In this example, 14 points on the edges of the hole are chosen for the constraints.

The F.E.A. model used for comparison is shown in figure 3.62. This model contains 1040 nodes and 960 elements. Figure 3.63 shows the convergence(N=21) of the proposed method for the deflection curves along the section y=0.375. Figure 3.64 shows the comparison between the F.E.A. model and the proposed method for the deflection curves along the

section y=0.375. The difference in the maximum deflection (x=0.88) is approximately 5.50%.
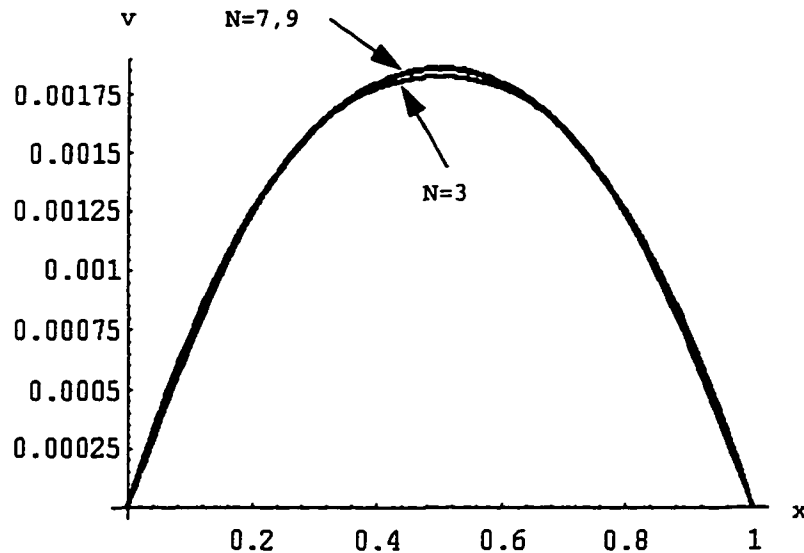

Figure 3.62 The F.E.A. model for example 3.15
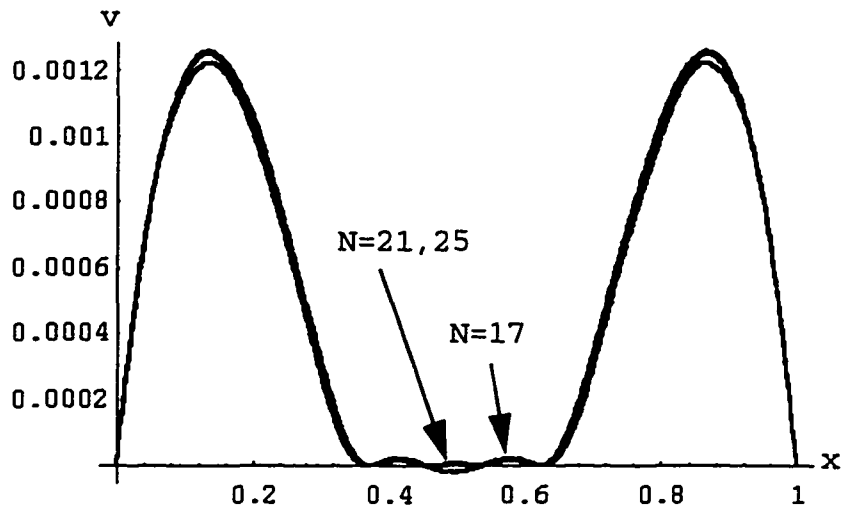

Figure 3.63 the computed deflection function along the section y=0.375

Figure 3.64 the comparison between the F.E.A. model and proposed method(N=21) for deflection curves taken along the section y=0.375.
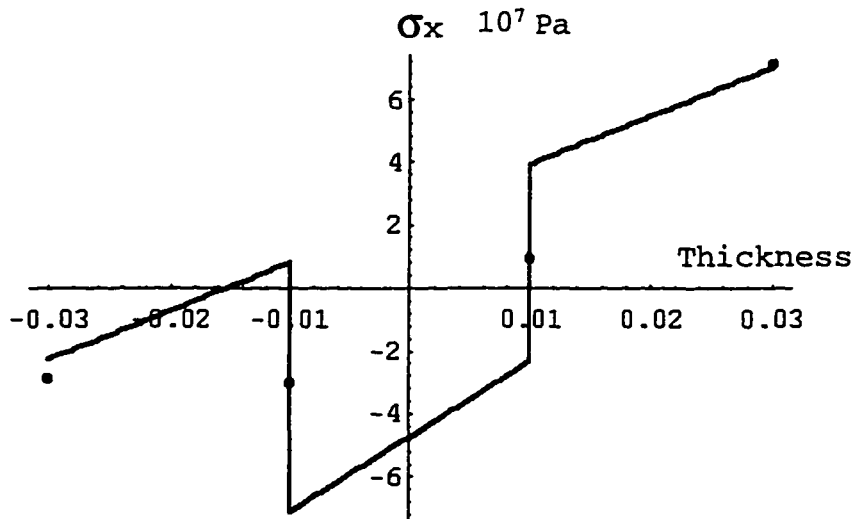
The deflection of the entire plate is shown in figure 3.65. The CPU time for calculating the deflection by the F.E.A. is 223 sec. The proposed method requires less than 4 sec.

Example 3.16

An illustration of the analysis of a plate with a square clamped hole is giving in the previous example. It is a relatively simple problem because the clamped edges can provide the necessary forces to satisfy the boundary conditions and no additional forces are necessary. For the case of a hole with free edges, a different technique is necessary.

Lin DEF Lc=1

FIGURE 3.65 THE DEFLECTION OF THE PLATE FOR EXAMPLE 3.15

Clamped

0.25

Clamped

Free

Clamped

0.25

0.375

Clamped

0.375
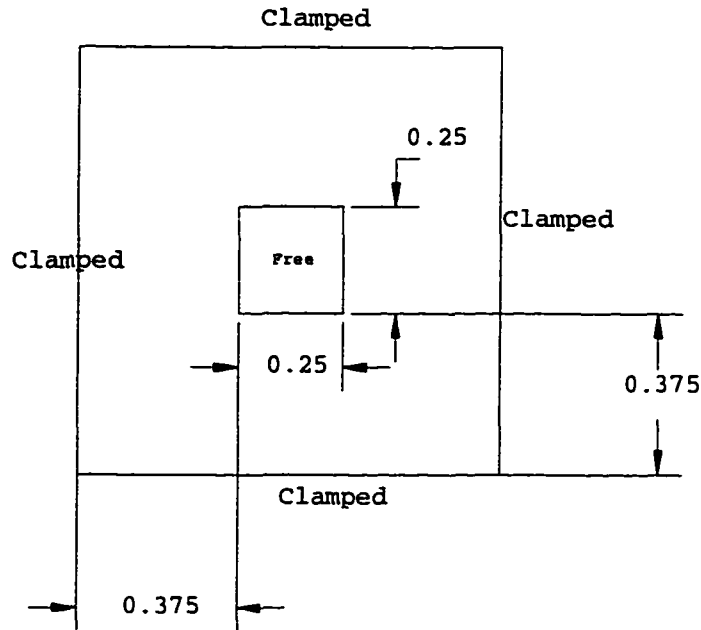
Figure 3.66 the configuration of the plate for example 3.16

Consider a unit square homogeneous clamped plate with the same configuration and subjected to the same thermal loading as in example 3.15. To begin with, a clamped plate without a hole is considered. The temperature loading is transformed to an equivalent moment M_t. The deflection under the equivalent moment M_t is equated to zero by assuming that the equivalent moment M_t is less than Euler loading(critical bucking loading). For the case where the equivalent moment M_t is greater than Euler loading(critical bucking loading), the plate can buckle. Due to the nonlinear behavior of buckling, the proposed method and the linear F.E.A. are unable to determine the buckling deflection of the plate.

The work(W_p) done the equivalent moment M_t when a plate is without a hole is zero by assuming there is no buckling. The work(W_h) done by the equivalent moment M_t over the region where the hole is located is as follows:

$$W_h = \int_{0.375}^{0.625} \int_{0.375}^{0.625} M_t(v'')dxdy \tag{3.62}$$

$$W_p = 0 \tag{3.63}$$

The total work done is:

$$W = W_p - W_h \tag{3.64}$$

The constraints of the plate are:

$$G_i = v'(0, y_i) = 0 \text{ for } i=1 \text{ to } 9 \tag{3.65a}$$

where $y_i = i/10$

$$G_{i+9} = v'(1, y_i) = 0 \text{ for } i=1 \text{ to } 9 \tag{3.65b}$$

where $y_i = i/10$

$$G_{i+18} = v'(x_i, 0) = 0 \text{ for } i=1 \text{ to } 9 \tag{3.65c}$$

where $x_i = i/10$

$$G_{i+27} = v'(x_i, 1) = 0 \text{ for } I=1 \text{ to } 9 \tag{3.65d}$$

where $x_i = i/10$

By assuming the same deflection function as equation (3.46), The strain energy U is the same as in example 3.10. The deflection surface of a clamped plate subjected to the thermal loading is zero and the moments along the edges of the hole can be calculated. Since the moments along the edges of the hole that is free must be zero, external moments are superimposed at the edge of the hole to simulate the effect of a hole.

The F.E.A. model used for comparison is the same as in example 3.15 with different boundary conditions. Figure 3.67 shows the convergence(N=16) of the proposed method for the deflection curve along the section y=0.375. Figure 3.68 shows the comparison between the F.E.A. model and the proposed method for the deflection curves along the section y=0.375. The differen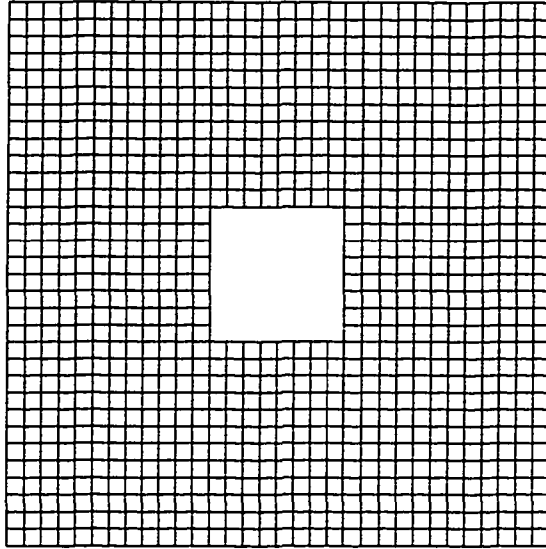ce in the maximum deflection (x=0.5) is approximately 1.26%. The deflection of the plate is shown in figure 3.69. The CPU time for calculating deflection by the F.E.A. is 512 sec. The proposed method requires less than 6 sec.

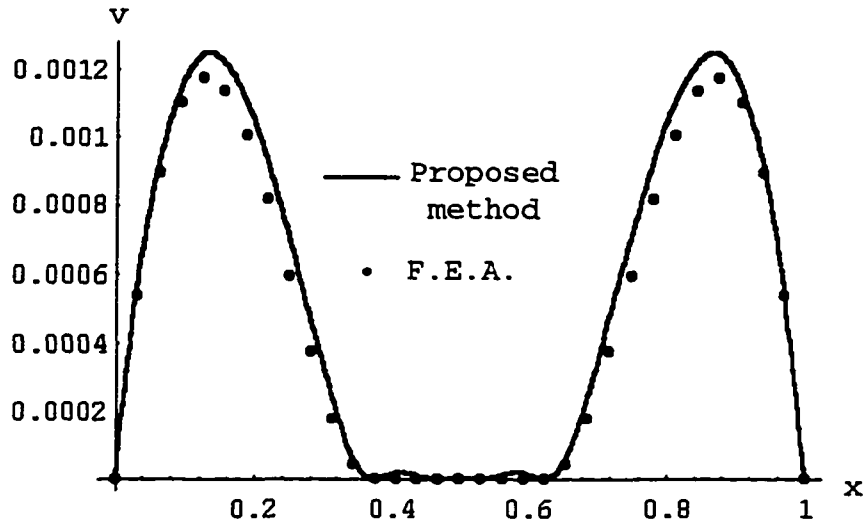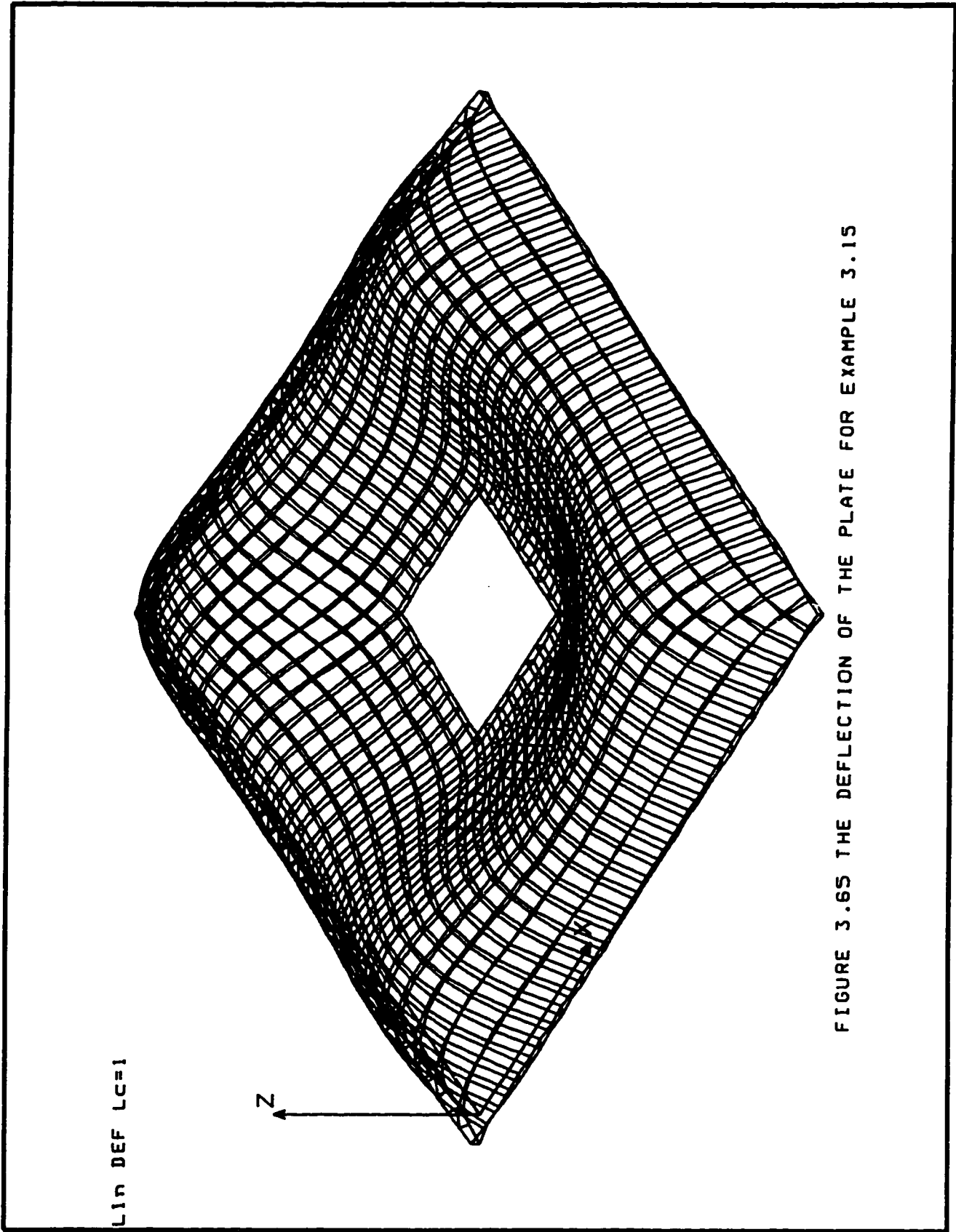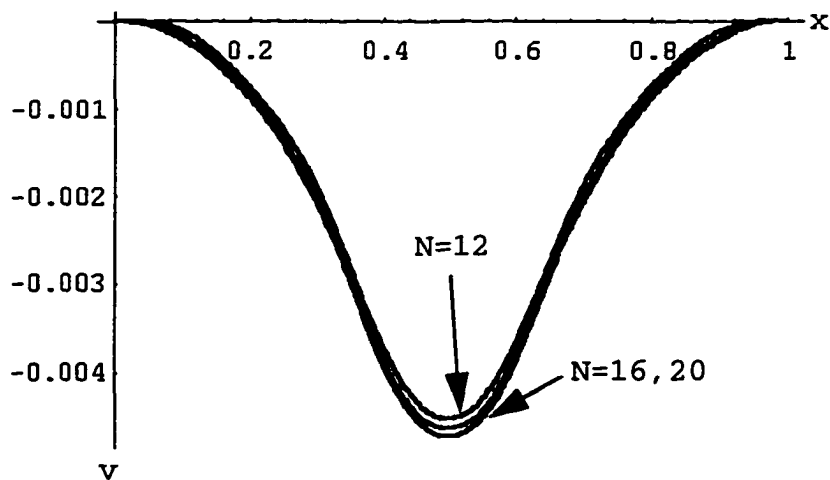Figure 3.67 the computed deflection function(N=12,16,20)
           taken along the section y=0.375
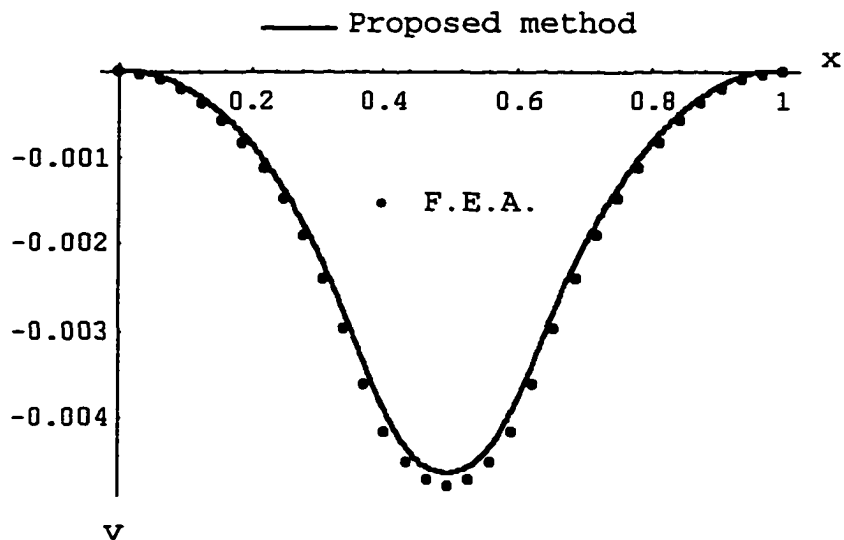
Figure 3.68 the comparison between the F.E.A. model and proposed method(N=16) for the deflection curves along the section y=0.375.

Lin DEF Lc=1

FIGURE 3.69 THE DEFLECTION OF THE PLATE FOR EXAMPLE 3.16
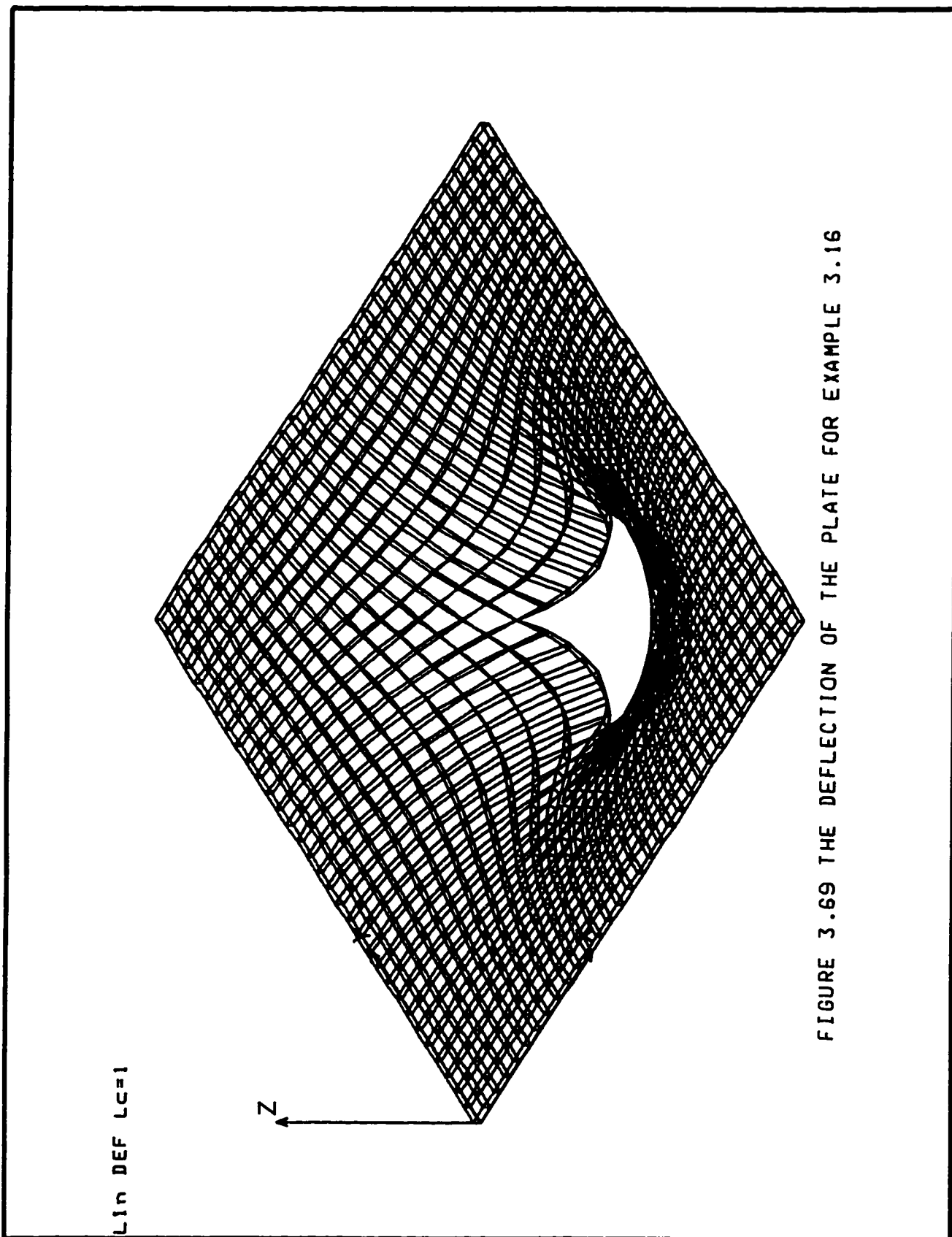
CHAPTER 4
ILLUSTRATIVE EXAMPLES

Introduction

In chapters 2 and 3, the transient temperature field of the structure is obtained by the simplified finite difference method. The thermal deflection of a structure subjected to an assumed thermal loading(temperature field) is also determined by using the proposed method. In order to solve the deflection of a structure under heat input, it is necessary to combine the two schemes discussed in the previous chapters in order to evaluate the deflection of the structure. In other words, the thermal elastic problem is treated in two steps:

(1) calculate the temperature field (transient thermal problem)

(2) transform the temperature field into mechanical loading and then calculate the deflection of the structure

The transient thermal analysis has already been treated in chapter 2. After the thermal loading (temperature field) is evaluated, the deflection of the structure can be determined by the same technique discussed in chapter 3.

116

117

There are six examples in this chapter. Examples 4.1
and 4.2 are beam problems and examples 4.3 to 4.6 are plate
problems. In order to illustrate the accuracy and
computational efficiency of the results from the proposed
method, it is necessary to compare the results and CPU times
with the F.E.A. method.

Example 4.1

In this example, a homogeneous multi-span beam shown in
figure 4.1 is subjected to a heat input(10 Watt) at two
locations (x=0.3 and 0.7) on the top surface of the beam.
The temperature value at x=0.2 to 0.4 and x=0.6 to 0.8
corresponding to the full penetration depth 0.1 can be
directly obtained through the results of example 2.3. The
temperature of the rest of the beam is zero during this
period.
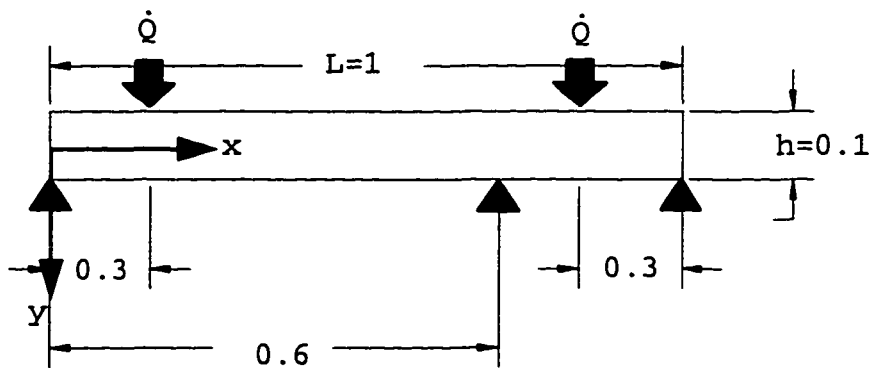
Figure 4.1 The configuration of the beam for example 4.1

After obtaining the temperature field($T(x,y)$) of the beam at that time, the equivalent thermal loading(M_t) can be obtained as:

$$M_t(x) = \sum_{j=1}^{n} b \int_{-h/2}^{h/2} \alpha E T(x, y) y \, dy \qquad (4.1)$$

Where b: the width of the beam

The strain energy can be expressed as function of deflection(v) as given in equation (4.2). The work done by the equivalent loading(M_t) also can be presented as a function of deflection.

$$U = \int_{0}^{l} \frac{EI}{2} (v'')^2 \, dx \qquad (4.2)$$

$$w = \int_{0}^{l} M_t(v'') \, dx \qquad (4.3)$$

The boundary conditions of the beam are v=0 at x=0,0.6L, L and $\partial^2 v/\partial^2 x = 0$ at x=0 and L. By assuming the deflection function v as a Fourier series:

$$v = A_0 + \sum_{n=1}^{N} A_n \cos\left(\frac{n\pi x}{L}\right) + \sum_{n=1}^{N} B_n \sin\left(\frac{n\pi x}{L}\right)$$

The strain energy U is the same as equation (3.26). The work done by the equivalent loading($M_t(x)$) is:

$$W = -\sum_{n=1}^{N} A_n n^2 \pi^2 \int_{0}^{L} M_t(x) \cos(n\pi x) dx - \sum_{n=1}^{N} B_n n^2 \pi^2 \int_{0}^{L} M_t(x) \sin(n\pi x) dx$$

$$(4.4)$$

The constraints are thus:

$$G_1 = A_0 + \sum_{n=1}^{N} A_n = 0 \qquad\qquad (4.5a)$$

$$G_2 = \sum_{n=1}^{N} n^2 A_n = 0 \qquad\qquad (4.5b)$$

$$G_3 = A_0 + \sum_{n=1}^{N} A_n \cos(n\pi) = 0 \qquad\qquad (4.5c)$$

$$G_4 = \sum_{n=1}^{N} A_n n^2 \cos(n\pi) = 0 \qquad\qquad (4.5d)$$

$$G_5 = A_0 + \sum_{n=1}^{N} A_n \cos\left(\frac{n\pi X_s}{L}\right) + +\sum_{n=1}^{N} B_n \cos\left(\frac{n\pi X_s}{L}\right) = 0 \qquad (4.5e)$$

Where $X_s = 0.6L$

The Lagrangian (merit) function L can be formulated as:

$$L = U - w + \sum_{i=1}^{5} \lambda_i G_i$$

By evaluating to zero the partial derivatives of the merit function with respect to parameters λ_i (i=1,2,3,4,5) A_0, A_n and B_n (n=1,2,...N), a set of (2N+6) linear equations with (2N+6) unknowns is obtained. Therefore all the unknown coefficients can be solved and the deflection function of the beam is determined.

The F.E.A. model used for comparison contains the full configuration of the beam with 11111 nodes and 1000 elements. The results from the proposed method for different number of terms N are shown in Figure 4.2. The assumed deflection function converges at N=10. The comparison between the proposed method and the F.E.A. is shown in Figure 4.3. The difference in the maximum deflection(x=0.3) is about 7.47%. The CPU time for calculating deflection by the F.E.A. is 76 seconds. The proposed method requires less than 2 sec.
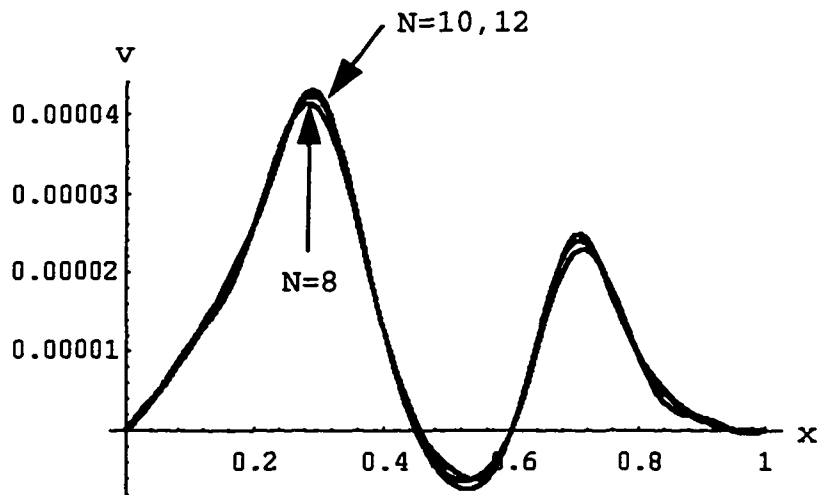
Figure 4.2 the computed deflection for N=8,10,12
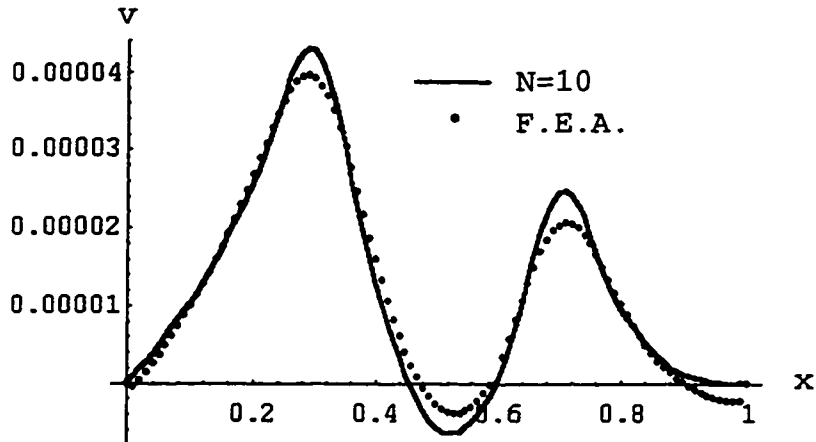
Figure 4.3 comparison of the deflection results from the proposed method(N=10) and the F.E.A.

Again, the results illustrate that the proposed method is much faster than the F.E.A. and that the two methods give very similar deflections values.

Example 4.2

The composite beam shown in figure 4.4 is assumed to be subjected to heat flux at the top surface of the beam. The temperature distribution through the thickness of the beam can be directly obtained from the results of example 2.2. The temperature through the depth of the beam is independent of x.
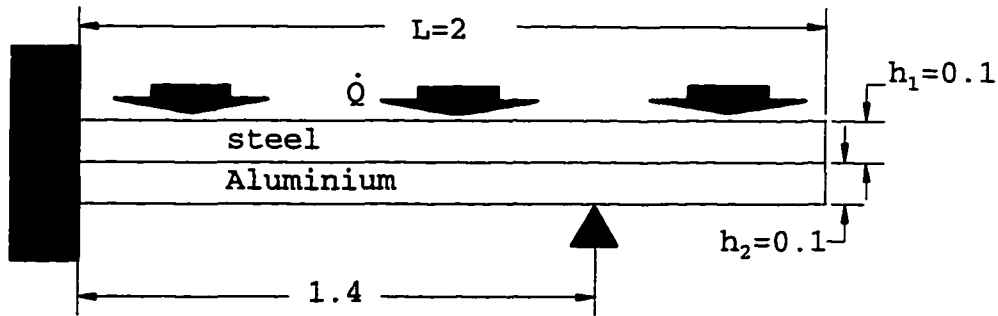
Figure 4.4 The configuration of the beam for example 4.2

The beam is clamped at x=0 and simply supported at x=1.4. The position of N.A.(y_0) and the total flexural rigidity D can be obtained by equations (3.33) and (3.34). The equivalent moment $M_t(x)$ is obtained as follows:

$$M_t = \int_{y_0}^{y_0+h_1} E_1\alpha_1 T y \, dy + \int_{y_0+h_1}^{y_0+h_1+h_2} E_2\alpha_2 T y \, dy \qquad (4.6)$$

The work done the equivalent moment $M_t(x)$ is:

$$w = \int_0^L M_t v'' dx \qquad (4.7)$$

The constraints in this case are:

$$G_1 = A_0 + \sum_{n=1}^{N} A_n = 0 \qquad (4.8a)$$

$$G_2 = \sum_{n=1}^{N} n B_n = 0 \qquad (4.8b)$$

$$G_3 = \sum_{n=1}^{N} A_n n^2 \cos(n\pi) = 0 \qquad (4.8c)$$

$$G_4 = \sum_{n=1}^{N} B_n n^3 \cos(n\pi) = 0 \qquad (4.8d)$$

$$G_5 = A_0 + \sum_{n=1}^{N} A_n \cos\left(\frac{n\pi X_s}{L}\right) + +\sum_{n=1}^{N} B_n \cos\left(\frac{n\pi X_s}{L}\right) = 0 \qquad (4.8e)$$

Where $X_s = 0.7L$

By assuming the same deflection function as in example 4.1, The Lagrangian(merit) function L can be formulated as:

$$L = U - w + \sum_{i=1}^{5} \lambda_i G_i$$

By equating to zero the partial derivatives of the merit function with respect to parameters λ_i (i=1,2,3,4,5) A_0, A_n and B_n (n=1,2,...N), a set of (2N+6) linear equations with (2N+6) unknowns is obtained. Therefore all the unknown coefficients can be evaluated and the deflection function of the beam is determined.

The F.E.A. model used for comparison contains the full configuration of the beam with 441 nodes and 400 elements. The results from the proposed method for different number of terms N are shown in Figure 4.5. The assumed deflection function converges at N=6. The comparison between the proposed method and the F.E.A. is shown in Figure 4.6a. The

difference in the maximum deflection(x=2) is 3.83%. The CPU time for calculating the deflection by the F.E.A. is 37 seconds. The proposed method only requires less than 1 sec.
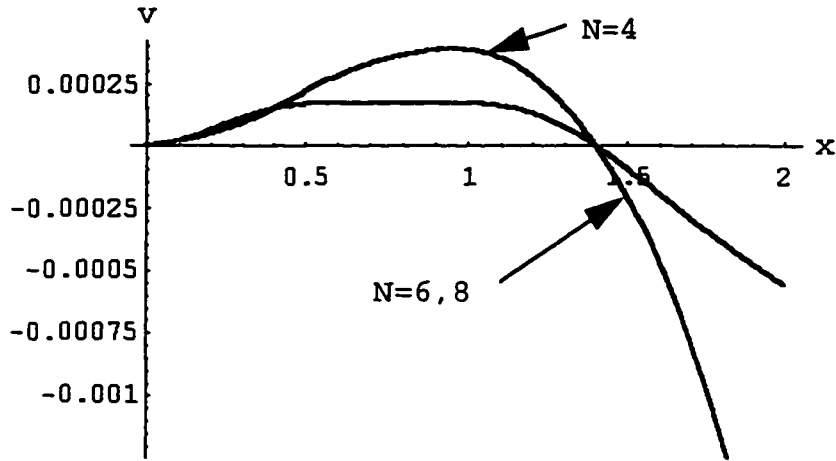

Figure 4.5 the calculated deflection of the beam for N=4,6,8

The stress distribution through the thickness also can be determined by the following procedure:

$$\sigma_{t(i)} = -\alpha_i E_i T \qquad \text{For layer } i(i=1 \text{ to } 2)$$

$$\sigma_{ave(i)} = \frac{E_i}{\sum\limits_{j=1}^{n} h_j E_j} \sum\limits_{i=1}^{n} \int\limits_{y_{i-1}}^{y_i} \alpha_i E_i T dy \qquad \text{For layer } i(i=1 \text{ to } 2)$$

$$\sigma_{m(i)} = \frac{E_i y}{D} \sum\limits_{j=1}^{n} \int\limits_{y_{j-1}}^{y_j} \alpha_j E_j T y dy \qquad \text{For layer } i(i=1 \text{ to } 2)$$

The resultant stress for any layer of the beam can be calculated as $\sigma = \sigma_t + \sigma_{ave} + \sigma_m$. The stress results of the proposed method and the F.E.A. are shown in figure 4.6b. The slip(shear) stress as shown in figure 4.6b which is the

resultant stress difference between the two material is 43 Mpa.
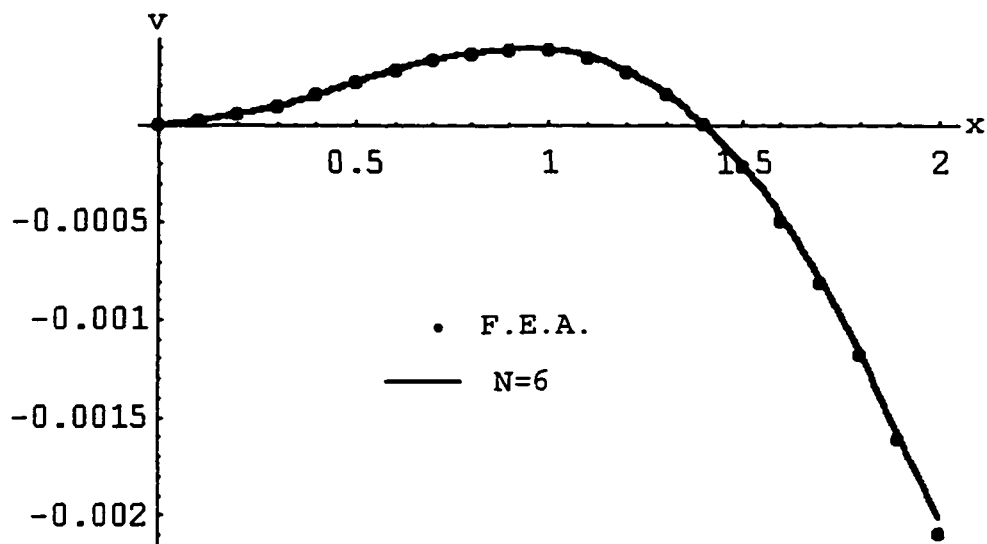
(a)
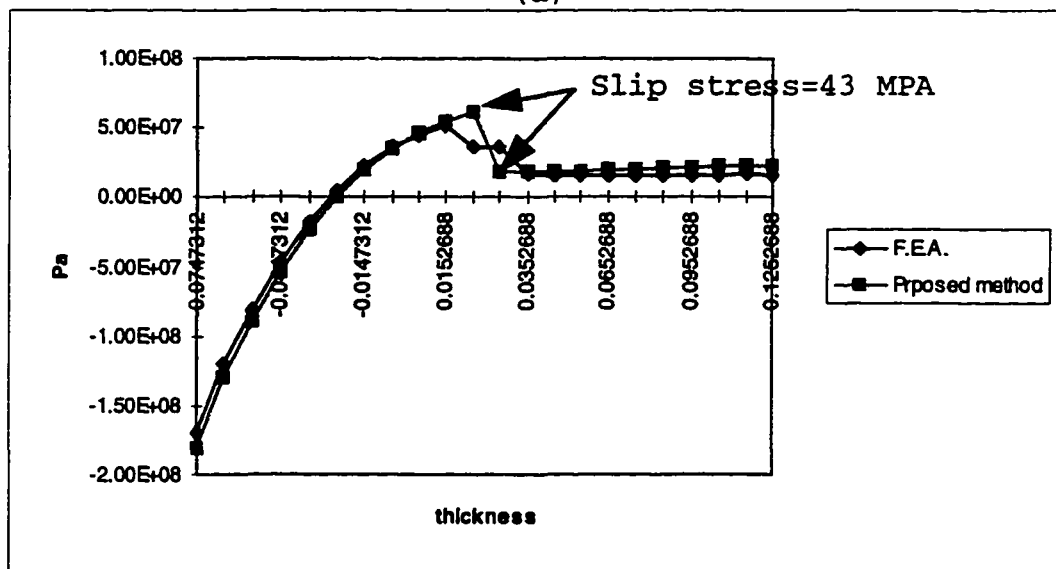
(b)

Figure 4.6 (a) deflection by the proposed method(n=6) and the F.E.A. (b) Resultant stresses σ through the thickness of the beam

Again, the results illustrate that the proposed method is much faster than the F.E.A. and that the two methods give almost identical numerical values.

Example 4.3

The problem of a homogeneous plate subjected an assumed thermal loading with all edges simply supported has been solved in example 3.10. A unit homogeneous square plate as shown in figure 4.7 (thickness(h)=0.1) is considered and subjected to a heat input(20 Watt) at x=0.3 y=0.3 of the upper surface. The assumed deflection function(v) is chosen to be a double sine series for both the x and y direction.
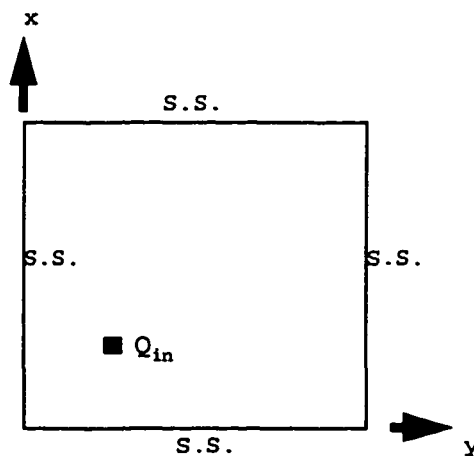
Figure 4.7 the configuration of the plate with boundary conditions in example 4.3

$$v(x, y) = \sum_{m=1}^{Nm} \sum_{n=1}^{Nn} A_{mn} \sin(m\pi x) \sin(n\pi y)$$

The strain energy U which is obtained by equation (3.42) is expressed as :

$$U = \frac{D\pi^4}{8} \sum_{m=1}^{Nm} \sum_{n=1}^{Nn} A_{mn}^2 (m^2 + n^2)^2$$

The temperature distribution $T(x,y,z)$ is developed as in example 2.5. The equivalent moment M_t and The work done by the equivalent moment M_t can be calculated from equations (3.43) and (3.44).

$$M_t(x, y) = \int_{-0.05}^{0.05} E\alpha T(x, y, z) (1 + v)z\,dz \tag{4.9}$$

$$W = \sum_{m=1}^{N} \sum_{n=1}^{N} A_{mn} [\int_{dA} M_t (\frac{\partial^2 v}{\partial x^2} + \frac{\partial^2 v}{\partial y^2})dA \tag{4.10}$$

Since the second derivative of a sine function vanishes at the edges of the plate, i.e. $\partial^2 v/\partial x^2 = 0$ at $x=0$ and $x=1$. and $\partial^2 v/\partial y^2 = 0$ at $y=0$ and $y=1$., all boundary conditions are satisfied by the assumed deflection function and no additional constraint equations are necessary. The Lagrangian function L is equal to the potential energy function in this case.

Using the same approach as in the beam examples, the partial derivatives of L with respect to each A_{mn} are set equal to zero. The unknown A_{mn} coefficients are obtained as:

$$A_{mn} = \frac{4\int_{dA} M_t(x, y) \sin(m\pi x) \sin(n\pi y)dA}{\pi^2 D(m^2 + n^2)} \qquad (4.11)$$

Due to the limitation of the number(32000) of the nodes in F.E.A. software, it is not possible to evaluate the temperature in the plate with equally space mesh. In order to predict a converge solution, three different F.E.A. models are used with the following structure:

1. 20 elements in the x direction, 20 elements in the y direction and 2 elements in the z direction.

2. 40 elements in the x direction, 40 elements in the y direction and 4 elements in the z direction.

3. 50 elements in the x direction, 50 elements in the y direction and 5 elements in the z direction.

The maximum deflections (at x=0.3, y=0.3) and CPU time for the three different F.E.A. models and the results from the proposed method are shown in table 4.1. The estimated converging value from the F.E.A. models using a very large number of elements for the maximum deflection is approximately the same as that calculated by the proposed method (see figure 4.8a).

x10^{-6} F.E.A. CPU time   Sec

Deflection

16 — 14000

15 — 12000

Proposed method:
deflection: 9.7×10^{-6}

14 — 10000

CPU time: 2 sec

13 — 8000

12 — 6000   CPU time

11 — 4000

10 — 2000

F.E.A. deflection

9

$\underline{40 \times 40}$ / 4

$\underline{20 \times 20}$ / 2 $\underline{50 \times 50}$ / 5

$\underline{200 \times 200}$ / 20

(a)

V

0.00001   N=11,15

8. 10^{-6}

6. 10^{-6}

N=9

4. 10^{-6}

N=7

2. 10^{-6}

0.2   0.4   0.6   0.8   1   X
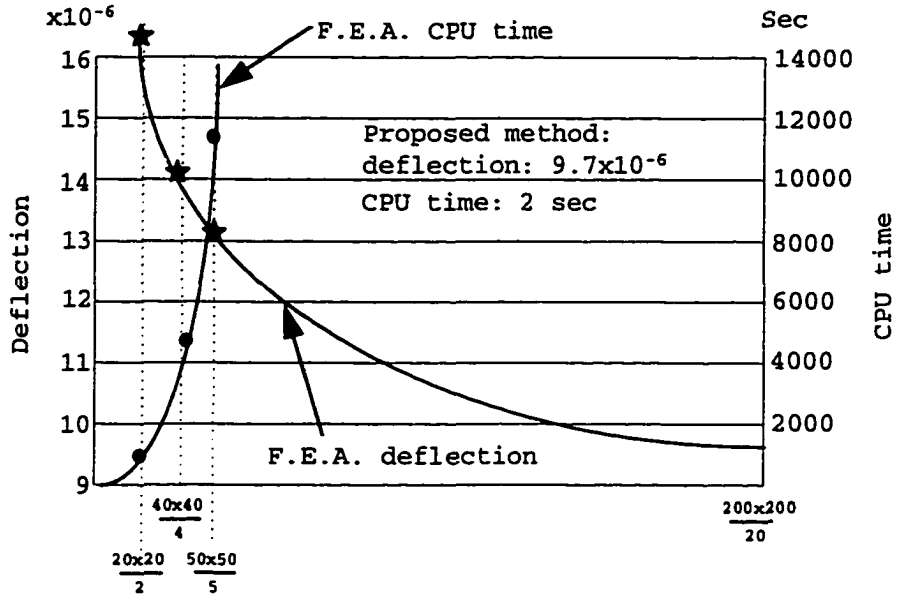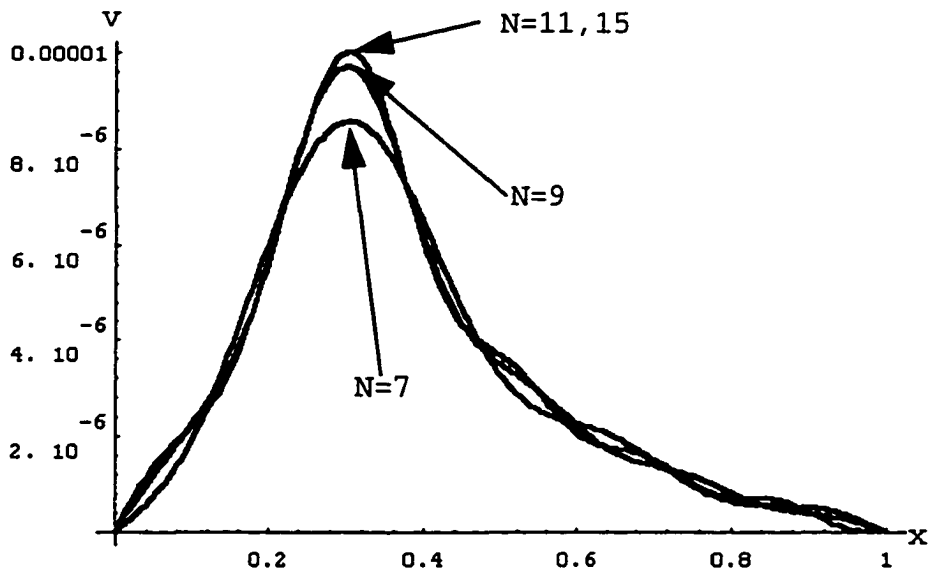
(b)

Figure 4.8 (a) the comparison of the results from the proposed method and the F.E.A. (b) the calculated deflection function along the section y=0.3

Table 4.1

	the CPU time (sec)	the deflection at x=0.3 y=0.3	node/ element #
F.E.A. model 1	386	16.4×10^{-6}	1323/800
F.E.A. model 2	2930	14.12×10^{-6}	8405/6400
F.E.A. model 3	11588	13.23×10^{-6}	15606/12500
The proposed method(N=9)	2	9.7×10^{-6}	

The results from the proposed method and the extrapolated F.E.A. results (figure 4.8a) are almost identical. The results from the proposed method with different number of terms N are shown in figure 4.8b. The assumed deflection function converges at N=11. The CPU times for calculating deflection by the F.E.A. are orders of magnitude larger than those for proposed method.

Example 4.4

In this example, the homogeneous unit square plate with clamped square hole is considered. The edges of the hole are clamped and the boundary of the plate is simply supported. The plate with boundary conditions and subjected to the same heat input in example 4.3 is shown in figure 4.9.

Following the same procedure as in example 3.15, a pseudo plate of the same size as the hole can be fitted into the hole, with its boundary clamped. The pseudo plate can then be integrated with the original plate, inside which the hole is located, and analyzed as a whole with the same procedure as in example 3.15. The pseudo plate inside the hole can be then disregarded.
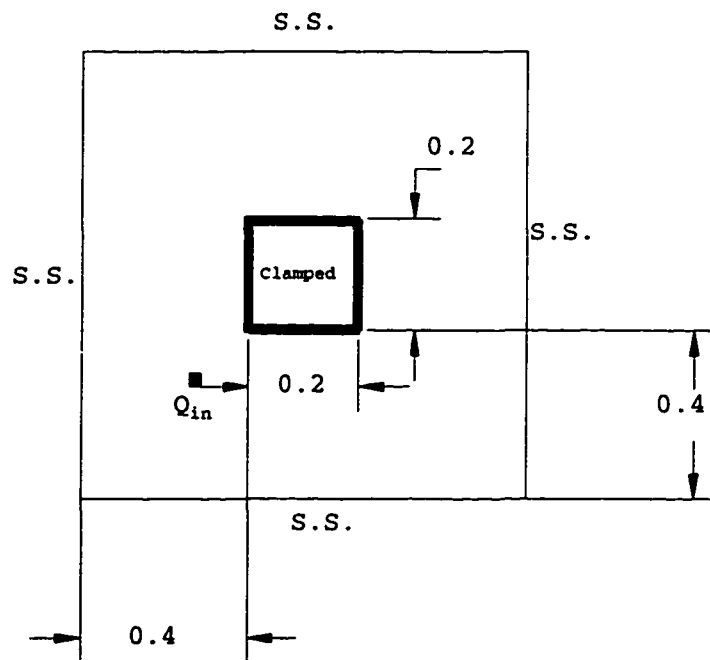
Figure 4.9 The configuration of the plate for example 4.4

By taking the same deflection function as in equation (3.46), the formulation of the Lagrangian function L is the same as in example 4.3. The constraints are zero deflection and zero normal slope along the edges of the hole. In this

example, 14 points are chosen on the edges of the hole for imposing the constraints.

Figure 4.10 shows the convergence (N=21) of the proposed method for the deflection curves along the section y=0.3.
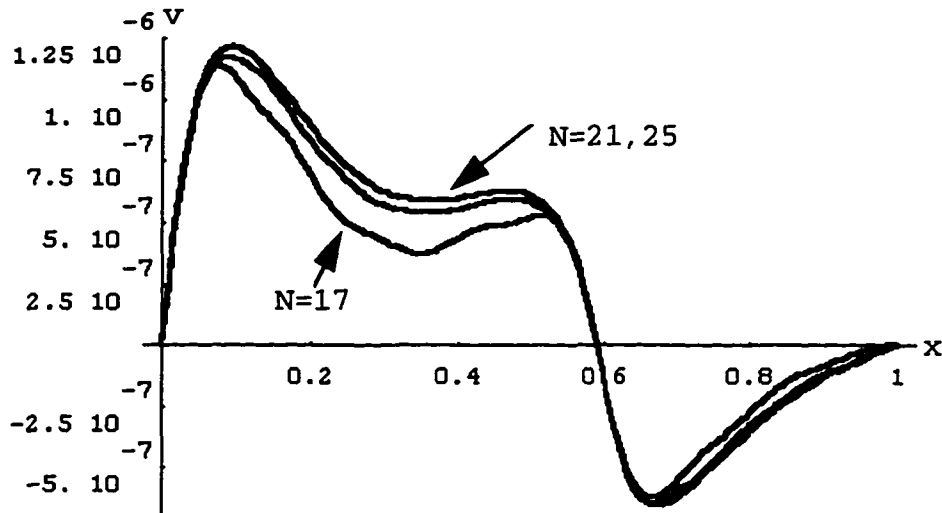
Figure 4.10 the calculated deflection function along the section y=0.3

Due to the accuracy of the results from the proposed method as demonstrated in example 3.15 and checked by the F.E.A. model and the extensive computations necessary for the F.E.A. model to simulate the exact temperature field of the plate, the F.E.A. model is omitted in the rest of the examples in this chapter. The convergence of the proposed method will be considered as the solution without further

checking. The proposed method requires less than 5 sec for obtaining the converging solution.

Example 4.5

In this example, a unit square composite plate with mixed boundary condition is considered. Since the proposed method allows the boundary conditions to be satisfied through the use of Lagrange Multipliers on a finite number of discrete points along the boundary, it is not difficult to handle a mixed boundary condition problem without any major modification of the assumed deflection or energy functions.

The strategy of applying the proposed method to a mixed boundary condition problem is to impose suitable constraints according to the desired boundary conditions at selected discrete points on the boundaries which are not completely satisfied by the assumed deflection function. The plate with the boundary conditions and thermal loading is shown in figure 4.11. The temperature field is the same as obtained in example 4.2.

By assuming the same deflection function and applying the same procedure as in the previous examples, the strain energy U, the work done by the equivalent moment M_t and the potential energy are therefore determined. The additional constraint points are chosen as the following sets of points along the edges of the plate:

set 1: $\partial v/\partial x=0$ at x=0 and y=0.1,0.2,0.3

set 2: $\partial v/\partial x=0$ at x=1.0 and y=0.1,0.2,0.3

set 3: $\partial v/\partial y=0$ at y=0 and x=0.1,0.2,0.3

set 4: $\partial v/\partial y=0$ at y=1.0 and x=0.1,0.2,0.3
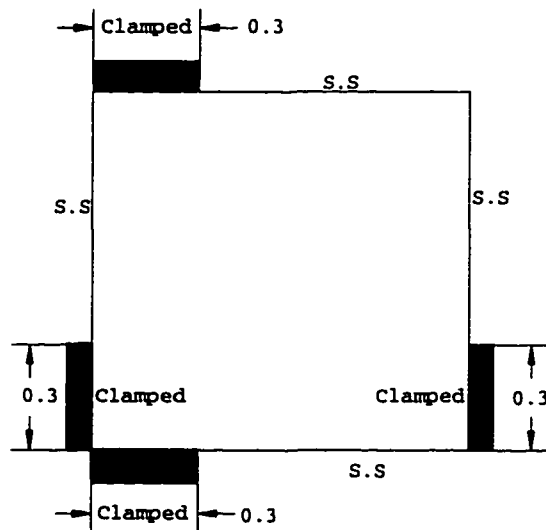
(a)
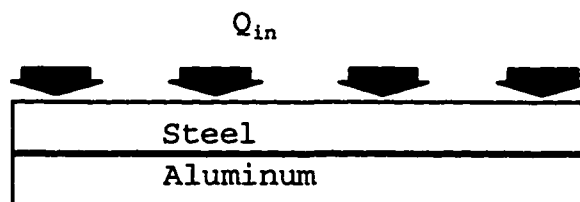
(b)

Figure 4.11(a) the plate with boundary condition for example 4.5 (b) the thermal loading plate for example 4.5

Therefore, The Lagrangian function L is the combination of the potential energy function and 14 constraints. Using the same approach as in example 4.4, The unknown A_{mn} coefficients are obtained. The results from the proposed method for different number of terms N are shown in figure 4.12a. The assumed deflection function converges when N=19 to 21. The proposed method requires less than 5 sec to obtain a converging solution.

The resultant stress for any layer of the beam direction can be calculated as:

$$\sigma = \sigma_t + \sigma_{ave} + \sigma_m$$

where

$$\sigma_{t(i)} = -(1 + \upsilon_i)\alpha_i E_i T \qquad \text{for } i = 1 \text{ to } 2$$

$$\sigma_{ave(i)} = \frac{E_i}{\displaystyle\sum_{j=1}^{n} h_j E_j} \sum_{i=1}^{n} \int_{z_{i-1}}^{z_i} \alpha E_i T(1 + \upsilon_i)dz \qquad \text{for } i = 1 \text{ to } 2, \ n=2$$

$$\sigma_{m(i)} = \frac{E_i y}{D} \sum_{j=1}^{n} \int_{z_{j-1}}^{z_j} \alpha_j E_j T(1 + \upsilon_i)z\,dz \qquad \text{for } i = 1 \text{ to } 2, \ n=2$$

$$\sigma_p = \sqrt{\sigma_x^2 + \sigma_y^2}$$

Because the thermal loading is the same as x and y direction, the stresses in x and y directions (σ_x, σ_y) are the same as the resultant stress. The shear stress (σ_p) can determined by combined the σ_x and σ_y.
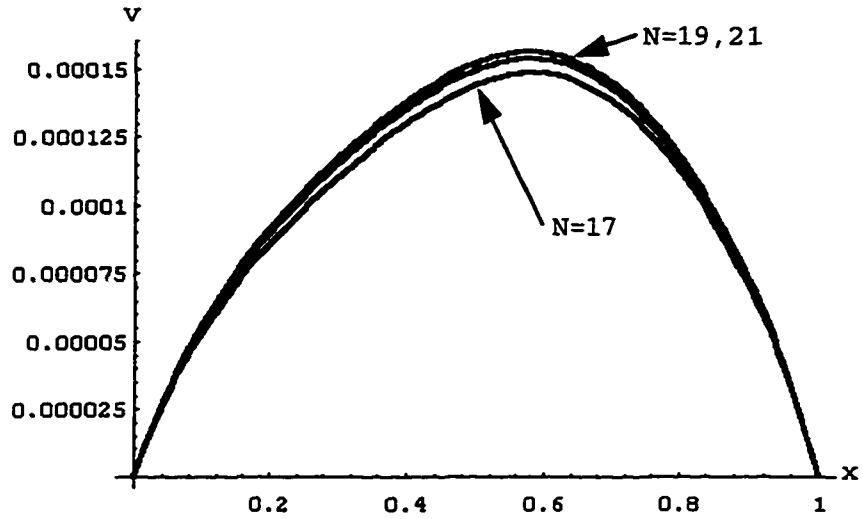
(a)
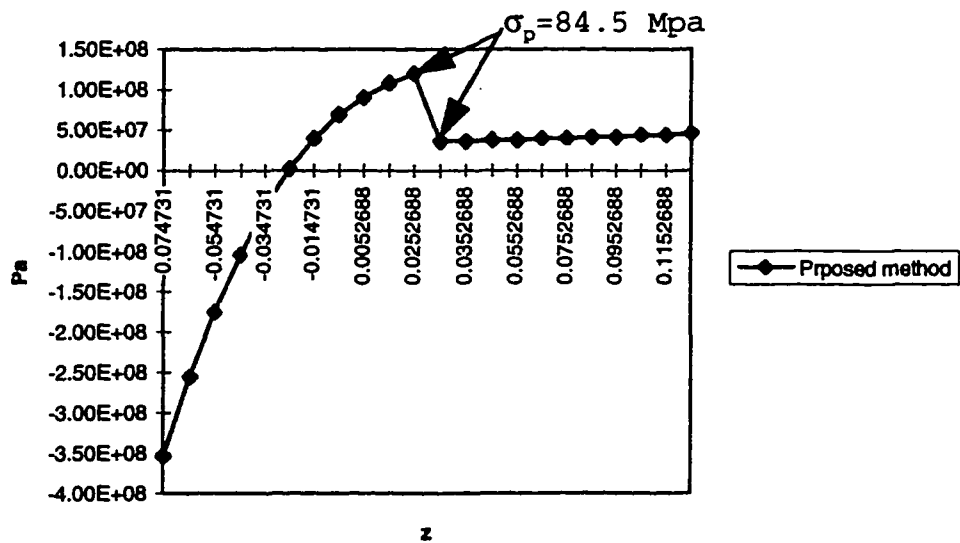
(b)

Figure 4.12 (a) the calculated deflection function along the section y=0.5 (b) Resultant stress through the thickness of the plate

The stress results from the proposed method and the F.E.A. are shown in figure 4.12b. The slip(shear) stress as shown in figure 4.12b which is the difference of the resultant stress between the two material is 84.5 Mpa.

Example 4.6

An illustration of how to analyze a plate with a square free hole is given in example 3.16. Consider a clamped composite plate with a central square hole to be subjected to the same thermal loading given in example 4.5 as shown in figure 4.13. The cross section of the plate is also assumed to be the same as in example 4.5.
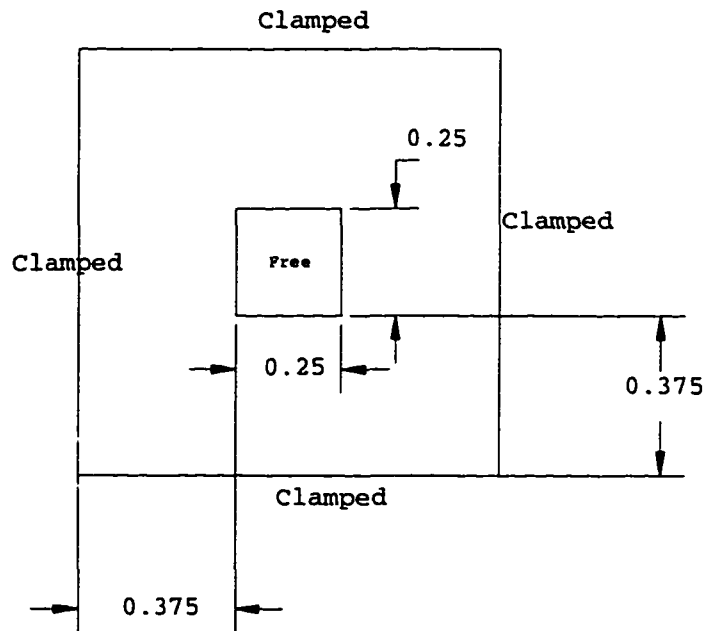
Figure 4.13 the configuration of the composite plate for example 4.6

Following the same procedure as in examples 4.5 and 3.16, the temperature loading is transformed to an equivalent moment $M_t(x,y)$ and the work(W_p) done by the equivalent moment M_t and the work(W_h) done by the equivalent moment M_t over the hole region are calculated.

$$W_h = \int_{0.375}^{0.625} \int_{0.375}^{0.625} M_t(x, y) v'' dx dy \qquad (4.12)$$

$$W_p = 0 \qquad (4.13)$$

The total work done is:

$$W = W_p - W_h \qquad (4.14)$$

The rest of the procedure of obtaining the deflection function is the same as in example 3.16. Figure 4.14 shows the convergence(N=16) of the proposed method for the deflection curve along the section y=0.375. The CPU time for calculating the deflection function by the proposed method in order to obtain the converging solution is less than 5 sec.
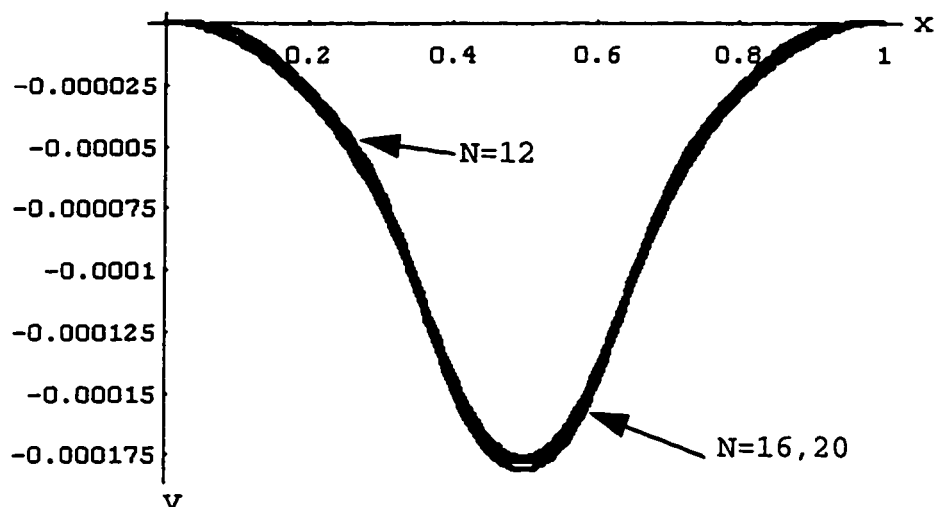
Figure 4.14 the computed deflection function(N=12,16,20)
taken along the section y=0.325

CHAPTER 5
CONCLUSIONS AND RECOMMENDATIONS

Conclusions

It can be concluded from this study that the proposed method provides an excellent tool for the analysis of a wide variety of thin elastic structures subjected to thermal loading.

The proposed method can be used to treat almost all type of thin elastic structures with different heat inputs and boundary conditions. The main advantage of the proposed method is that the boundary conditions can be changed without major modification of the formulation as illustrated in the different cases considered in this studies.

The proposed method also can be applied to many plate problems with discrete and mixed boundary conditions as illustrated in example 4.5 and for plates with different shapes and types of holes. In all these cases, the boundary conditions can be changed without major modification of the formulation.

Whenever applicable, the proposed method has several advantages as summarized in the following:

140

1. The proposed method provides continuous (closed form) expressions for the deflection and stress solution while the F.E.A. only provides discrete results at the nodes in the considered mesh.

2. The F.E.A. can not directly provide the slip(shear) stress at the common surface of two different materials for a composite material structure which is subjected to a thermal loading. The proposed method can readily determine this information.

3. The proposed method can evaluate the converging solution in significantly shorter CPU time for both thermal loading and elastic structural analysis.

4. Very large F.E.A. models with fine meshes or special mesh distributions may be needed for some problems in order to obtain the same converging results as the proposed method. For example, in example 4.3, the 12500 equal size elements model requires about 3 hours CPU running time to evaluate the results and this model still does not converge. On the other hand, less than 5 seconds are required to obtain the converging solution by the proposed method.

Recommendations

The proposed method, although possessing valuable advantages in analyzing thermal deflection and stress in thin elastic structural elements, has the following disadvantages:

1. The finite difference segment of the proposed method can only obtain numerical temperature distributions (not continuous functions), the size of the control volume in the transient thermal analysis becomes very important in providing the closest thermal equivalent loading.

2. For a clamped beam or a clamped plate, there are zero deflection results due to the nature of the thermal equivalent moment. However, if the load is close to or greater than the Euler load, the structure undergoes buckling and the proposed method cannot deal with this non-linear condition to determine the deflection.

The following studies are recommended for future extension of the method presented here:

1. It is suggested that an efficient procedure should be developed in order to apply the proposed method to problems with combined thermal loading and mechanical loading. This should not present any

difficulties since superposition can be used in this case.

2. It is suggested that the proposed method is extended to deal with non-linear problems such as beams or plates with large deflections by iterative or piece-wise linear analysis or averaging techniques.

3. It is suggested that a procedure is developed to apply the proposed method for structures where buckling can occur.

4. It is suggested to extend the proposed method for treating structures subjected to fluctuing thermal loading in order to predict their fatigue life.

APPENDIX

DETAILED ILLUSTRATION OF THE PROCESS OF DETERMINING THE THERMAL DEFLECTION AND STRESS FOR A COMPOSITE BEAM SUBJECTED TO A GIVEN HEAT INPUT

Consider a composite beam with boundary conditions and subjected to heat input(Q_{in}=10 Watt for 120 seconds) at x=0.3 on the top surface of the beam as shown in figure A.1. The transient temperature distribution for the beam at the end of the heating time is first obtained before calculating the thermal deflection.
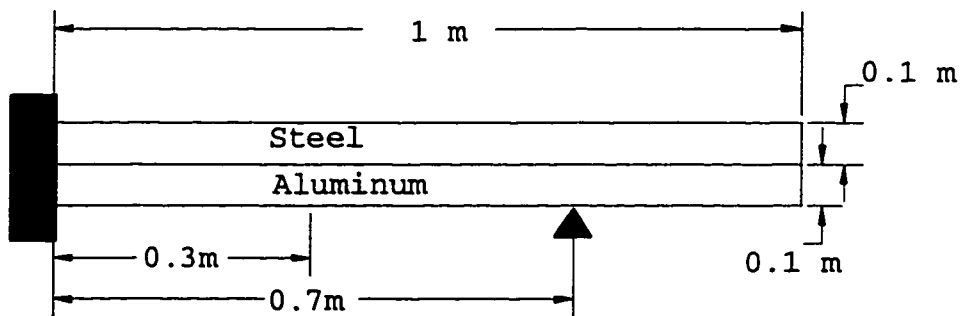
Figure A.1 The configuration of the beam

Width of the beam, b=0.01 m
Material 1 : Steel
Density of material ,ρ_1=7900 (Kg/m^3)
Thermal conductivity K_1 = 45 (W/m-°K)
Specific heat c_1=460 (J/kg-°K)
Young's Modulus of elasticity E_1=2.1x10^9(Pa)
Thermal diffusivity β_1= K_1/($\rho_1 c_1$)=1.238x10^{-5}(W-m^2/J)

144

Material 2: Aluminum
Density of material,ρ=2700 (Kg/m^3)
Thermal conductivity, K = 200 (W/m-$^{\circ}$K)
Specific heat, c=900 (J/kg-$^{\circ}$K)
Young's Modulus of elasticity E=7.9x10^8(Pa)
Thermal diffusivity β_2= K_2/($\rho_2 c_2$)=8.230x10^{-5}(W-m^2/J)

The Temperature Distribution

The temperature distribution for the beam is calculated by using the simplified finite difference method. The first step is to calculate the surface area and volume of each control volume (layer) by selecting the thickness(Δh) of the incremental layer in the first material (Steel) as 0.01 m to allow for 10 penetration steps. In order to simulate the temperature at the position of the heat input, the radius of the control volume (layer) should has much smaller volume than the other layers and is taken as half of Δh and the finial temperature of layer 1 can be assumed to be the temperature at the position of the heat input.

The radius and required heat penetration times (calculated from equation (A.1)) of the control volumes are shown in table A.1.

$$t_p = 0.0891 \frac{D_p^{2}}{k} \qquad\qquad (A.1)$$

Table A.1

Control volume #	D_p	t_p
1	0.005	0.1578
2	0.015	1.4202
3	0.025	3.9449
4	0.035	7.7320
5	0.045	12.7815
6	0.055	19.0933
7	0.065	26.6675
8	0.075	35.5041
9	0.085	45.6031
10	0.095	56.9644
11	0.105	69.5880
12	0.115	93.4741
13	0.125	98.6225
14	0.135	115.0333
15	0.145	132.7065
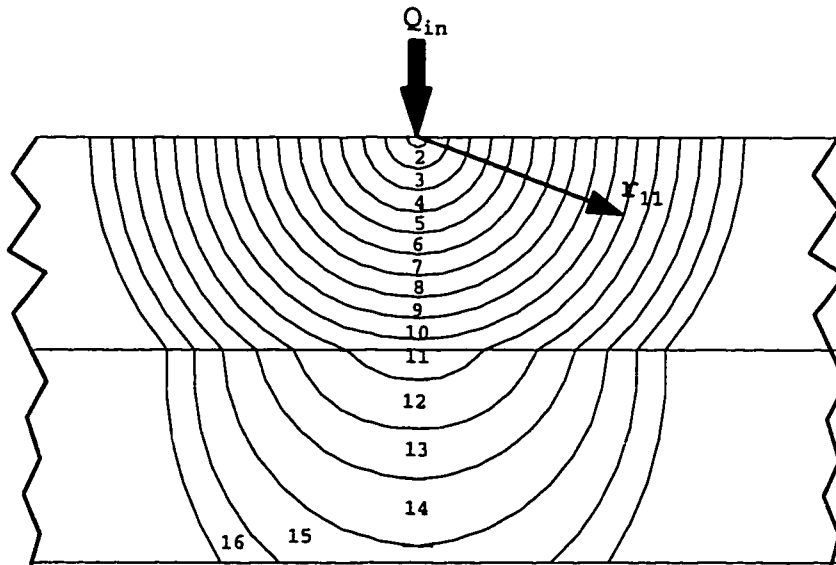
Figure A.2 The control volumes of the beam

The surface area and volume of each control volume are shown in figure A.2. They are calculated as following:

The volume and surface area of material 1 in layer 1 is:

$$V_{1,1} = \frac{b \Delta h^2 \pi}{8}$$ (A.2)

$$A_{1,1} = \frac{b \Delta h \pi}{2}$$ (A.3)

From layers 2 to 10, the shape of the surface area is half-cylindrical, the thickness of each layer is $\Delta h (=0.01)$ and their volume and surface in material 1 are:

$$V_{1,j} = \frac{b(4j - 1)\Delta h^2 \pi}{2} \quad \text{for } j=2 \text{ to } 10$$ (A.4)

$$A_{1,j} = \frac{b(2j - 1)\Delta h \pi}{2} \quad \text{for } j=2 \text{ to } 10$$ (A.5)

Since the first 10 layers do not involve material 2, the volumes and surface areas in material 2 of the first 10 layers are zero.

$$V_{2,j} = 0. \qquad \text{for } j=1 \text{ to } 10$$ (A.6)

$$A_{2,j} = 0. \qquad \text{for } j=1 \text{ to } 10$$ (A.7)

The Layer 11 as shown in figure A.3 has both materials 1 and 2. The volume and surface area of layer 11 in material 1 is:

$$V_{1,11} = b\left(area\_oab + area\_odc + \Delta obc - \frac{Dp_{10}^2 \pi}{2}\right)$$ (A.8)

$$A_{1,j} = 2bDp_{11}\theta_{11} \qquad\qquad (A.9)$$
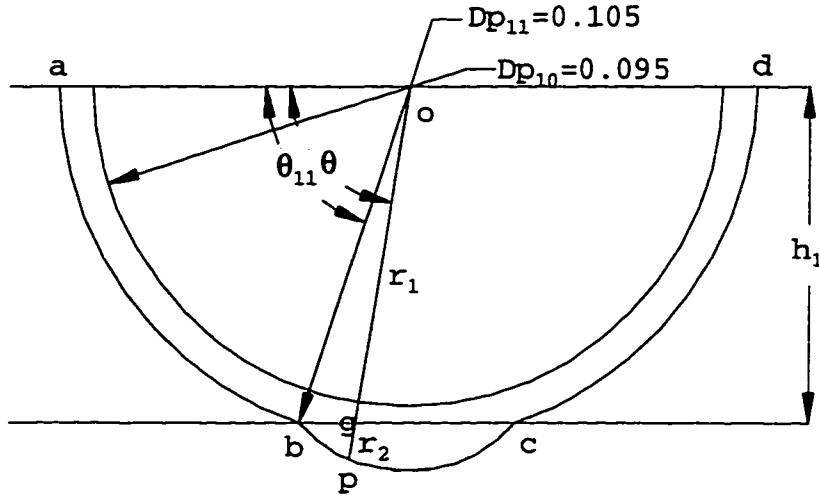
Figure A.3 The layer 11

Since the point p (in material 2) and b (in material 1) are on the same heat exchange surface, they have the same penetration distance Dp_{11}.

$$Dp_{11} = r_1 + r_2\sqrt{\frac{\beta_1}{\beta_2}} \qquad\qquad (A.10)$$

where r_1: line_og=$h_1$csc(θ)
r_2: line_gp

From equation (A.10), the function of curve_bpc can be determined by equation (A.11) in cylindrical coordinate system:

$$r = r_1 + r_2 = P - Q\csc(\theta)) \qquad\qquad (A.11a)$$

where

$$P = \sqrt{\frac{\beta_2}{\beta_1}} Dp_{11}$$

$$Q = (1 - \sqrt{\frac{\beta_2}{\beta_1}})h_1$$

$$V_{2,11} = b(\int_{\theta_{11}}^{\pi - \theta_{11}} r^2 d\theta - \Delta obc))$$ (A.11b)

$$A_{2,11} = curve\_bpc = b \int_{\theta_{11}}^{\pi - \theta_{11}} r d\theta$$ (A.11c)

The volume and surface area in material 2 of layer 11 can be calculated through the integration of equations (A.11b) and (A.11c). The volumes and surface areas in the rest of the layers are calculated in a similar way. The volume and surface area for each layer are shown in table A.2.

Table A.2

control volume#	volume in material 1	volume in material 2	area in material 1	area in material 2
1	0.0001963	0	0.00157	0
2	0.001570	0	0.00471	0
3	0.003141	0	0.00785	0
4	0.004712	0	0.01099	0
5	0.006283	0	0.01413	0
6	0.007854	0	0.01727	0
7	0.009424	0	0.02042	0
8	0.01099	0	0.02356	0
9	0.01256	0	0.02670	0
10	0.01413	0	0.02984	0
11	0.01463	0.0026607	0.02648	6.801E-4
12	0.01259	0.0123351	0.02424	1.337E-3
13	0.01183	0.0197077	0.02318	1.923E-3
14	0.01141	0.0266998	0.02252	2.499E-3
15	0.01130	0.0284328		

After defining the volume and area of the control volumes, the finite difference equations ,as shown in equations (A.15) to (A.17), are set up to calculate temperature of each layer. The time step (Δt) is chosen as the time required to penetrate through the first layer.

$$\Delta t = t_{p1} = 0.1578 \text{ Second} \tag{A.12}$$

The heat density (HD) of each layer is:

$$HD_i = (\rho_1 c_1 V_{1,\,i} + \rho_2 c_2 V_{2,\,i})\Delta h \quad \text{for } i=1 \text{ to } 15 \tag{A.13}$$

$$KA_i = K_1 A_{1,\,i} + K_2 A_{2,\,i} \quad \text{for } i=1 \text{ to } 14 \tag{A.14}$$

For the first layer :

$$T_{1,\,t+1} = \frac{\Delta t (KA_1)}{HD_1} Q_{in} + (1 - \frac{\Delta t (KA_1)}{HD_1}) T_{1,\,t} + \frac{\Delta t (KA_1)}{HD_1} T_{2,\,t} \tag{A.15}$$

For the layer 15:

$$T_{15,\,t+1} = \frac{\Delta t (KA_{14})}{HD_{15}} T_{14,\,t} + (1 - \frac{\Delta t (KA_{14})}{HD_{15}}) T_{15,\,t} \tag{A.16}$$

For the remaining layers:

$$T_{i,\,t+1} = \frac{\Delta t (KA_i)}{HD_i} (T_{i-1,\,t} + T_{i+1,\,t}) + (1 - \frac{2\Delta t (KA_i)}{HD_i}) T_{i,\,t}$$

$$\text{for } i=2 \text{ to } 14 \tag{A.17}$$

After setting the initial temperatures of the layers and the initial current time(t_c) to zero, the finite difference procedure begins.

In each time step: $t_c = t_c + \Delta t$

For $tp_{k-1} \leq t_c < tp_k$, applying the finite difference equations from layers 1 to k. Due the theory of heat penetration distance, the temperatures of the rest layers remain the same as the temperature of the last time frame.

$$T_{i, t+1} = T_{i, t} \quad \text{for} \quad i > k \qquad (A.18)$$

The finial temperatures of each layer can be determined after the current time reaches the final heat input time (120 seconds). The temperature of the first layer represents the temperature of the position of the heat input.

Table A.3		
Layer#	Ave. penetration distance D	Temperature (°C)
1	0.00	240.73
2	0.01	113.88
3	0.02	72.83
4	0.03	49.62
5	0.04	34.46
6	0.05	23.98
7	0.06	16.57
8	0.07	11.31
9	0.08	7.57
10	0.09	4.93
11	0.10	3.06
12	0.11	1.92
13	0.12	1.22
14	0.13	0.76
15	0.14	0.52

The temperatures of the rest of the layers represent the temperatures at the average penetration distances (D) of each layer as shown in equation (A.19). The final temperature and average penetration distance D of each layer are shown in Table A.3.

$$D_1 = 0$$

$$D_i = \frac{Dp_{i-1} + Dp_i}{2}$$

<div align="right">(A.19)</div>

The temperature distribution throughout the beam is obtained by expanding the temperatures of the layers to two-dimensional space. First, as shown in figure A.4, define the origin of the Cartesian coordinate system at the left-end bottom of the beam and the position of the heat input (0.3,0.2). The heat penetration distance (D_1) to a point $P_1(x_1,y_1)$ in material 1 can be calculated from equation (A.20). For a point $P_2(x_2,y_2)$ in material 2, the penetration distance from this point to the position of the heat input can be calculated in equation (A.21) from the theory of heat penetration distance. The temperature of points P_1 and P_2 can be solved as shown in equation (A.22) by utilizing the table A.3. The temperature distribution ($T(x,y)$) of the beam is therefore determined.
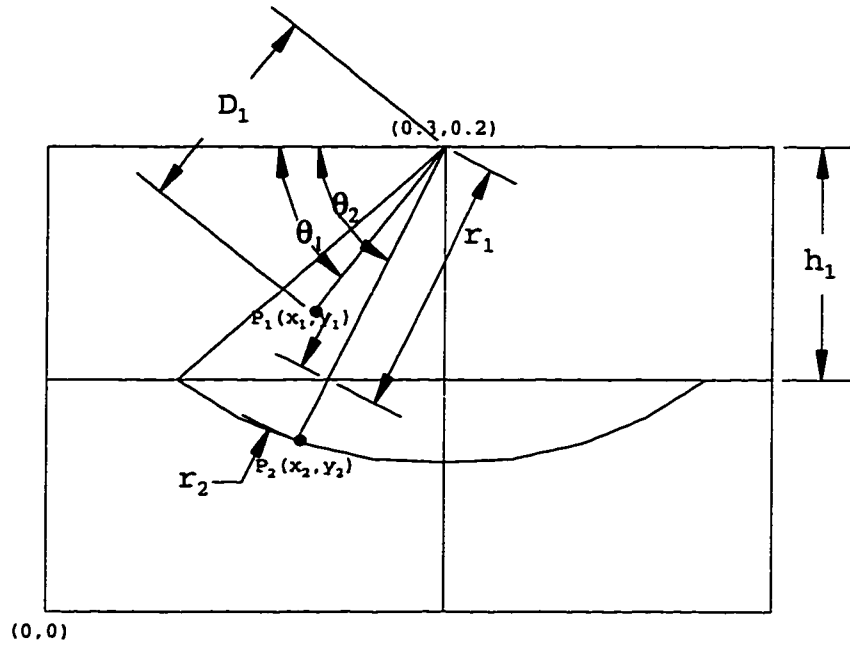
Figure A.4

$$D_1 = \sqrt{(x_1 - 0.3)^2 + (y_1 - 0.2)^2} \tag{A.20}$$

$$D_2 = r_1 + r_2\sqrt{\frac{\beta_1}{\beta_2}} \tag{A.21}$$

where $r_1 = h_1 \csc(\theta_2)$

$$r_2 = \sqrt{(x_2 - 0.3)^2 + (y_2 - 0.2)^2} - h_1 \csc(\theta_2)$$

$$\theta_2 = \tan^{-1}(\,|\,(y_2 - 0.2)/(x_2 - 0.3)\,|\,)$$

For any $D_k \geq D > D_{k-1}$

$$T(D) = T(D_{k-1}) + (\frac{D - D_{k-1}}{D_k - D_{k-1}})\,(T(D_k) - T(D_{k-1})) \tag{A.22a}$$

for and $D \geq 0.14$

$$T(D) = 0 \tag{A.22b}$$

The Thermal Deflection and Stress Distribution

After obtaining the temperature distribution ($T(x,y)$) of the beam, the neutral axis (shown in figure A.5) of this composite beam is determined by utilizing equation (3.2) before calculating the equivalent moment.

$$\int_{y_0}^{y_0+0.1} E_1 y\, dA + \int_{y_0+0.1}^{y_0+0.2} E_2 y\, dA = 0 \tag{A.23}$$

From which:

$$y_0 = -0.07473 \text{ m}$$
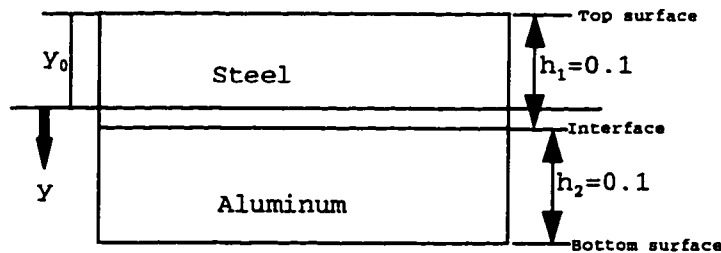
Figure A.5 The cross section of the beam

The total flexural rigidity D is obtained as following:

$$D = b[E_1(\frac{h_1^3}{12} + h_1(\frac{h_1}{2} + y_0)^2] + b[E_2(\frac{h_2^3}{12} + h_2(h_1 + \frac{h_2}{2} + y_0)^2]$$

where b: width of the beam (A.24)

The equivalent moment $M_t(x)$ is obtained as follow:

$$M_t(x) = \int_{y_0}^{y_0+h_1} E_1\alpha_1 T(x, y)y\, dy + \int_{y_0+h_1}^{y_0+h_1+h_2} E_2\alpha_2 T(x, y)y\, dy \tag{A.25}$$

The work done by the equivalent moment $M_t(x)$ is:

$$w = \int_0^L M_t v'' dx \qquad (A.26)$$

By assuming the deflection function $v(x)$ as a Fourier series:

$$v = A_0 + \sum_{n=1}^{N} A_n \cos\left(\frac{n\pi x}{L}\right) + \sum_{n=1}^{N} B_n \sin\left(\frac{n\pi x}{L}\right) \qquad (A.27)$$

The strain energy U and the work done by the equivalent loading $(M_t(x))$ are:

$$U = \frac{EI\pi^4}{4L^3} \left[\begin{array}{l} \sum_{n=1}^{N} (A_n^2 + B_n^2) n^4 + \\ \sum_{n=1}^{N} \sum_{\substack{m=1 \\ m \neq n}}^{N} (A_n B_n) \frac{4n^2 m^3}{(n^2 - m^2)\pi} (\cos(n\pi)\cos(m\pi) - 1) \end{array} \right] \qquad (A.28)$$

$$W = -\sum_{n=1}^{N} A_n n^2 \pi^2 \int_0^L M_t(x) \cos\left(\frac{n\pi x}{L}\right) dx - \sum_{n=1}^{N} B_n n^2 \pi^2 \int_0^L M_t(x) \sin\left(\frac{n\pi x}{L}\right) dx$$

$$(A.29)$$

The constraints in this case:

For v=0 at x=0

$$G_1 = A_0 + \sum_{n=1}^{N} A_n = 0 \qquad (A.30a)$$

For v'=0 at x=0

$$G_2 = \sum_{n=1}^{N} n^2 A_n = 0 \qquad (A.30b)$$

For v''=0 at x=L

$$G_3 = A_0 + \sum_{n=1}^{N} A_n \cos(n\pi) = 0 \qquad (A.30c)$$

For v'''=0 at x=L

$$G_4 = \sum_{n=1}^{N} A_n n^2 \cos(n\pi) = 0 \qquad\qquad (A.30d)$$

For v=0 at x=X_s=0.7L

$$G_5 = A_0 + \sum_{n=1}^{N} A_n \cos\left(\frac{n\pi X_s}{L}\right) + + \sum_{n=1}^{N} B_n \cos\left(\frac{n\pi X_s}{L}\right) = 0 \qquad (A.30e)$$

The Lagrangian(merit) function L can be formulated as:

$$L = U - W + \sum_{i=1}^{5} \lambda_i G_i$$

By equating to zero the partial derivatives of the merit function with respect to parameters λ_i (i=1,2,3,4,5) A_0, A_n and B_n (n=1,2,...N), a set of (2N+6) linear equations with (2N+6) unknowns is obtained. For N=8,10,14 the unknown coefficients of the deflection functions are shown in Table A.4. The results from the proposed method for different number of coefficients N are shown in figure A.6.

Table A.4

| I	N=8 sine	cosine	N=10 sine	cosine	N=14 sine	cosine
1	-2.92E-6	1.92E-4	-1.09E-4	7.50E-3	0.034467	-1.10127
2	-3.37E-4	9.50E-5	-1.26E-2	-2.56E-4	1.92731	0.12065
3	-1.55E-4	-3.17E-4	4.19E-4	-1.39E-2	-0.21661	2.31035
4	2.46E-4	-1.63E-4	1.21E-2	4.82E-5	-2.24208	-0.2765
5	1.32E-4	1.42E-4	-4.12E-4	8.48E-3	0.28756	-1.85022
6	-6.04E-5	7.62E-5	-4.88E-3	-2.78E-4	1.32188	0.24548
7	-3.22E-5	-1.82E-5	1.42E-4	-2.26E-3	-0.17696	0.82149
8	1.66E-6	-8.01E-6	8.08E-4	5.31E-6	-0.4426	-0.10813
9			-1.29E-5	2.05E-5	0.05565	-0.20461
10			-2.89E-5	-7.15E-7	0.07967	0.02373
11					-0.00813	0.02533
12					-0.00623	-0.00212
13					3.77E-4	-0.00107
14					9.88E-5	3.42E-5
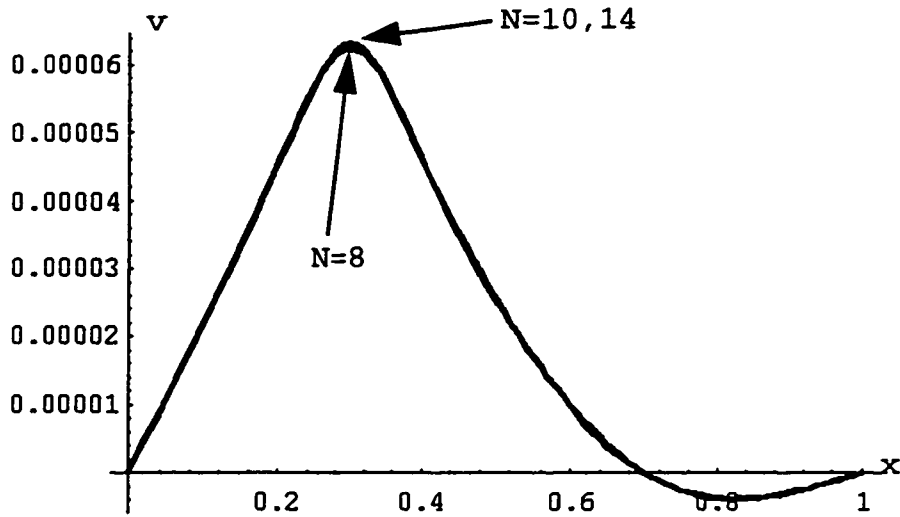
Figure A.6 The results from the proposed method for different number of coefficients N

The resultant stress is the superposition of the thermal stress (σ_t), uniform stress (σ_{ave}) and bending stress (σ_m). In order to satisfy the equilibrium conditions, the total force due to the stress distribution in x-direction has to be zero and the total moment about the neutral axis should be also zero.

For material 1:

$$\sigma_t = -\alpha_1 E_1 T(x, y) \qquad\qquad (A.31)$$

$$\sigma_{ave} = \frac{E_1}{h_1 E_1 + h_2 E_2} \left(\int_{y_0}^{y_0+h_1} \alpha_1 E_1 T(x, y) dy + \int_{y_0+h_1}^{y_0+h_1+h_2} \alpha_1 E_1 T(x, y) dy \right)$$

$$(A.32)$$

$$\sigma_m = \frac{E_1 y}{D} \left(\int_{y_0}^{y_0+h_1} \alpha_1 E_1 T(x, y) y dy + \int_{y_0+h_1}^{y_0+h_1+h_2} \alpha_2 E_2 T(x, y) y dy \right)$$

where $y_0 \geq y \geq y_0+h_1$ (A.33)

For material 2:

$$\sigma_t = -\alpha_2 E_2 T(x, y)$$ (A.34)

$$\sigma_{ave} = \frac{E_2}{h_1 E_1 + h_2 E_2} \left(\int_{y_0}^{y_0+h_1} \alpha_1 E_1 T(x, y) dy + \int_{y_0+h_1}^{y_0+h_1+h_2} \alpha_1 E_1 T(x, y) dy \right)$$

(A.35)

$$\sigma_m = \frac{E_2 y}{D} \left(\int_{y_0}^{y_0+h_1} \alpha_1 E_1 T(x, y) y dy + \int_{y_0+h_1}^{y_0+h_1+h_2} \alpha_2 E_2 T(x, y) y dy \right)$$

where $y_0+h_1 \geq y \geq y_0+h_1+h_2$ (A.36)

The resultant stress in materials 1 and 2 of the beam can be calculated as:

$$\sigma = \sigma_t + \sigma_{ave} + \sigma_m$$ (A.37)

The maximum temperature, as shown in table A.5 and figure A.7, through the thickness of the beam occurs at the x position of the heat input (x=0.3m). The resultant stress at x=0.3 can be determined by using equations (A.31) to A.37) and shown in figure A.8. The maximum shear stress as shown in figure A.8 at the interface of the two materials is 60.9 Mpa.

Table A.5 The temperature distribution through the thickness
of the beam at x=0.3

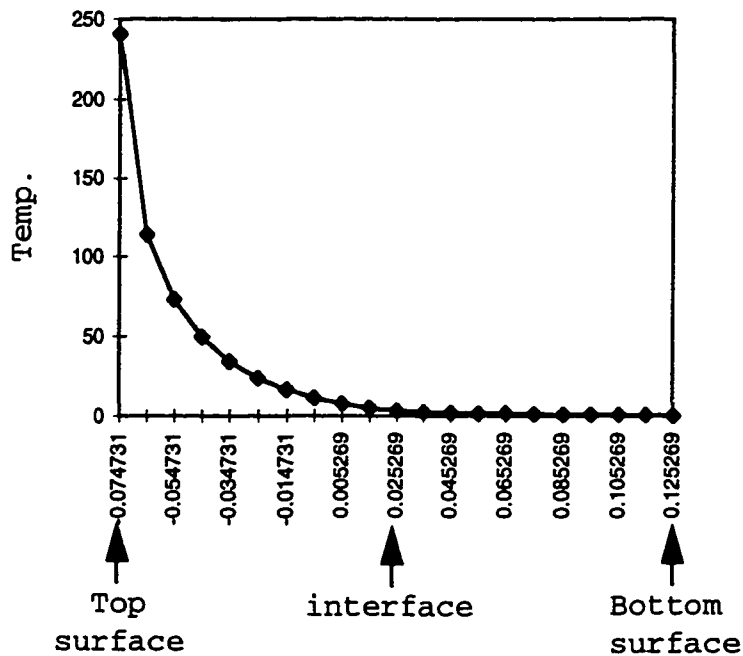| $y-y_0$	temperature	$y-y_0$	temperature
0.00	240.73	0.11	2.59
0.01	113.88	0.12	2.12
0.02	72.83	0.13	1.75
0.03	49.62	0.14	1.46
0.04	34.46	0.15	1.19
0.05	23.98	0.16	0.99
0.06	16.57	0.17	0.81
0.07	11.31	0.18	0.68
0.08	7.57	0.19	0.58
0.09	4.93	0.20	0.0
0.10	3.06		

Figure A.7 Temperature distribution in the beam
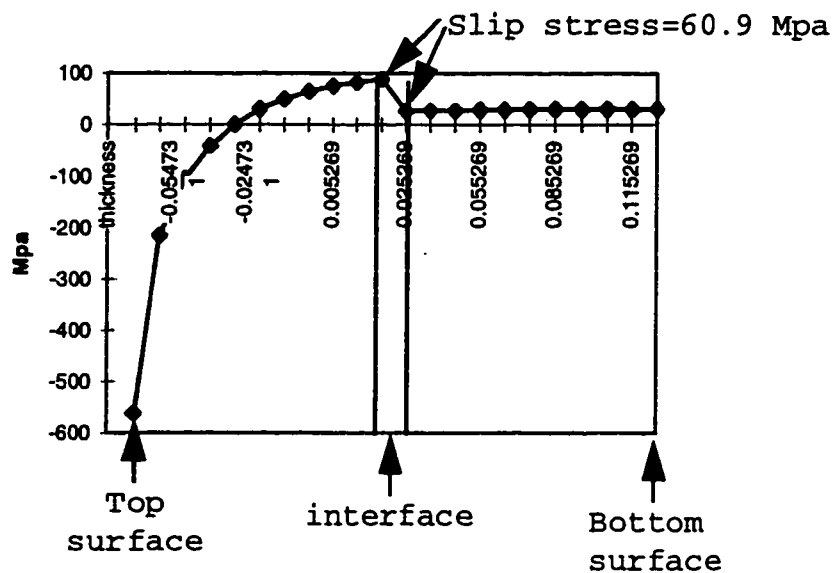at x=0.3 t=120 sec

Figure A.8 The resultant stress and the shear stress between
two materials at x=0.3

REFERENCES

1. Burton, W. Scott & Noor, Ahmed K. "Three-dimensional solutions for thermomechanical stresses in sandwich panels and shells", Journal of Engineering Mechanics vol. 120 No. 10 Oct 1994. pp. 2044-2071.

2. Chandrashekhara, K. & Bhimaraddi, A. "Thermal stress analysis of laminated doubly curved shells" Computers and Structures vol. 52 No. 5 Sept 3 1994. pp. 1023-1030.

3. Zako, Masaru & Tsujikami, Tetsuya & Uetsuji, Yasutomo "Three-dimensional thermal stress analysis of composites" Journal of the Society of Materials Science, Japan vol. 43 No. 487 Apr 1994. pp. 402-407.

4. Yin, Wan-Lee "Simple solutions of the free-edge stresses in composite laminates under thermal and mechanical loads" Journal of Composite Materials vol. 28 No. 6 1994. pp. 573-586.

5. Saha, Pabitra K. & Ahmed, Nesar U. & Basu, Prodyot K. & Nagar, Arvind "3-D thermal stress analysis of laminated panels " Recent Developments in Computational Mechanics American Society of Mechanical Engineers, Aerospace Division (Publication) AD vol. 39 1993. Publ by ASME, New York, NY, USA.

6. Kollar, L. P. "Three-dimensional analysis of composite cylinders under axially varying hygrothermal and mechanical loads" Computers and Structures vol. 50 No. 4 Feb 17 1994. pp. 525-540.

7. Karditsas, Panayiotis J. "Thermal and structural behaviour of various first-wall concepts" Fusion Engineering and Design vol. 25 No. 1-3 Aug 1994. pp. 273-287.

8. Cresdee, R. B. & Edwards, W. J. & Thomas, P. J. & Ross, G. F. "Analysis of beam distrortion during hot dip galvanizing" Materials Science and Technology vol. 9 No. 2 Feb 1993. pp. 161-167.

9. Ray, Ajit Kumar & Banerjee, Barun & Bhattacharjee, Biswanath "Non-linear analysis of heated rhombic plates" International Journal of Solids and Structures vol. 31 No. 5 1994. pp. 705-710.

10. Lee, Kang Yong & Jang, Yong Hoon "Thermal stress analysis of an infinite plate containing a rigid inclusion of arbitrary shape" Engineering Fracture Mechanics vol. 46 No. 4 Nov 1993. pp. 709-714.

11. Aboutalebi, M. Reza & Hasan, Mainul , "Thermal modelling and stress analysis in the continuous casting of arbitrary sections" Steel Research vol. 65 No. 6 Jun 1994. pp. 225-233.

12. Fuchiyama, Takashi & Noda, Naotake & Tsuji, Tomoaki & Obata, Yoshihiro, "Transient thermal stress in a circular plate of functionally gradient materials with temperature-dependent material properties" Transactions of the Japan Society of Mechanical Engineers, Part A vol. 59 No. 564 Aug 1993. pp. 1925-1930.

13. Ootao, Yoshihiro & Akai, Tomikazu & Tanigawa, Yoshinobu "Three-dimensional transient thermal stress analysis of a nonhomogeneous hollow circular cylinder with respect to rotating heat source" Transactions of the Japan Society of Mechanical Engineers, Part A vol. 59 No. 568 Dec 1993. pp. 2953-2959.

14. Dighde, Rajesh M. & Meekisho, Lemmy L. "Transient thermal analysis of Tekken weldability test by the finite element method" Manufacturing Science and Engineering American Society of Mechanical Engineers, Production Engineering Division (Publication) PED vol. 64 1993. Publ by ASME, New York, NY, USA. pp. 885-893.

15. Wang, Ming-Jong & Wang, Wei-Chung "Transient thermal stress analysis of a near-edge elliptical defect in a semi-infinite plate subjected to a moving heat source" International Journal of Pressure Vessels and Piping vol. 57 No. 11994. pp. 99-110.

16. Elbella A. & Seireg, A. A. "Optimum design of crown brakes", Transactions of the A.S.M.E., Journal of Mechanical Design, vol. 112 1990. pp. 557-562.

17. Spilker, R. L. & Engelemann, B. E., "Hybrid-stress isoparametric elements for moderately thickness and thin multilayer plates", Computer Method in Applied Mechanics and Engineering, vol. 56, 1986, pp. 339-361.

18. Venkatesh, A. & Roa, K. P., "Analysis of laminated shells with laminated stiffeners using rectangular shell finite elements", Computer Methods in Applied Mechanics and Engineering, vol. 38, pp. 255-272.

19. Logan, D. L., A First Course in the Finite Element Method, PWS-KENT Pulibishing Company, Boston, 1991.

20. Timoshenko, S. P. & Goodier, J. N., Theory of Elasticity 3rd edition, McGraw-Hill Book Company, New York, 1970.

21. Gere, J. M. &.Timoshenko, S. P., Mechanics of Materials 3rd edition, McGraw-Hill Book Company, New York, 1956.

22. Ugural, A. C. & Fenster, S. K., Advanced strength and Applied Elasticity, Elsevier Science Publishing Co., Inc, New York, 1975.

23. Al-Shareedah, E. M. & Seireg, A. A., "The design of slabs with constraining columns using the undetermined multilpers method", Computer in Mechanical Engineering, vol. 4, No. 4, 1986, pp. 59-68.

24. Al-Shareedah, E. M. & Seireg, A. A., " Use of undetermined multilpers in the solution of plate problem", Computer in Mechanical Engineering, vol. 4, No. 3, 1985, pp. 59-68.

25. Al-Shareedah, E. M. & Seireg, A. A., "Use of undetermined multilpers in the design of stiffened plates", Computer in Mechanical Engineering, vol.4, No. 5, 1986, pp. 57-64.

26. Chen, Tzu-Yang, The Use of Undermined Multipliers in the Analysis and Optimum Design of Elastic Structures, Ph.D. dissertation, University of Florida, 1989.

27. Saada, A. S., Elasticity: Theory and Application, New York: Pergaman Press, 1974.

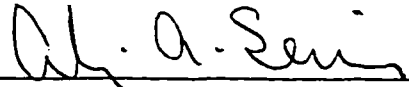28. Love, A. E. H., A Treatise on the Mathmatical Theory of Elasticity, 4th ed.,Dover Publications, New York, 1944.

BIOGRAPHICAL SKETCH

Un-Chin Chai was born on September 4, 1964, in Keelong, Taiwan, Republic of China.

He received his B.S. in mechanical engineering from National Taipei Institute of Technology, Taipei, Taiwan R.O.C. in June 1986. He then served in the army to fulfill mandatory military service from August 1986 to June 1988. After finishing the service in the army, he worked full time for two years as a teaching assistant and technician in mechanical engineering department of Chong-Chou Institute of Technology. Encouraged by his father and wife, he decided to continue his studies in the U.S.A. He received his M.S. in mechanical engineering from Bradley University, Peoria, IL. in December 1992.

In August 1993, he joined the department of mechanical engineering, University of Florida, Gainesville, where he studied machine design under the direction of Dr. Ali A. Seireg.

164

I certify that I have read this study and that in my opinion it conforms to acceptable standards of scholarly presentation and is fully adequate, in scope and quality, as a dissertation for the degree of Doctor of Philosophy.

Ali A. Seireg, Chair
Ebaugh Professor of
   Mechanical Engineering

I certify that I have read this study and that in my opinion it conforms to acceptable standards of scholarly presentation and is fully adequate, in scope and quality, as a dissertation for the degree of Doctor of Philosophy.

Chen-Chi Hsu
Professor of Aerospace
   Engineering, Mechanics,
   and Engineering Science

I certify that I have read this study and that in my opinion it conforms to acceptable standards of scholarly presentation and is fully adequate, in scope and quality, as a dissertation for the degree of Doctor of Philosophy.
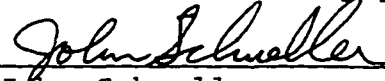
Carl D. Crane, III
Associate Professor of
   Mechanical Engineering

I certify that I have read this study and that in my opinion it conforms to acceptable standards of scholarly presentation and is fully adequate, in scope and quality, as a dissertation for the degree of Doctor of Philosophy.

Gloria J. Wiens
Associate Professor of
   Mechanical Engineering

I certify that I have read this study and that in my opinion it conforms to acceptable standards of scholarly presentation and is fully adequate, in scope and quality, as a dissertation for the degree of Doctor of Philosophy.
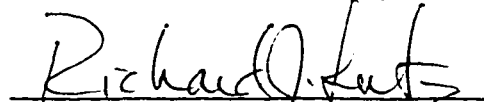
John Schueller
Associate Professor of
Mechanical Engineering

This dissertation was submitted to the Graduate Faculty of the College of Engineering and to the Graduate School and was accepted as partial fulfillment of the requirements for the degree of Doctor of Philosophy.

August, 1996

Winfred M. Phillips
Dean, College of Engineering

Karen A. Holbrook
Dean, Graduate School